

# UNIVERSITEIT TWENTE.

Faculty of EEMCS  
Department of Electrical Engineering  
Biomedical signals and systems

## Development of an 11000 electrode high-density multi- electrode-array system for neural network recording

---

12 January 2011

report nr: BSS 11-04

Master Thesis

Author : Deligkaris, Kosmas

---

Committee : Prof.dr.Wim Rutten  
Dr.ir. Joost le Feber  
Dr.ir. Jan Stegenga  
Prof.dr. Michel van Putten

---

## Acknowledgments

This report would not be feasible without the cooperation of many people. First and foremost, I would like to thank my supervisor for more than one year, Joost le Feber. His guidance and help were vital for my progress in and out of my academic studies. The guidance of the group's chairman, Wim Rutten, besides the relevant courses, is also one of the primary factors affecting the quality of this work. Discussions with Jan Stegenga during our common laboratory hours were informative and fun at the same time. Michel van Putten, as a neurophysiologist significantly contributed to the quality of the document, especially in the introductory part where many unclear statements were made in the original version. Furthermore, acknowledgments go to all the committee members, as a committee, who were extremely helpful and understanding of personal problems. I should not forget to mention Karin and Irina from the BSS group. They did all the plating and maintenance of the cultures and tried their best, even when I did not keep my end of the deal.

Besides the people in my group, personal discussions in Reutlingen, accompanied by email exchange, with the people from ETH (especially Jan Mueller and David Jackael) helped to speed up things a little bit. I hope they also gained something from our discussions. Acknowledgements also go to Michele Friscella and Douglas Bakkum.

## Contents

1. Background and Motivation .....	1
1.1 Recording cellular activity .....	1
1.1.1 Generation and propagation of electrical signals.....	1
1.1.2 Intracellular and extracellular recordings.....	3
1.2 MultiElectrode Arrays .....	4
1.2.1 Overview .....	4
1.2.2 Modeling extracellular potentials generated by neural cells.....	7
1.2.3 Preparation of networks on traditional MEAs.....	9
1.2.4 Network development.....	10
1.2.5 On high-resolution MEAs.....	12
1.3 The ETH 11000 electrode, CMOS system .....	15
1.4 Formulation of research questions.....	17
2. Methods and materials.....	18
2.1 Hardware .....	18
2.1.1 System Description .....	18
2.1.2 Chip description .....	19
2.1.3 Electrode array and configuration .....	22
2.2 Culture preparation and maintenance .....	23
2.3 Experimental procedures.....	24
2.3.1 Verifying hardware's and software's integrity with physiological saline ...	24
2.3.2 Trial experiments with active and silenced cultures .....	24
2.4 Algorithms and techniques.....	25
2.4.1 Electrode selection overview.....	25
2.4.2 Online spike-detection algorithm.....	26
2.5 Data analysis .....	28
3. Results.....	30
3.1 Verification of experimental set-up.....	30
3.1.1 Saline experiments.....	30
3.2.4 First spike shapes and ISI Histograms .....	31
3.2 Dynamics in developing high density networks .....	32

3.2.1 Basic electrode configuration and raster plots.....	32
3.2.2 Firing rates and active electrodes.....	36
3.2.3 Burst profiles.....	37
3.2.5 Spike shape clustering.....	40
3.3 Electrode configurations.....	42
3.4 Neurochemical treatment (Magnesium).....	47
4. Discussion and conclusions.....	48
4.1 Overview.....	48
4.2 Data analysis.....	50
5. Future work and Recommendations.....	53
Appendix.....	55
A.1 Experimental set-up for temperature recordings.....	55
A.2 Trial hippocampal recordings – verifying integrity of our software.....	56
A.3 Selecting burst criterion.....	60
A.4 Complementary raster plots.....	63
A.4.1 Culture 512.....	63
A.4.2 Culture 529.....	65
A.5 MFR of individual electrodes.....	67
A.6 Software description.....	68
A.6.1 Hidens neurodish router.....	68
A.6.2 Labview software overview.....	72
A.7 Spike shapes.....	73
References.....	80



# 1. Background and Motivation

## 1.1 Recording cellular activity

Certain classes of cells can produce electrical signals by changes in their membrane potential difference (intra vs. extra cellular potential). These cells are called excitable and characteristic examples are neurons (including retina ganglion cells and cardiomyocytes) and muscle cells. Such cells can be used to study spontaneous activity or the effects of chemical substances. Our analysis from now on will be based on neuronal cells.

### 1.1.1 Generation and propagation of electrical signals

The cell membrane is selectively permeable to specific ions. Ionic channels and transporters allow or initiate movement of ions. Ionic movements in turn, can produce electrical signals. The permeability of the cell's membrane depends on the membrane potential itself. Luigi Galvani, a biologist from Bologna, Italy, first discovered electrical activity in animals, eliminating the concept of "spirits able to generate muscle twitch" which was very popular at his time. Hermann von Helmholtz later found that the axons of nerve cells generate electrical activity not as a byproduct of their activity but as a means of transmitting information. At 1859 he even measured the propagation speed of such signals, which was found to be much slower than electrical signals in a wire. These signals were following the principle of all or none and are named Action Potentials (AP).

Julius Bernstein, a student of Helmholtz, first formulated the membrane hypothesis. He measured the normal, resting potential of a neuron at 70 millivolts, with the inside of the cell having more negative charge than the outside. He reasoned, that due to different ion concentrations inside and outside of the cell and together with the selective membrane permeability this resting potential is due to potassium ions leaving the cell, until an equilibrium phase is reached. In this equilibrium phase, the diffusional force is equal to the electrical force and gives rise to the -70mV resting potential. Finally, he concluded that during an action potential this membrane permeability breaks down and potassium ions flow freely restoring the membrane's potential to 0 mv.

The ionic hypothesis of Alan Hodgkin and Andrew Huxley correctly explained the fact that during an action potential the membrane's potential does not return to 0 levels, but goes up to 40mV. After World War II ended they both returned from military service and found, together with Bernard Katz of University College London, that the

upstroke of the action potential depends on the amount of sodium outside the cell, while the downstroke phase is affected by the amount of potassium. They suggested that, during an action potential some ion channels are selectively permeable to sodium ions during the upstroke phase and later on, other channels are open during the downstroke phase (Figure 1).

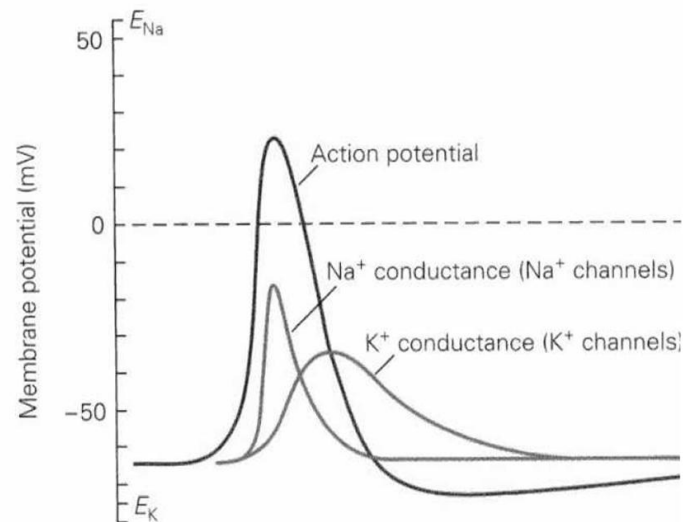


Figure 1. An action potential with the corresponding sodium and potassium membrane conductances. The conductance for a specific ion is the result of the effective number of open ion channels for that particular ion. Taken from [1].

The concentration of sodium ions is much larger outside the cell, while the cytoplasm contains a higher concentration of potassium ions compared to the extracellular fluid. When an action potential is initiated, sodium channels open, allowing sodium ions to enter the cell (carrying positive charge) and depolarize the cell. Later, voltage-sensitive potassium channels open and the sodium channels are inactivated, bringing the cell back to its normal resting potential.

Furthermore, due to excess potassium concentration outside the cell, the membrane's potential becomes temporarily hyperpolarized (more negative than its resting state). These events give rise to what is known as **refractory period** and is a parameter exploited during cell recordings. Neurons can produce action potentials as fast as the refractory period will allow which is approximately 1 msec.

The question arises then, how the sodium channels open in the first place. The answer is that they are voltage-sensitive and when the cell's potential has been sufficiently depolarized they open. Furthermore, initiation of an action potential in a specific region of the cell is enough to depolarize near-by areas (after some delay) so that an action potential can propagate. Most cells exhibit what is known as saltatory conduction. A myelin sheath (dielectric) covers large parts of the cells' axons. Gaps in the myelin sheath are called Nodes of Ranvier. An action potential in one node of

Ranvier gives rise to passive currents flowing through the axon's myelinated section until it reaches the next Node of Ranvier where another action potential is generated (Figure 2).

Modern research has verified that mutations in the genes coding for ion channels lead to diseases. For example, a disorder called familial idiopathic epilepsy is associated with mutations in genes coding for potassium channels. Furthermore, demyelination of neurons is more commonly known as multiple sclerosis and has devastating physiological and psychological effects on the individual. However, the pathophysiology of this disorder is only partially understood.

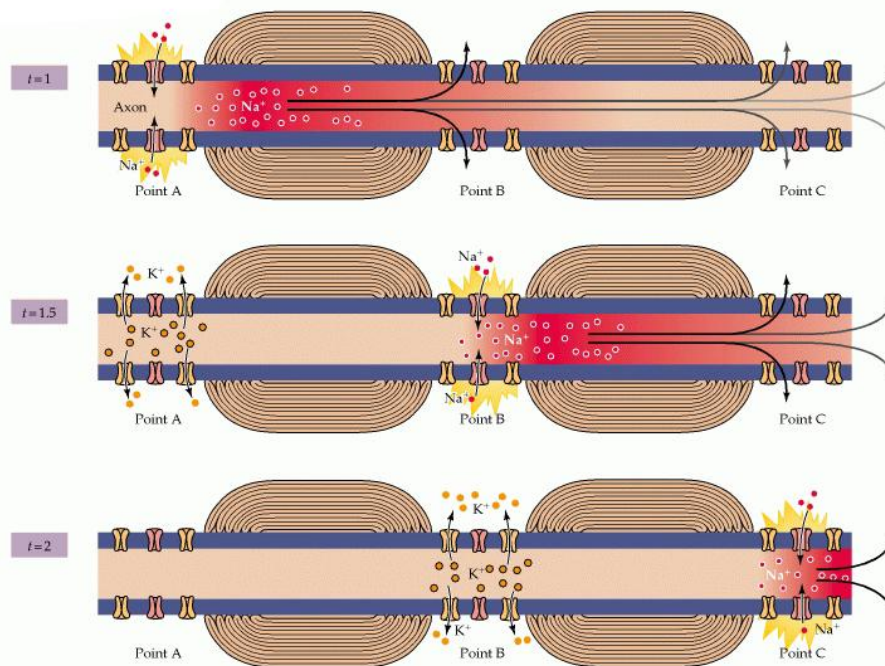


Figure 2. Mechanism of saltatory conduction. At time  $t = 1$  sodium ions enter the first Node of Ranvier causing an action potential. Passive current flows through the myelinated area and reaches the next Node of Ranvier. (point B,  $t = 1.5$ ), causing depolarization and another action potential. After the upstroke phase (depolarization), potassium ions leave the cell, hyperpolarizing the cell. Propagation continues, "jumping" from one Node of Ranvier to the next. Taken from [2].

### 1.1.2 Intracellular and extracellular recordings

The membrane's potentials can be recorded either intracellularly or extracellularly. By inserting a microelectrode in the cell one can record with great detail the intracellular currents flowing in the cell. With an external electrode, voltage or ionic current recordings are possible.

The patch clamp technique is widely used nowadays and allows monitoring of the electrical potential and currents from the entire cell, measurement of single channel

currents and injection of substances into the interior of the cell among others [2]. However, cells get damaged and as a consequence long-term recordings cannot take place. Furthermore, the number of cells that can be used in an experiment is quite limited. Only a few cells can be patched simultaneously.

Intracellular recordings can measure ionic currents with great details but in a limited number of cells and for a limited time. Extracellular recordings with substrate-integrated micro electrodes on the other hand are non-invasive and can be used for long-term recordings. However, they cannot record ionic currents, but only the extracellular potential fluctuations. When ions move inside or outside the cell, during an action potential, they give rise to a potential difference between the measurement electrode and the reference electrode. However, extracellular signals are much lower in amplitude than intracellular signals. Figure 3 shows the schematic illustration of an extracellular recording system [1].

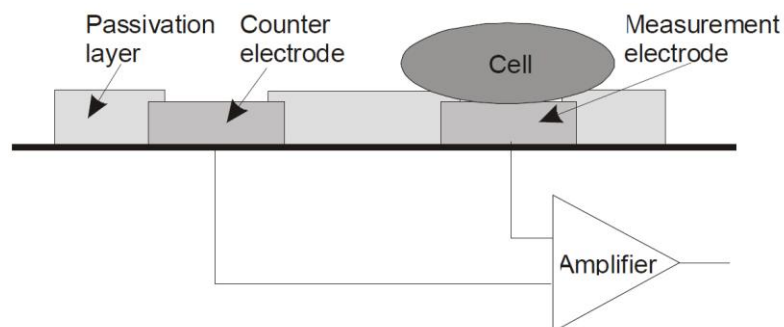


Figure 3. Schematic of an extracellular measurement setup. Taken from [1].

## 1.2 MultiElectrode Arrays

### 1.2.1 Overview

A MultiElectrode Array (MEA) is an array of electrodes, allowing recording and stimulation of cells. Typical numbers of electrodes are 60 – 100. These electrodes are integrated into the substrate which is usually glass, transparent to light. The microelectrodes are typically inert conductors (gold, platinum...). The electrodes need to be isolated from each other so, biocompatible non conductive layers are used (like  $\text{Si}_3\text{N}_4$  and  $\text{SiO}_2$ ). Glass rings are mounted to form a culture around the electrode area so that neurons can be cultured on the substrate, bathing in the medium.

Figure 4 shows an example of a commercially available MEA. It is also demonstrated how an electrode contacts the cells. There is a slight probability that an electrode might pick up signals from different neurons (multi-unit activity) and a neuron might contribute signals to many electrodes, although this depends on the

distance of the neurons to the electrode and the diameter of the electrode. Other commercial MEAs are illustrated in Figure 5.

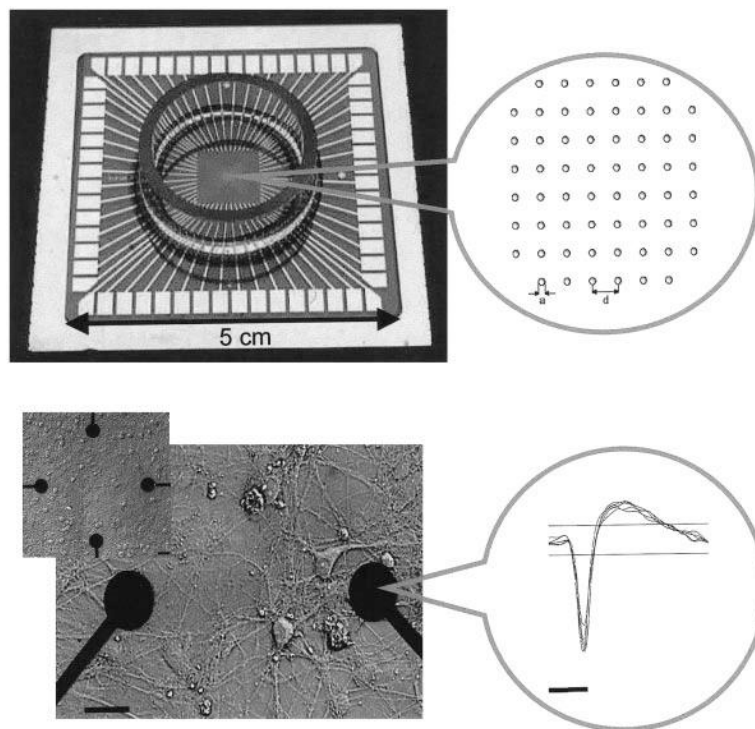


Figure 4. A commercially available substrate integrated multi-electrode array (MEA) containing 60 electrodes. The diameter of a single electrode (a) and the distance between electrodes (d) range from 10-50  $\mu\text{m}$  and 100-500  $\mu\text{m}$ , respectively. (b) *Ex-vivo* developing cortical network growing on a substrate integrated MEA (only the four center electrodes are visible, two of which are enlarged). The exposed electrode tip occupies only part of the circular terminal (bar = 30  $\mu\text{m}$ ). Aligned action potentials recorded from one electrode are shown at the right. The distance between the horizontal lines depicts  $\pm 8$  root mean square units, which, for this particular electrode amounts to approximately  $\pm 7 \mu\text{V}$  (time bar = 1 ms). Taken from [3].

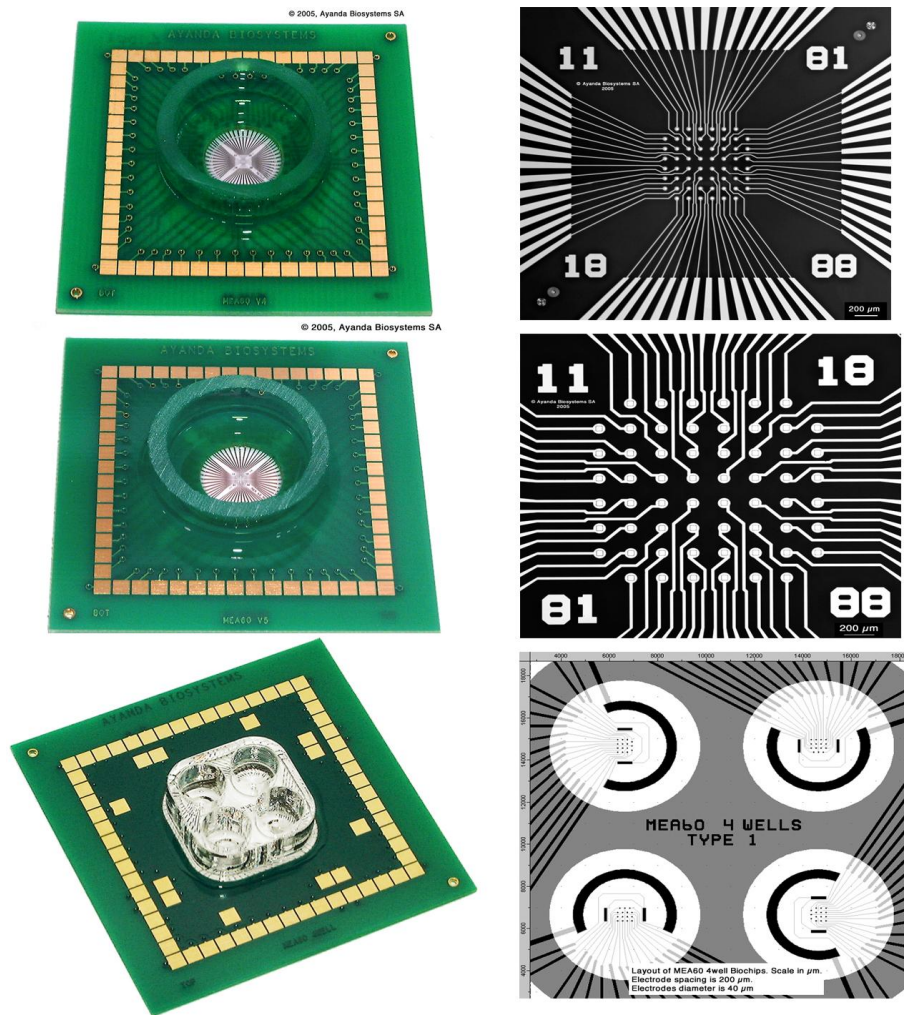


Figure 5. Different types of commercial MEAs. On the left the MEA design is shown and on the right the MEA layout. Upper MEA is a traditional 60-electrode array of 8x8 electrodes, without the corner electrodes. Electrode spacing is 100 µm and electrode diameter is 30 µm. Noise levels are 25-30 µV for aluminum electrodes. In the middle MEA electrodes are of larger size (40 µm x 40 µm, square) and spacing (200 µm). Finally, the lower MEA is a 4-well MEA suitable for conducting many experiments at once. Property of Ayanda Biosystems (<http://www.ayanda-biosys.com>).

Multi electrode arrays (MEAs) can be used with primary dissociated cultures or acute brain slices. In primary dissociated cultures one specific cell type can be grown and the external environmental conditions are much easier to control than in vivo. On the other hand, is not possible to directly draw conclusions from in vitro experiments upon the in vivo behavior of the cell [4].

MEAs offer possibilities in studying electrogenic tissue, of brain or cardiac origin and are considered to be important in experimental neuroscience, neurotechnology and biosensing [5-9]. Recordings from dissociated cultures or brain slices of extracellular potential fluctuations [3, 8-14] allow us to study network development [10-12, 14-17], learning and memory capabilities [3, 11-12, 18-24], the effects of

various chemicals [6, 25-30] and different patterning protocols for patterned cell adhesion [8, 31-34].

### 1.2.2 Modeling extracellular potentials generated by neural cells

Two main types of signals can be identified in an extracellular recording. One is the local field potential (LFP) which has a relatively low frequency content whereas an action potential (AP) has more high frequency content.

The extracellular spike recorded from a specific neuron is considered to be repeatable, although this is questionable since the extracellular action potential (EAP) can change, especially during bursts [10, 21]. The magnitude of the recorded EAP depends on the morphology of the cell, the transmembrane currents, the sealing resistance of the cell-electrode interface and the orientation and distance from the electrode to the source [35-36]. The transmembrane currents are affected by the type and number of ion channels, which depend on the type and size of the cell [4].

Gold et al. [35] have investigated by experimental and modeling techniques the effects of the above considerations on the extracellularly recorded waveform. They found that the electrode position had a significant impact on the recorded shape. More specifically, when the electrode position was close to the cell's body then the EAP was mainly biphasic with one negative peak followed by a slower positive rebound, without any initial positive peak (Figure 6). In contrast, close to the apical trunk the initial positive peak becomes more pronounced. Furthermore, the axon's initial segment has a slightly lower depolarization threshold and is activated slightly (0.5 ms) before the soma. Therefore, an electrode in this position would record a depolarization at about 0.5 ms before the start of the three-phase EAP. Myelinated areas of axons and nodes of Ranvier do not contribute to the recorded EAP. Finally, the distance of the electrode position was found to affect the width of the negative peaks. The larger the distance the more EAPs may sum up, increasing the total width of the EAP.

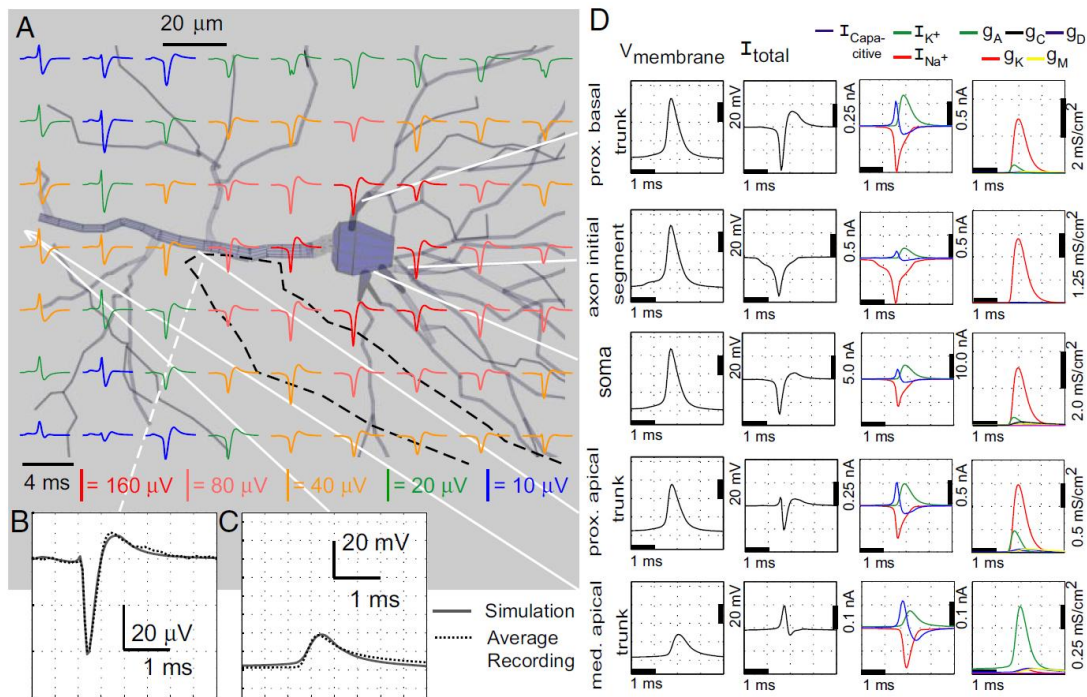


Figure 6. A: EAPs in the transverse section containing the tip of electrode track (dotted line), about 5  $\mu\text{m}$  caudal to the soma and apical trunk (the z-axis is the axis perpendicular to the plane of the section). Close to the soma, there is no initial, positive peak in the EAP. At locations along the apical trunk, the initial peak becomes pronounced. B: comparison of extracellular recording (strongest channel of the tetrode) and simulation at the estimated electrode position. There is only a slight hint of a positive deflection before the negative Na-dominant phase of the waveform. C: comparison of intracellular recording and the simulation in the apical trunk approximately 120  $\mu\text{m}$  from the soma. D: further simulation details. In the soma (middle row) the positive capacitive current, proportional to the change in membrane potential, coincides with the larger Na current (3rd column) because the membrane potential change is driven by local Na current. In dendritic compartments (4th and 5th rows) the membrane depolarization is initially driven by Na current from the soma, until local Na currents are activated and the action potential regenerates. In the brief time before the local Na currents activate, the positive capacitive current is the dominant membrane current and a capacitive-dominant phase is visible in the net current (2nd column). Consequently, the EAP has a more pronounced capacitive phase close to the apical trunk. Also shown, the Na current starts to enter the axon initial segment (2nd row) in a gradual way, driven by the action potential in the first node of Ranvier (not shown) and before the start of the main action potential at the soma. This results in a slightly negative slope in the extracellular potential before the start of the main EAP. Taken from [35].

The shape of an EAP does not depend only on the position of the electrode. The morphology of a neuron affects the waveshape also. The distribution of active ionic conductances can affect its form [37]. In general, the  $\text{Na}^+$  conductance is responsible for the large negative peak observed in an EAP and its inactivation together with activation of the  $\text{K}^+$  conductance give rise to the repolarization phase of the EAP. Not all recorded wave shapes look like the EAPs in Figure 4 and Figure 6. Figure 1 is only indicative of  $\text{Na}^+$  and  $\text{K}^+$  conductances. Conductances found in cells include fast inactivating  $\text{Na}^+$ , A type  $\text{K}^+$  (proximal and distal varieties), C type voltage and  $\text{Ca}^{2+}$  dependent  $\text{K}^+$  conductance, D type  $\text{K}^+$  conductance and K type  $\text{K}^+$  conductance among others [37]. In order to analyze how the EAP waveform depends on the density of active ionic conductances, Gold et al. [37] created a model and performed four different simulations, each with different ionic conductance distributions. The models had nearly identical intracellular action potentials (IAP) so that only the influence of different ionic conductances was investigated. Their results indicate that

the shape of a recorded EAP depends not only on the position of the electrode but also on the conductance density distribution (Figure 7), since in different regions of the neuron different types of conductances can be found.

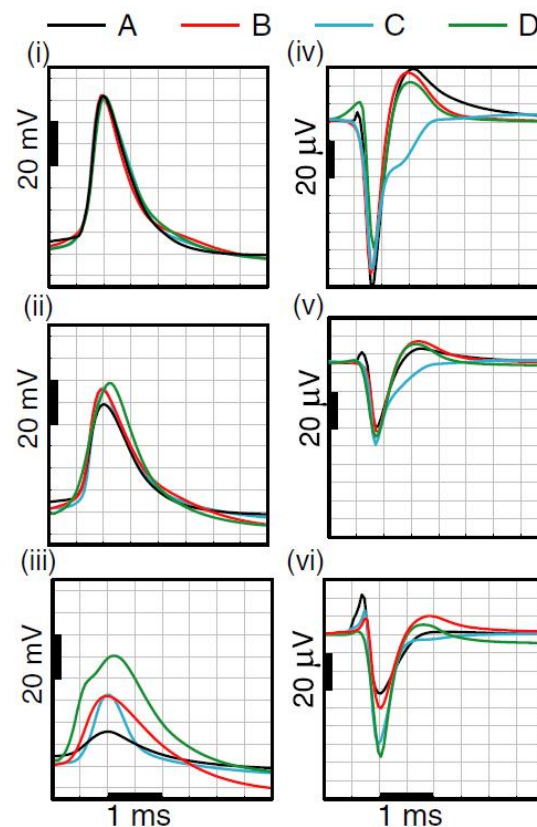


Figure 7. Comparison of Intra and Extracellular Action Potentials for four conductance density models. Left column: IAP at soma (i), and on the apical trunk at 100 (ii) and 200μm (iii). The IAPs at the soma are indistinguishable. Right Column: EAP measurements near the soma (iv), near the apical trunk 50 μm (v) and near the apical trunk 100 μm (vi) from the soma. In model C, repolarization depends on the A type  $K^+$  conductance which inactivates much faster than other types of conductances and makes the repolarization phase of the EAP at the soma somewhat “curvy”. Taken from [37].

### 1.2.3 Preparation of networks on traditional MEAs

The procedure of plating a culture on conventional MEAs includes decapitation of new-born rats which are then plated on top of a glass substrate integrated with electrodes of diameter 10 – 30 μm. Cells taken from older animals usually have lower probabilities of survival [3]. Only the soma of each neuron is being plated on the MEA. Axons and dendrites do not exist at that time but they form later, during development of the network in vitro. The distribution of cell types in vitro has been found to be the same as that in vivo for networks of cortical neurons. Approximately 10% is inhibitory and the rest excitatory [38-39]. In the preparation of cortical networks cell purification procedures are not common and the culture contains all the types of cells present in the cortex, including glial cells [3].

The cells are plated within a chamber of diameter 20 mm [3]. A liquid medium (Rominj's serum - free medium) necessary for growth is added containing a balanced solution of ions and other substances [40]. The network can then grow, form connections, and after approximately 7 days in vitro (D.I.V.) shows spontaneous activity.

It may be evident that the number of cells (or cell density) might affect the development of the network [41]. Obviously, if there are just a couple of neurons they may not survive long enough to form a network. Useless cells tend to die due to lack of growth factors secreted by their postsynaptic partners [2]. However, with a higher number of cells in a MEA the recorded patterns are much more complicated to analyze and therefore a balance should be found between density and survival. Furthermore, the lower the density of the culture, the lower the probability that one electrode in a conventional MEA will be close enough to record its activity.

A typical culture with 150000 cells in such a MEA can survive for months [3, 42]. In the literature many different densities have been investigated, from 100 cells/mm<sup>2</sup> to 2000 cells/mm<sup>2</sup> [3, 42-46]. Jun et al. [44] assessed densities as low as 100 cells/mm<sup>2</sup> for finding the minimum neuron density and their results indicate that for spontaneous activity a minimum of 200 cells/mm<sup>2</sup> is needed and for bursts the number goes to 400 cells/mm<sup>2</sup>. Ito et al. [47] have recently investigated the minimum cell density necessary for burst generation. Five different plating densities were investigated (2000, 1000, 500, 250 and 100 cells/mm<sup>2</sup>) and it was found that the minimum density for burst generation is 250-500 cells/mm<sup>2</sup>. Furthermore, cell densities of surviving neurons at 30 DIV were much lower than initial cell densities ( 1 DIV ).

#### 1.2.4 Network development

Every ex-vivo developing cortical network shows spontaneous activity, starting from the end of first week [10, 12], which changes according to the age of the network [3, 10-14]. Two distinct classes of firing can be distinguished, tonic activity and bursts. Tonic activity is seemingly uncorrelated activity while bursts are composed of synchronous firing and an increase in the recorded activity.

Chiappalone et al. [10] and van Pelt et al. [12] have both investigated the spontaneous activity patterns during in vitro development. Their results indicate that the network goes through developmental changes which also affect the recorded activity. Both report on significant developmental changes between the second and third week in vitro. At first, the network forms a surplus of network connections which at a certain point (2-3 weeks in vitro) will be reduced. At the end of the third week in vitro (WIV) dendritic spine and shaft synapses have attained their maximum

numbers [48-49]. During the 4<sup>th</sup> WIV dendritic spine synapses are pruned, but not shaft synapses [12].

At a very early stage, the networks exhibit mostly uncorrelated firing, without signs of organization and the activity of the network, measured by the mean firing rate, is close to zero. From that point, the network's activity increases, reaching a peak at approximately the end of the third week and starts decreasing (Figure 8A). A similar pattern is observed for the bursting activity (Figure 8B). Furthermore, the burst duration was also found to be dependent on the age of the culture with young cultures exhibiting fewer bursts but of higher duration than mature cultures (Figure 9). As stated by van Pelt et al. [12]:

*“It is remarkable that the time point of maximal synapse number appears to coincide with the time at which network bursts attain their longest duration, and that the period of strong reduction in synapse number coincides with the period in which network bursts develop extremely short rising phases”.*

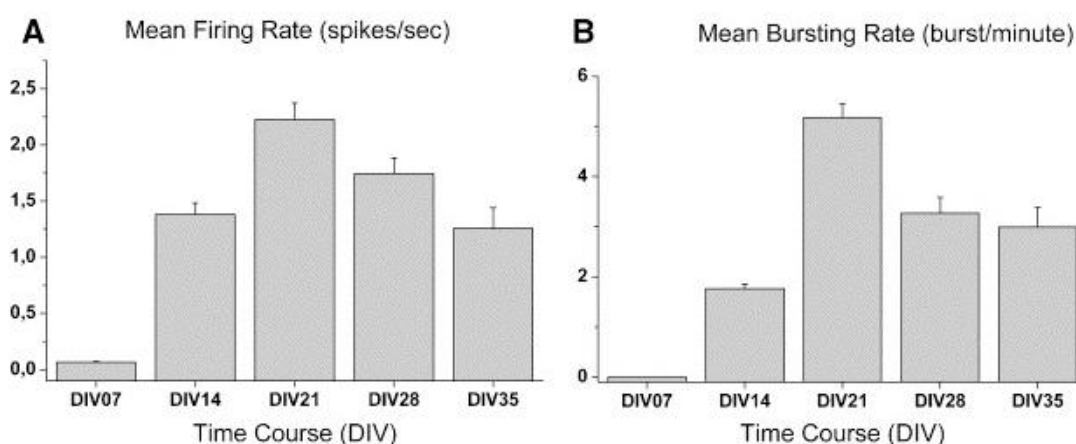


Figure 8. Changes in the spontaneous mean firing rate (MFR, spikes/s) and mean bursting rate (MBR, burst/min) during the five ages of the monitored cortical networks. (A) MFR averaged over all the recording electrodes from 10 cortical cultures at the considered developmental stages. (B) MBR averaged over all the bursting channels (i.e., channels presenting at least 2 bursts in a recording trial of 5 min) from 10 cortical cultures at the considered developmental stages. All the data are presented as mean + SEM. Reproduced from [10].

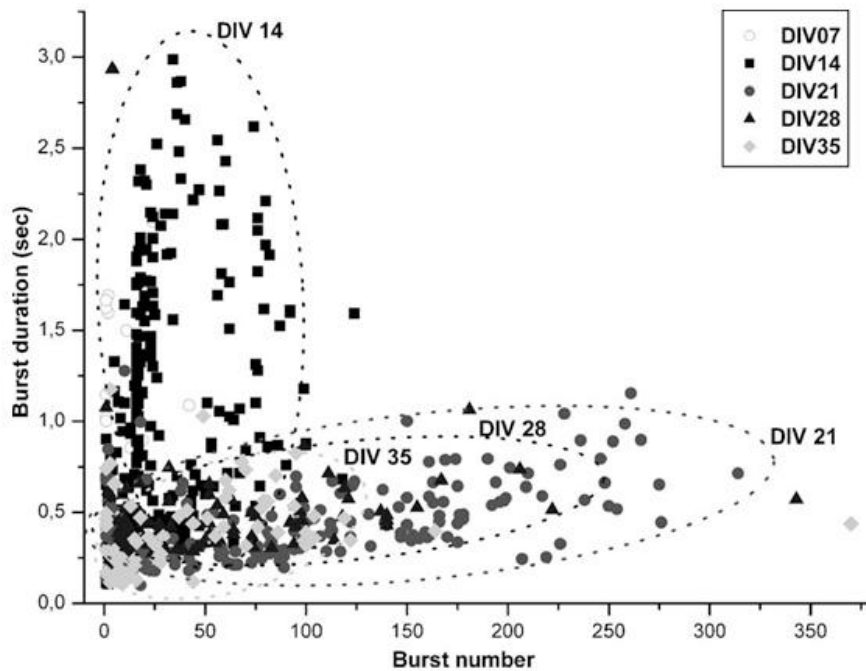


Figure 9. Burst duration and burst number at different ages. All the experiments are reported in the graph. Each point represents a bursting channel producing a certain number of bursts (horizontal axis) whose mean duration can be read on the vertical axis. It is worth noting the change of the network state between the second (14 DIV) and the third (21 DIV) week. The subsequent ages (28 DIV and 35 DIV) tend to group in a region that is the intersection between the two clusters at 14 and 21 DIV, possibly indicating a more stable condition. Reproduced from [10].

Wagenaar [50] investigated the development of high and low density cultures. For the MFR development results were similar to that of Chippalone et al. [10] but sparse cultures showed a more delayed development. A procedure was also created to analyze bursting. The burstiness index (BI) as defined by Wagenaar takes values of 0 (no bursts) up to 1. A value of 1 means that all spikes occurred in bursts. He found that although the MFR reaches a plateau and then decreases, the BI continues to increase even after the MFR decreases.

### 1.2.5 On high-resolution MEAs

The main problem of conventional MEAs is that they do not allow a one to one investigation of neural activity. The recorded activity is from a very small percentage of the population. Therefore, a detailed analysis in the investigation of pre-synaptic and post-synaptic patterns is not feasible. When analyzing plasticity between two spike trains, the pathways could be poly-synaptic and in the transition from mono to poly-synaptic pathways the properties of plasticity might be significantly altered. The low number of electrodes together with the high-density of cells necessary for recording can only yield insight in the overall activity of the network and not in relations between poly-synaptically connected cells.

One possible solution could be the patterning of the array with neurotrophic factors in order to direct neuron cell bodies to electrodes [8, 31-34, 44-45]. This way, large regions of neurotrophic factors can attract cell bodies, whereas narrow lines can direct process growth [51]. However, it was found [44] that with increasing cell density the cells tend to grow processes independent of the patterned surface and with lower density cultures the network is not active (Figure 10).

Another approach is the development of high-density MEAs, consisting of thousands of electrodes with electrode densities similar to densities of the culture. A 1 to 1 correspondence between electrodes and cells might then be achieved.

Berdondini, Imfeld et al. [52-53] have presented a high resolution system for data acquisition of electrophysiological recordings based on an active pixel sensor array (Figure 11). Main components of the platform are an integrated microelectrode array, low noise amplifiers and high-speed random addressing logic. The device's concept is based on image/video data capture methods implemented on hardware. 64 x 64 electrodes arranged as an array of pixel elements constitute the MEA. Electrode sizes are 20  $\mu\text{m}$  x 20  $\mu\text{m}$  and the electrode separation is 20  $\mu\text{m}$  while the total active array is 2.56 mm x 2.56 mm. The resulting electrode density is then 625 electrodes/ $\text{mm}^2$  [53].

Typical noise levels are quite high (11  $\mu\text{V}_{\text{RMS}}$ ) but signal to noise ratios of 5-10 have been accomplished [52]. Other drawbacks of the system include limited usage of each chip (4-5 experiments, 30 DIV for each experiment) and an increase in the number of non working electrodes after intensive use. Furthermore, no in-pixel stimulation capabilities exist, but rather only through dedicated electrodes.

Another approach from the same group includes locally dense microelectrode arrays (Figure 12) [54] in which 60 microelectrodes are arranged in four areas separated by 1.1 mm. Each area features 15 microelectrodes with 10  $\mu\text{m}$  inter-electrode spacing. Electrode diameters were 30 and 22  $\mu\text{m}$ . Finally, the ADC resolution was 12 bits and sampling frequencies ranged from 10 to 50 kHz/channel. Recordings showed that 60% of the electrodes pick up signal from one neuron. The other electrodes would pick up signals from two neurons with one being the dominant (90% of the events), allowing a very accurate mapping of electrodes to cells. Furthermore, with increasing sampling rate propagation of the spikes could be identified. Typical noise levels were 8.2  $\mu\text{V}$  (22  $\mu\text{m}$  electrode diameter) or 6.5  $\mu\text{V}$  (30  $\mu\text{m}$  electrode diameter). We must note here, that although the larger diameter electrode has lower noise levels, it is more prone to picking up signals from more than one source. The main disadvantage of this system is the limited active area. As illustrated in Figure 12 the area covered by electrodes is small compared to the area of the MEA.

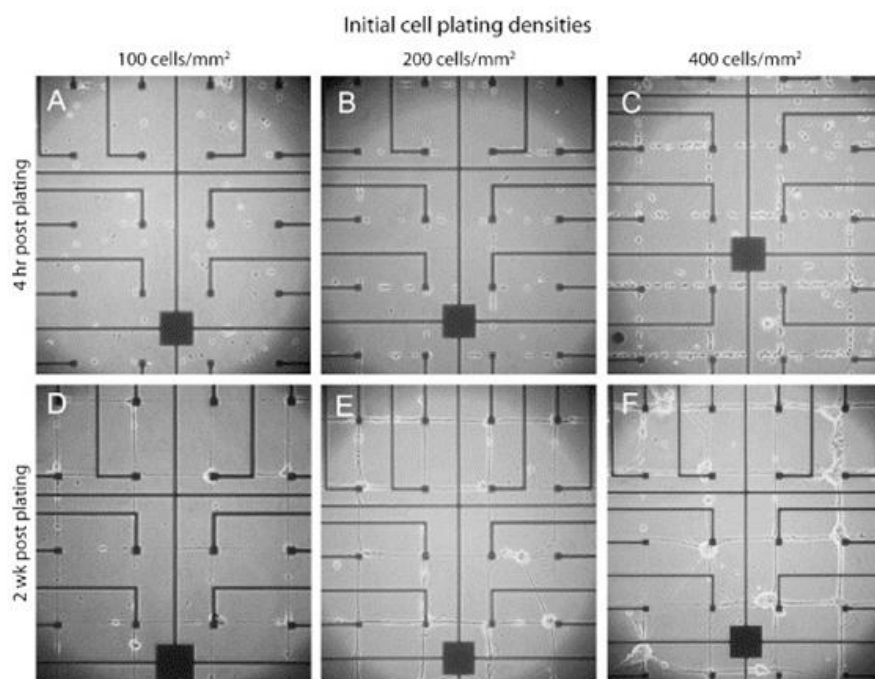


Figure 10. Phase micrographs of live neurons growing as networks on patterned poly-l-lysine MEAs. Cells were plated at initial seeding densities of 100, 200, and 400 cells/mm<sup>2</sup>. Images are presented illustrating cultures at 4 h and 2 weeks after plating. The big black box is the ground of the system. Small, rectangular boxes represent places for cell bodies while the black lines aim in directing process growth. Notice that with increasing plating density neurons tend to escape from the patterning scheme. Reproduced from [44].

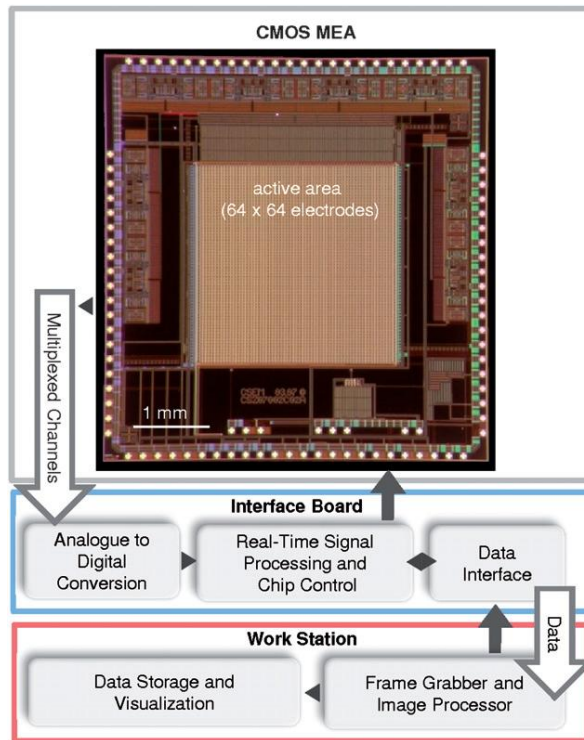


Figure 11. Overview of the high resolution electrophysiological platform. The system is composed of three hardware levels, i.e. the CMOS–MEA chip, the interface board and a work station equipped with a frame grabber for capturing and storing the video stream. Taken from [52].

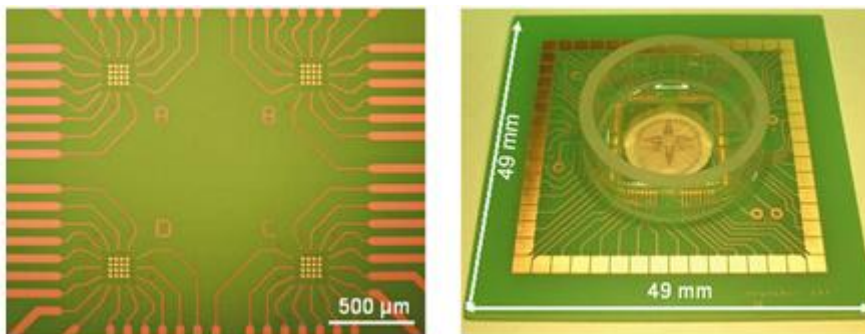


Figure 12. View of a locally dense microelectrode array. Reproduced from [54].

### 1.3 The ETH 11000 electrode, CMOS system

Typical MEA system designs contain the electrode array separated from the signal conditioning electronics [55-57]. Each electrode requires a connection to the external electronics, limiting the array size. Furthermore, the signal should be conditioned as close as possible to its source to prevent noisy data. The requirements of high signal-to-noise ratio and a large number of electrodes seem difficult to be accomplished together. This stems from the fact that for high density MEAs the available space for each electrode and its accompanying electronics is limited. However, the smaller the size of electronics the higher the thermal noise.

The end result is that when using high-density MEAs noise levels are quite high, making difficult the extraction of electrophysiological signals [58].

The majority of commercial MEAS currently in production are termed passive. This means that no active elements (amplifiers, multiplexers) are integrated on chip. Each electrode requires an external connection to filters and amplifiers. This approach poses a limit on the maximum number of electrodes on the substrate, since each electrode requires a connection to external electronic circuitry. Furthermore, the signal is not amplified close to its source. In the pathway from the electrode to the amplifier, cross-talk may occur which hampers the signal to noise ratio (SNR).

The Bio-engineering laboratory of ETH (Swiss Federal Institute of Technology, Zurich), headed by Prof. Andreas Hierlemann conducts research on developing microelectronics-based tools for solving problems in biology. Recently they have developed a switch-matrix based high-density microelectrode array in CMOS technology suitable for physiological recordings [59]. The device has been sent to several collaborating groups for debugging, including:

- Laboratory for systems biology, RIKEN, Japan
- University of Freiburg, IMTEK, Germany.
- University of Bern, Switzerland.
- Twente university, the Netherlands.

In the BSS group, people working on the theme of Neurotechnology, lead by prof. Wim Rutten have therefore access to the high-density chips for physiological recordings. The system consists of a microelectrode array of 11011 electrodes, 126 of which can be arbitrarily selected using reconfigurable electrode-readout-channel mapping. The front-end circuitry is then placed outside the array itself, allowing sufficient space for low-noise circuitry and providing high-density of electrodes. Electrode diameter is 7  $\mu\text{m}$ , electrode pitch 18  $\mu\text{m}$  and electrodes have also the ability of stimulation. Noise levels are low (3.9  $\mu\text{V}_{\text{RMS}}$ , 1 Hz to 100 kHz, bare Pt-electrodes) and electrode density is 3150 electrodes/ $\text{mm}^2$ . The increased electrode density allows plating of low density cultures (cells/ $\text{mm}^2$ ) while the low noise levels allow recording of low-amplitude spikes.

Two main advantages of using integrated circuit or CMOS technology include connectivity and signal quality [4, 59]. Using on-chip multiplexing architectures allows the use of a large number of electrodes. When the signal is conditioned close to the electrode the SNR increases, allowing better observation of weak physiological signals such as extracellular spikes.

A disadvantage of such IC chips is that silicon is not transparent to light, which makes the observation of cells through a light microscope impossible. Furthermore, the

chip must be protected from the bath medium used to culture the cells and the culture must be protected from toxic substances used in the chip. For example, CMOS metal aluminum dissolves in saline solution [4]. However, deposition of platinum makes the electrodes biocompatible.

## 1.4 Formulation of research questions

Cultured neuronal networks on MEAs provide a useful platform to study cognitive processes like learning and memory. Essential in such research is the ability to estimate network connectivity. Most tools to estimate functional connectivity are based on the analysis of activity patterns, and there are indications that such estimated functional connectivity provides information about physiologic, synaptic connections. However, a thorough validation is hampered by the fact that it is not possible to visually trace axons on the chip due to the high density of seeded cells. This high density is necessary because at lower cell densities the probability that one of the 60 electrodes record activity falls significantly. This means that due to the undersampling of the culture's activity with the 60 electrodes, the culture may be active but no electrode would be close to a cell to record its activity.

Recently, we obtained the switch-matrix based, high-density microelectrode array device designed by ETH, Zurich, for use in our group [59]. The high density of the electrodes allows us to record activity even from low-density cultures, with the appropriate electrode selection. So, a first challenge is the development of an efficient way to select the 126 electrodes to record from. Then, activity analysis and the culture's development will be investigated. To sum up, basic research questions include:

- How can we efficiently find the most suitable electrodes to record from?
- How stable is the recorded activity from this set of electrodes?
- What are the differences in spontaneous firing patterns in high and low density cultures?
- What is the minimum network size/density that we can record activity from?
- How representative is a set of electrodes?

## 2. Methods and materials

### 2.1 Hardware

#### 2.1.1 System Description

In this section the system's electronic components will be described. A block diagram of the whole system is shown in Figure 13. The chips are plugged in the chip-support board, called the Neurolizer, which provides all necessary clock and digital control signals together with the required analog references to the chips. Data are serialized on the board and sent through a serial connection (LVDS protocol) to an FPGA board. The FPGA runs Linux operating system, performs CRC checks of the chips, separates data streams from different chips and finally, transmits the data to the PC used for data analysis, visualization and storage. The PC runs a server application, named the server, which can be accessed from several clients requesting data or sending commands. The server contains emulators of the chips. When a command is sent to a chip the same command is applied on the emulator of the appropriate chip. The client can then request from the server information about the chip routing, gain and filter settings etc. through a TCP/IP connection.

Figure 14 shows the system's data flow. The FPGA board sends the received data first to the server. The server contains a buffer of 25seconds. This value can be changed in the *defines.h* file located at:

```
cmosmea_external/ntk_tools/trunk/resources/defines.h
```

The client(s) can then request data from the server, specifying the amount of data (10, 20, 100 ms) and the interval between successive requests. If there are not enough data, the client has to wait before receiving the data package. If the client reads data too slow, the buffer will fill and the client will lose data. The color of the buffer will then change to red. More than two clients can request data from the same plug, there is no "interference" between the two. Finally, the client can request data in two modes, *stream* or *live*. In the *stream* mode, the server keeps track of the position of the latest data and sends the next package according to that index. In the *live* mode the server always sends the newest data.

When a command is sent, if it is successfully executed it will then proceed to the server's emulator. It is also important to note that when a command is sent there is no accurate timing; it depends on the computer load, speed and SNR of the transmission pathways (Ethernet) among other conditions.

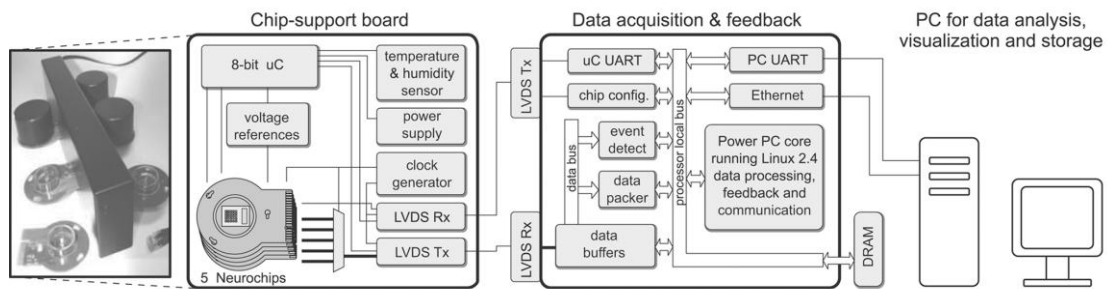


Figure 13. Block diagram of the system. A photograph of the support board with plugged in chips is shown on the left. Taken from [59].

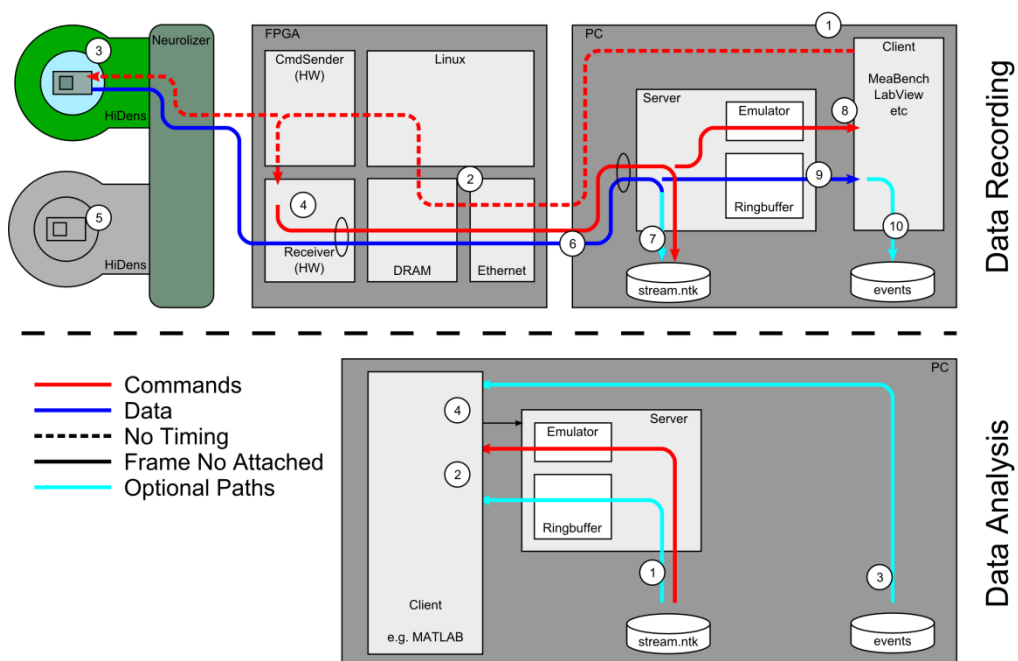


Figure 14. System data flow. Commands follow a different path than data. Notice that there is no accurate timing in a command execution. Data can be saved directly from the server (which can also attach commands in the recorded file) or by the client (e.g. Labview, which only see the data and not the commands). The client can select which chip to read from through the server or the client (which communicates with the server). Taken from [60].

### 2.1.2 Chip description

The chip is mounted on a custom-made printed circuit board (PCB) with an electroplated nickel/gold edge-connector. A glass ring is glued on the PCB and a water-resistant epoxy is used to encapsulate the bond wires and pads. The packaged device is shown in Figure 15 and a micrograph of it in Figure 16. The 126 channels and the associated signal amplification and stimulation circuitry are outside the reconfigurable electrode array.

There are three signal conditioning stages on the chip. The first two stages include signal amplification and filtering, whereas the third only includes amplification. The first stage includes a high pass filter, a low pass filter and an amplification of 30 dB. The second stage includes a low pass filter, an additional gain of 0, 20, 30 dB and a DC-Offset compensation scheme. Chip settings (gain, cut-off frequencies) are all set to the same values for all channels. After the second stage, eight channels are multiplexed and amplified at 0, 6, 14 or 20 dB and finally, digitized with an 8-bit ADC. The recording controller then transfers the data off-chip. The command decoder is responsible for commands of array configuration, gain and filter settings. Finally, 2 10-bit DACs provide stimulation capabilities.

Figure 18 shows the schematic of the three signal conditioning stages. The gain of the first stage is defined by the capacitance ratio  $C1/C2$  and is 30 dB. The LPF cut-off frequency can be selected to 15 or 50 kHz. The default HPF cut – off is below 1 Hz. A switch provides a complete bypass of the first stage to test features in DC.

The second amplification stage is a non inverting amplifier implemented as a two stage Miller compensated opamp. Switching between different resistors  $R_1$ ,  $R_2$ ,  $R_3$ , adjusts the gain selection. The LPF cut-off frequency can be adjusted to 5 or 16 kHz. The DC-offset compensation scheme can remove DC signals of up to 55 mV in steps of 5 mV.

After the 3d stage data are transferred to the digital part of the chips. The 16 ADCs run at a clock speed of 3.2 MHz and need 10 clock cycles for one 8-bit conversion. One frame of output consists of 160 bytes, 128 of which are used for data and the rest for status information about the device (gain, filter settings etc...). The chip address, the frame counter and the command counter are also inserted. A command is only executed if there are no CRC errors and if the chip address is correct. After a successful command execution the command counter increases. Commands are used to change the amplification factor and adjust DC-Offset compensation.

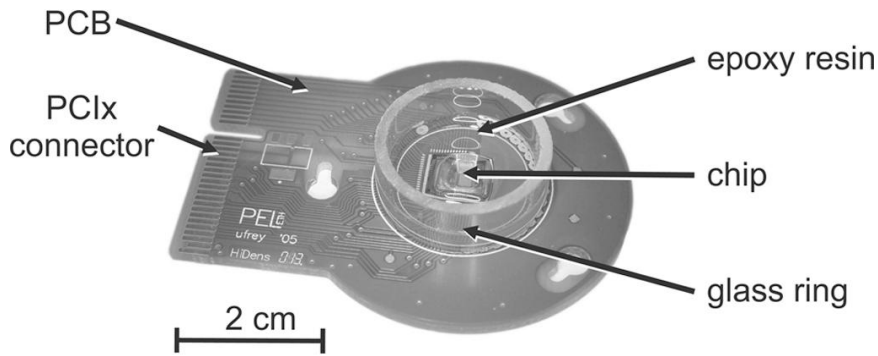


Figure 15. Packaged device. Taken from [59].

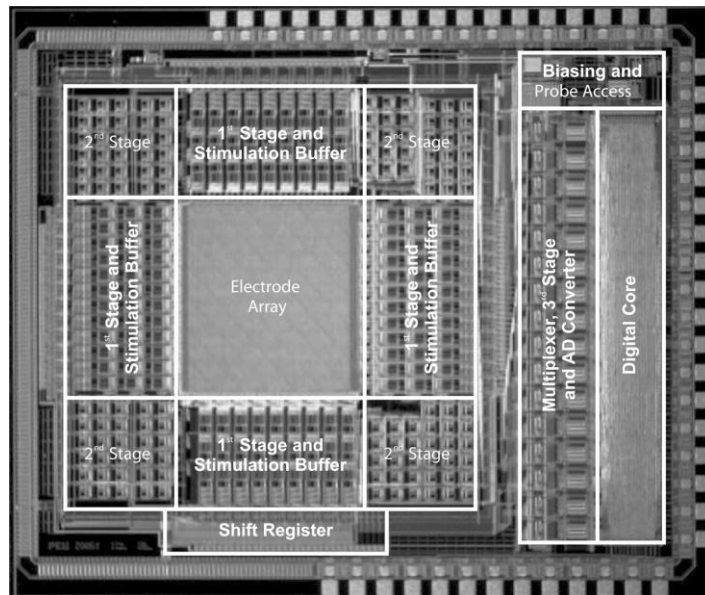


Figure 16. Micrograph of the fabricated device. The size of the chip is  $7.5 \times 6.1 \text{ mm}^2$ , the size of the electrode array is  $2 \times 1.75 \text{ mm}^2$ . Taken from [59].

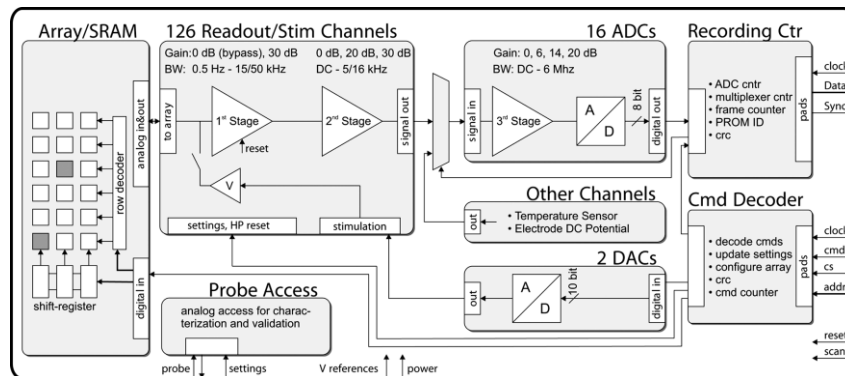


Figure 17. Block diagram of the chip architecture and the on-chip electronics. Taken from [59].

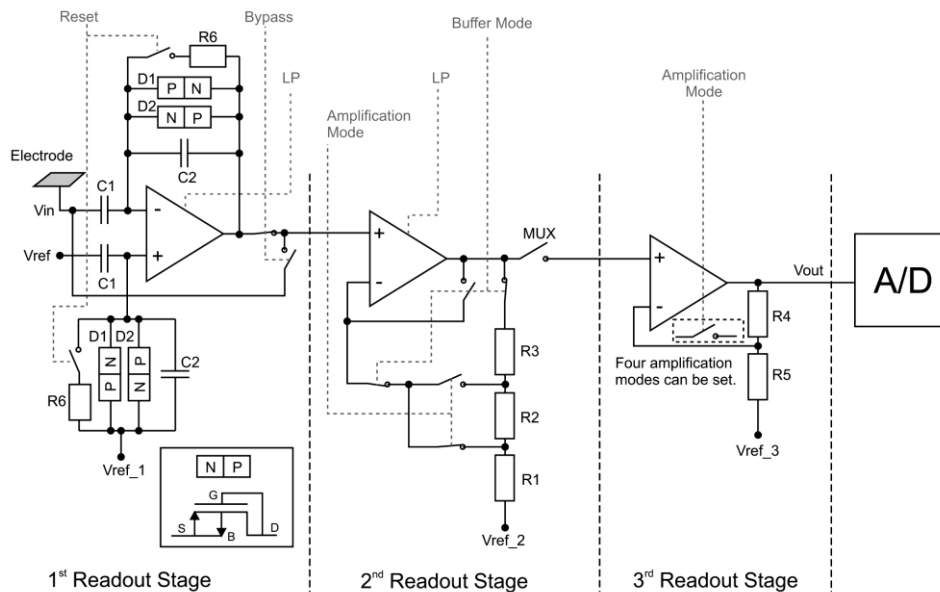


Figure 18. Amplification stages of the readout channels with the first stage featuring a low HPF cut-off frequency. Taken from [59].

### 2.1.3 Electrode array and configuration

The flexibility of the system is provided by an analog switch matrix implemented underneath the microelectrode array. Its general form is shown in Figure 19. Electrodes are connected to channels through vertical and horizontal wires. The reconfigurable switches control the connections of the wires. Each channel can be connected to any electrode but there are some limitations. Firstly, in Figure 19 it is shown that for the electrodes belonging to the same row, the seventh electrode uses the same transfer line (horizontal wire) as the first one. Or to put it differently, every sixth electrode occupies the same transfer line. This has two implications:

1. A maximum number of six consecutive electrodes in a row can be used.
2. When electrode<sub>n</sub> is used, electrode<sub>n+k\*6</sub> from the same row cannot be used (k = -2, -1... 1, 2...).

This poses some limitations in the final array but due to the large number of electrodes they can be overcome. Limitations also apply for the vertical wires.

According to the designers of the set-up, the largest block of electrodes possible is a 6x17 rectangular configuration.

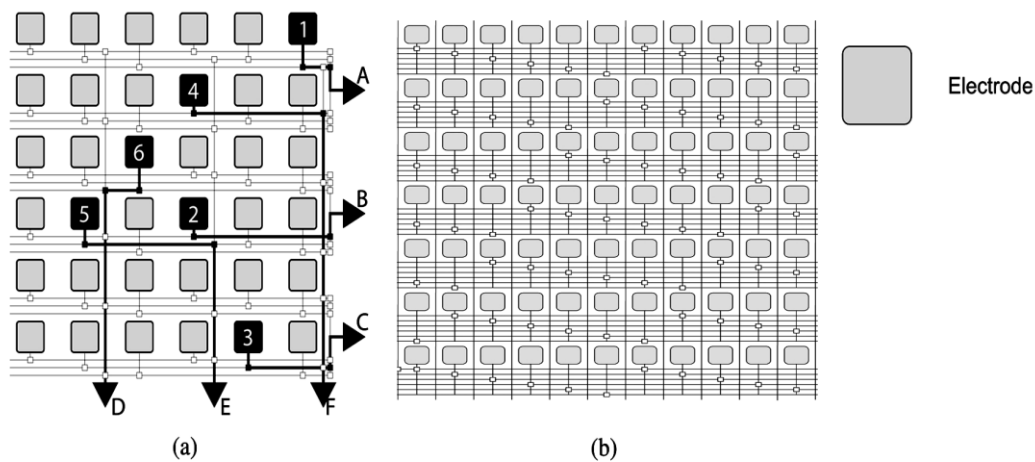


Figure 19. Illustration of the switch matrix reconfigurable array. The selected electrodes (1-6) are being routed to the output channels (A-F). Taken from [59].

The final configuration is controlled by specialized software (NeuroDishRouter) which solves the routing problem. Another software (BitStreamer) creates the command file that can be sent to change the configuration. Possible configurations are blocks of electrodes, random electrodes or single spots. NeuroDishRouter can also create a sequence of files to scan the whole array.

## 2.2 Culture preparation and maintenance

Active and healthy cultures are the most basic materials for our experiments. Newborn Wistar rats were decapitated and cortical neurons were obtained and cultured within a circular chamber on the CMOS chip. For high density cultures the seeding concentration was 3 million cells/ml. A drop of 30  $\mu\text{l}$  was then applied on the array chamber, resulting in an initial plating density of 2500 cells/ $\text{mm}^2$ . The culture chamber was filled with 600  $\mu\text{l}$  serum-free medium [40]. Cultures were stored in an incubator, under standard conditions of 37 $^{\circ}$  C, 100% humidity and 5% CO $_2$  in air.

In the incubator the cultures' surrounding air is in contact with the incubator's environment, allowing the exchange of gases. The cultures are not visually inspected in their various development stages due to the non-transparent nature of silicon. The medium was refreshed three times a week in each culture. Approximately half of the medium is taken out and slightly more is added (because of medium evaporation).

## 2.3 Experimental procedures

After a medium change, the cultures were left in the incubator for 3 hours before any experiment took place. Measurements took place inside a dry incubator. Each culture was covered with a film allowing gas but not water exchange to protect it from bacteria and infections. The incubator was dry so that there was no risk for the electronics. However, medium evaporation takes place and it was found that when leaving a culture for 2 days with the lid not properly sealed the entire medium evaporates and the culture dies.

### 2.3.1 Verifying hardware's and software's integrity with physiological saline

The first phase of the experiments was to verify the suitability of the hardware and newly-developed software for performing the experiments. The chips were filled with 600  $\mu$ l of saline and signals were recorded for 50 minutes. In the duration of the experiments, gain, electrode configurations and other settings were changed in order to verify their correct operation. Typical noise levels were also registered. Only connected electrodes were taken into account. Temperature was recorded in order to set the externally controlled temperature (incubator) to appropriate levels. The maximum temperature of the chips should not exceed 37 °C. The temperature was recorded with two conditions. In the first case, the incubator's temperature was set to 34.7°C and in the second case to 33°C. A sensor was attached underneath the MEAs to record their temperature for 50 minutes (see appendix for the experimental set-ups). This duration seemed appropriate for the experiments of this project. No long recordings took place so a temperature recording of hours or days was deemed unnecessary.

For verifying the integrity of our newly-developed software we used sample data from the University of Kaiserslautern and compared results from our software to the results of the hidens toolkit. Spike shapes and raster plots were produced to get an idea of the signals obtained.

### 2.3.2 Trial experiments with active and silenced cultures

Following verification of the experimental set-up, recordings were made in order to analyze the activity and development of high- density cultures. Recordings were made with a random electrode configuration to assess culture's properties and electrode activity and stability of the set. The cultures' activity was then analyzed for different DIV assessing their activity patterns. Data from these experiments were used to analyze the activity of cultures, the stability of electrodes, the performance of the electrode selection algorithm, spike shapes and burst profiles. As a final step,

magnesium was added in the medium in order to verify that identified events are actually cell extracellular potentials and not artifacts. Magnesium is known to stop all spontaneous activity of the culture. If the activity recorded in the baseline phase was indeed from spontaneous activity of the network and not artifacts, then the identified activity in the magnesium phases should be minimum.

Magnesium sulfate was used with a molecular weight of 95.22 gr. For adding 1mM of magnesium to 600  $\mu$ l of medium we need 57  $\mu$ gr of the substance. MgSo was diluted in physiological saline (57 mgr in 1 ml) and then 1  $\mu$ l of that substance was added to the 600  $\mu$ l of serum-free medium. The amount added is insignificant compared to the total amount in the culture and should not alter the activity of the network.

A baseline recording took place, followed by addition of 1  $\mu$ l of plain, R12 medium to check for protocol effects (adding 1  $\mu$ l of a substance, control phase). Then, 1  $\mu$ l of MgSo was added for the Mg phase. The Mg-filled medium was then washed out twice and replaced by 600  $\mu$ l of medium for the washout phase. The duration of the recordings was 20 minutes and the first 5 minutes of each phase were ignored because handling of the cultures was shown to affect their activity, mostly in the first 5 minutes [50]

## 2.4 Algorithms and techniques

### 2.4.1 Electrode selection overview

The electrode selection algorithm should be able to find a local/global set of electrodes that will allow us to record high quality signals. By quality of the signals we mean low noise levels, large spike amplitude and high enough firing rates. With high density cultures selection of such an electrode set should not be difficult, but with lower densities a more thorough search through the search space should be done.

As a first step, a “brute-force” attack was used for this search. This method evaluates all possible sets of solutions to find the best one. Therefore, all electrodes were used in some sample recordings and their suitability was evaluated. This procedure is termed “Scanning algorithm”.

#### 2.4.1.1 Scanning algorithm and electrode evaluation

This procedure scans all electrodes of the array in sequential blocks, generated by NeuroDishRouter. The scanning procedure includes the following steps:

- Select configuration
- Send configuration to the server
- Record with online spike detection algorithm
- Repeat for all configurations

Each configuration needs 1 minute in total. Specific command files for each configuration were created. After sending the configuration and before spikes are accepted, the DC-Offset compensation scheme is applied. This scheme is already implemented in the Lab view hidens toolkit. Its automatic application after a configuration change was implemented for the needs of this project. Furthermore, noise values need to be re-established, so the first 10 seconds of a new configuration are ignored. This amount of time seemed satisfactory based on our observations. Noise levels need 3-4 seconds to stabilize, so a value of 10 seconds is more than enough. The detailed procedure is explained in the following section.

The output file is an events-file containing information about the events. It is then loaded into Matlab which produces the final configuration of the electrodes after their evaluation. Electrodes are evaluated based on certain thresholds:

- The Mean Firing Rate (MFR) should be above a minimum value.
- The average noise levels should be below a maximum value.
- The number of points above threshold levels should be above a maximum value.
- The spike's amplitude should be above a minimum value.

#### 2.4.2 Online spike-detection algorithm

The online spike-detection algorithm is threshold based. The RMS noise value for each electrode is calculated and when the threshold (5.5 times the noise levels) is passed (negative only) an event is identified and recorded. The threshold value is adjustable. However, three more constraints were added to improve efficiency.

##### 1. Saturated electrodes

Each electrode can have DC potential fluctuations, also called drift. The DC offset compensation scheme is applied in the second stage of the amplifiers, so if the first stage is saturated, the DC offset compensation scheme will not solve the problem.

When an electrode is saturated, the noise is extremely low and because of that, spikes can be wrongly identified when the signal's value crosses the threshold (which depends on the noise levels). The false positive rate then is extremely high for that electrode. In the Hidens matlab toolbox when such a signal is observed it is ignored. For the purposes of the online spike detection algorithm a constraint was added. If the noise of the electrode is too low, spikes are not identified in that electrode. The electrode should have a minimum noise level. The value of this parameter can be changed in the settings tab of the software and values used were up to 8  $\mu$ Vs.

## 2. Idle time after a configuration change (DC-Offset)

When changing configurations it is important to automatically apply a DC-offset compensation after some time due to the fact that each electrode has a different DC value. This functionality has been implemented in the software and affects the online spike-detection algorithm. When such a compensation is applied, due to the sudden change in the recorded values, spikes would be wrongly identified. Therefore, spikes are ignored after application of the DC offset compensation in the scanning algorithm for 5 seconds. Channels are compensated in parallel. Each configuration change need 5 seconds for all channels, not for each. A boolean control was implemented (when the value of this boolean control is false, spikes are not identified) and for 5 seconds after the configuration change, spikes are ignored to allow sufficient time for the change to take place.

## 3. Idle time before DC-offset compensation

For the electrode selection algorithm, or when manually changing configurations, one recording is made in which all electrodes are used by using sequence recordings. When a configuration is changed, data should be ignored for some time after the change, allowing the noise levels to stabilize for the given new configuration, like in constraint 2. Otherwise, spikes will be wrongly identified during the transition from one configuration to the other. A boolean control was implemented (when the value of this Boolean control is false, spikes are not identified) and for 5 seconds after the configuration change, spikes are ignored to allow sufficient time for the noise levels to be estimated. After these 5 seconds, the automatic DC-Offset compensation scheme takes place so the total idle duration is 10 seconds.

The output of the detection algorithm is a file containing information regarding:

- Time of the event
- Electrode (not channel) recording the event
- Waveform (6 msecs, in  $\mu$ Vs)
- Noise Levels during the event

## 2.5 Data analysis

For data analysis we used mean firing rates (MFR), mean bursting rates (MBR), raster plots and other graphs illustrating the activity development of the cultures. The MFR and MBR are defined as the number of events and bursts per minute respectively. A burst is defined as a collective, sudden increase in the activity of the network. All spike trains were divided into time segments of 2.5 minutes. Calculations for the firing rates at a specific DIV include the average and std of these time segments. This approach has been followed for a single reason. The activity of the network might not be stationary; By averaging (using appropriate time-segments) a better indication of the firing rates is obtained. Furthermore, the MFR (and MBR accordingly) might change and by re-calculating the burst threshold according to the MFR in each time segment the accuracy of the burst identification (explained later in this section) is improved.

Raster plots indicate the firing patterns of the network. One can visually discriminate if the culture exhibits bursts or not. A disadvantage of this method is that one can only observe a finite amount of time. Usually this interval is approximately 1-5 minutes. With higher intervals details on the exact timing of spikes are lost. Together with raster plots the binned number of events is illustrated for easy visualization of the activity pattern. The bin size was set to 30 ms, a value small enough to yield detailed description of the activity fluctuation and an easy to visualize plot.

Individual electrode activity was analyzed for all cultures. The MFR of individual electrodes was calculated and data sets were later interpolated (cubic spline interpolation) and averaged to give one average for all cultures and electrodes. The stability of the electrode set can be evaluated by observing the number of electrodes that appear or disappear from one experiment to the next. As a final step we calculated the number of active electrodes in each experiment for all cultures. An electrode was considered active if it showed more than two spikes per minute and the number of active electrodes is plotted for each culture and DIV.

Finally, during the cultures' development the properties of spike shapes and burst profiles are shown. The spike shapes were clustered according to two properties:

- Peak to peak amplitude (Vpp)

- Peak balance (PB)

The peak balance is an indication of the spike shape and it allows discrimination between different spike shapes. It is the difference of the areas of the two positive phases of the spikes, before and after the negative phase respectively. Almost all burst shapes are shown in order to see their amplitude, duration and general shape.

The number of events per bin is also counted and bursts are identified by an automatic procedure, previously used in [61]. The threshold for burst detection has been set to 9.5 times the average MFR of the time segment analyzed. This value was carefully selected after evaluation, see appendix for the details. When a burst was found its profile was calculated for 0.5 seconds before and 0.5 seconds after its center (center defined as the peak of the amplitude). Threshold crossings were treated in order of size and overlap between profiles was prevented by setting all the bins around the detected burst to 0 (duration 2 seconds) after the calculation of the burst profile. The value of 0.5 seconds proved adequate to capture the burst profiles and the duration of 2 seconds was deemed low enough so as not to erase nearby bursts since inter-burst intervals are in the order of 10ths of seconds [10]. After obtaining the burst's profile we calculated the number of events in it. The width of the burst was calculated as the distance between the 10% points before and after its peak. The number of events in this segment was then counted. The number of events in bursts divided by the total number of events in each segment give the Burst/dispersed ratio. This is an indication of how many spikes are in and out of bursts. A value of 100 % means that all spikes occurred in bursts.

Different sets of electrode configurations were compared in order to analyze the effects of different configurations on the activity recorded. Recordings with different configurations include comparison among three random and block configurations. Finally, a scan of the whole array was performed to find suitable recording electrodes. To answer the question of which one is the limiting factor in choosing an appropriate set of electrodes, colormaps of active electrodes were produced for their MFR, average spike amplitude and average noise levels. Different sets of electrode configurations were then compared to the optimum one. This optimum set is a subset of the suitable electrodes found. More specifically, a random configuration, a block configuration, a conventional configuration (rectangular array of electrodes) and the best configuration are compared to each other. The conventional configuration is one similar, but obviously not the same as in conventional MEAs, due to electrode routing limitations, size and pitch.

## 3. Results

### 3.1 Verification of experimental set-up

#### 3.1.1 Saline experiments

As a first part of the project, the incubator's appropriate temperature was investigated and noise levels were established. The maximum temperature for a culture is defined around 37°C. From the two experiments conducted (with incubator settings for the external temperature: 34.7°C and 33°C ) it can be seen that when the external temperature is set to 33°C, the temperature of the culture stays below 37°C for almost one hour after starting the experiment (Figure 20). Therefore, in all subsequent experiments the external temperature used was 33°C.

Figure 21 shows noise levels for the three experiments during which the external temperature was set to 33°C. Saline experiments conducted on three chips. Noise values from all channels were recorded. Three basic categories can be distinguished, extremely low noise channels (saturated channels, less than 3  $\mu\text{V}_{\text{RMS}}$ ) and two other separated distributions. The left one is composed of unconnected channels (6 – 9  $\mu\text{V}_{\text{RMS}}$ ) and the second from connected channels (10 – 16  $\mu\text{V}_{\text{RMS}}$ ).

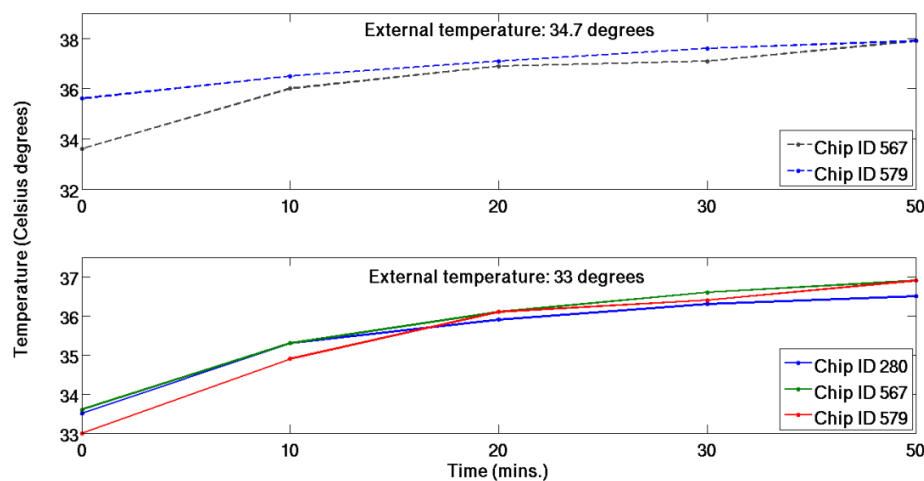


Figure 20. Temperature was recorded 0, 10, 20, 30 and 50 minutes after starting the operation of the device (server receiving data). See appendix for screenshots of the experimental set-ups.

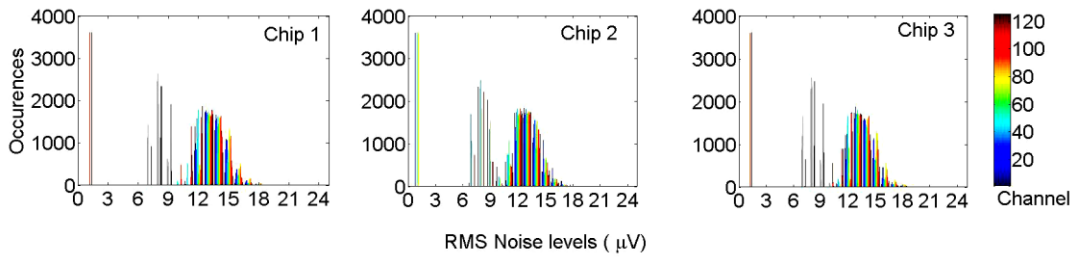


Figure 21. RMS Noise levels during saline experiments. Saline experiments conducted on three chips. Noise values from all channels were recorded. Three basic categories can be distinguished, extremely low noise channels (saturated channels, less than  $3 \mu V_{RMS}$ ) and two other separated distributions. The left one is composed of unconnected channels ( $6 - 9 \mu V_{RMS}$ ) and the second from connected channels  $10 - 16 \mu V_{RMS}$ .

### 3.1.2 First spike shapes and ISI Histograms

First spike shapes observed with active cultures are shown in Figure 22a. Spike shapes are clearly distinguishable from background noise. All histograms of each culture (all data used for analysis) were summed up and the results are presented in Figure 22b. It is obvious that there almost 0 spikes with ISI of less than 1 msec. furthermore, a peak is observed in all cultures at 40 – 50 ms.

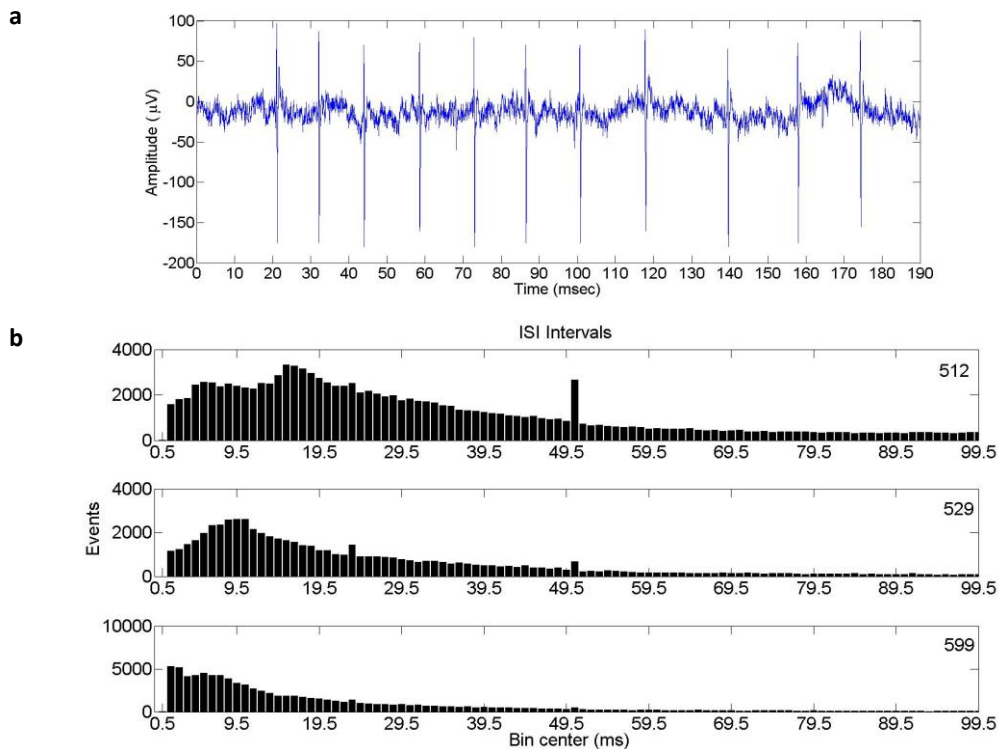


Figure 22. (a) Illustration of recorded spike shapes. (b) Interspike intervals for all experiments and all cultures. All I.S.I. were summed up, producing these final figures. The first bin, with bin center of 0.5 includes values of 0 to 1 msec.

## 3.2 Dynamics in developing high density networks

### 3.2.1 Basic electrode configuration and raster plots

The random electrode configuration used for the experiments is illustrated in Figure 23. Raster plots of the three cultures showed transitions among different patterns of activity as the culture matures. Raster plots of the development of culture 599 are illustrated in Figure 24 (10-19 DIV) and Figure 25. (21 – 28 DIV). Below each raster plot the number of events in each bin is shown (bin width = 30 ms). Bursts are shown in these plots with an asterisk situated on the center of each burst. Both uncorrelated firing and bursts were observed during the culture's development. More specifically, an increased number of bursts was observed in 10 DIV (Figure 24a), and in 25 and 28 DIV (Figure 25b-c). Small and large fluctuations of the spontaneous activity are observed even when the bursting frequency is low (Figure 25a) with the strongest fluctuations identified as bursts. A clear transition can be seen from 10 to 11 DIV (Figure 24a,b) from bursting (extremely low or high number of events per bin) at 10 DIV to a more stable firing pattern at 11 DIV. Raster plots for the other cultures can be found in the appendix.

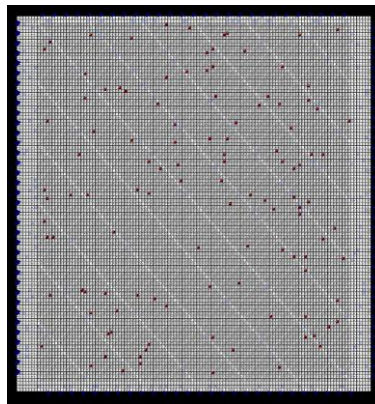


Figure 23. Random electrode configuration used for activity analysis of the three cultures. This configuration was used in all experiments and all cultures, unless written otherwise. The size of the array is 2.0 x 1.75 mm<sup>2</sup>.

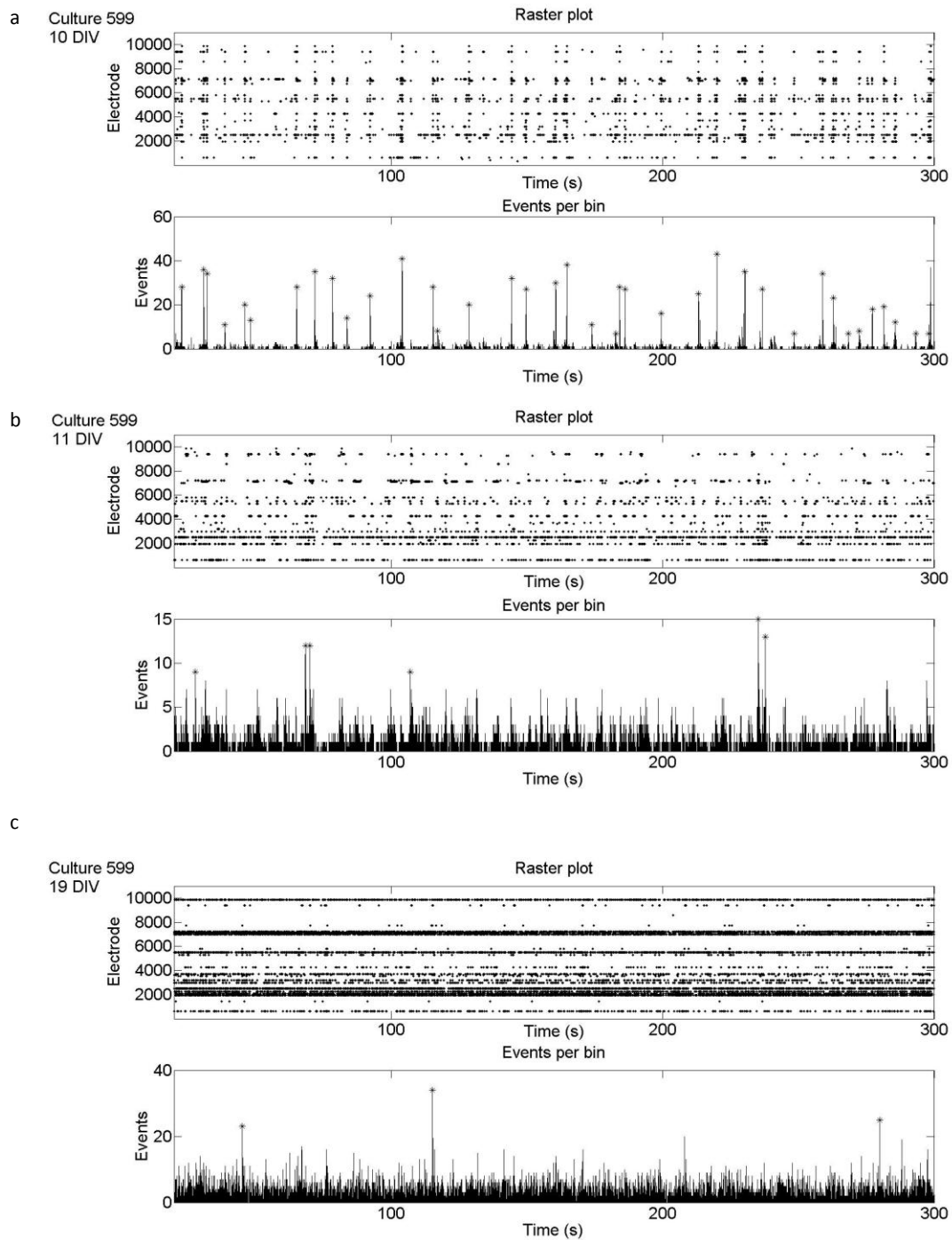


Figure 24. Raster plots of culture 599 at an early stage of development (10 – 19 DIV, a-c). On the top, a raster plot of 5 minutes is shown. The bottom plot indicates the number of events in each bin (bin size is 30ms). Spike trains were divided in segments of 2.5 minutes. For each segment, the bursting threshold was set to 9.5 times the mean firing rate for the specific segment.

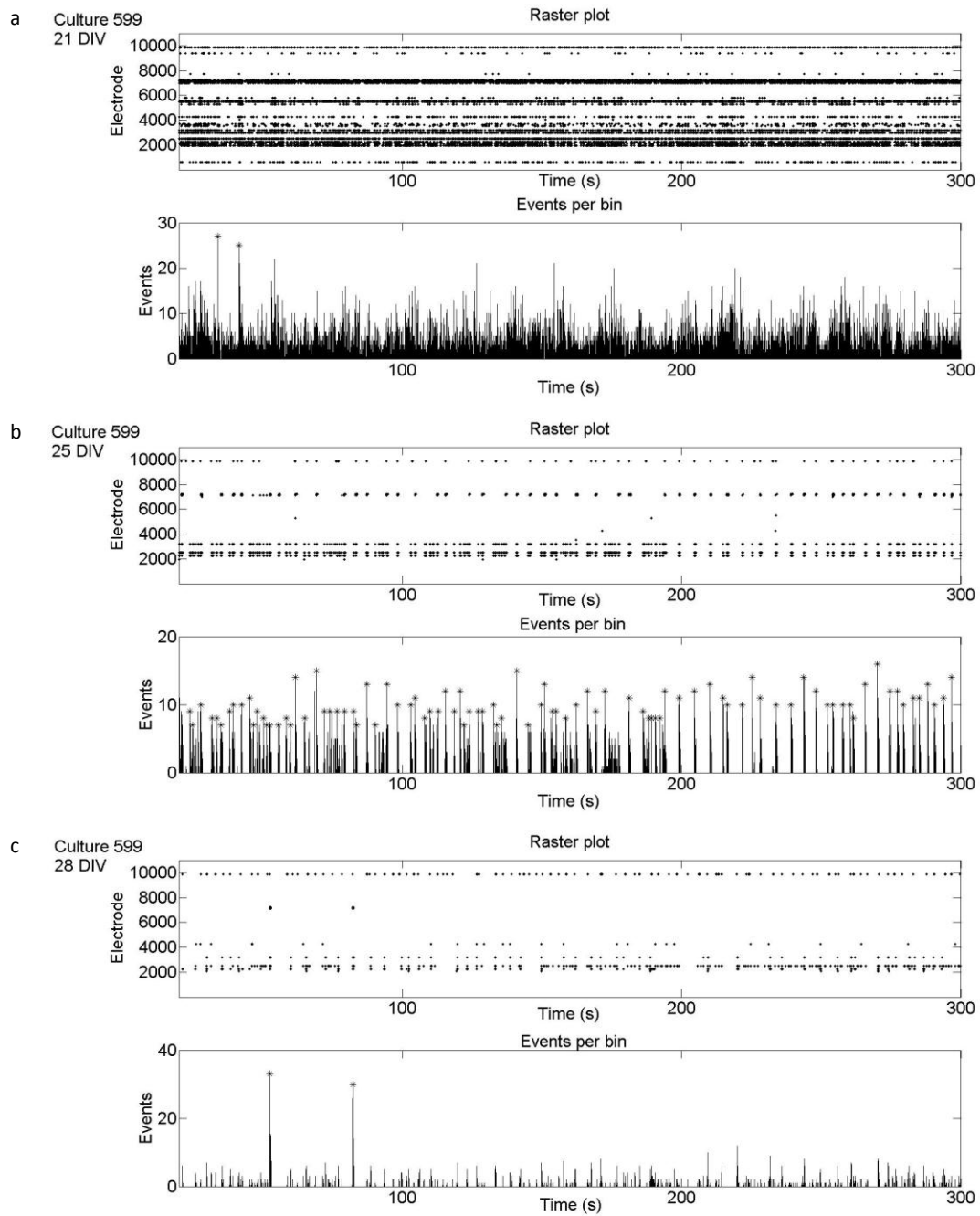


Figure 25. Raster plots of culture 599 at a mature stage of development (21 – 28 DIV, a-c). On the top, a raster plot of 5 minutes is shown. The bottom plot indicates the number of events in each bin (bin size is 30ms). Spike trains were divided in segments of 2.5 minutes. For each segment, the bursting threshold was set to 9.5 times the mean firing rate for the specific segment.

Zoomed plots displaying in detail the uncorrelated firing and bursts are shown in Figure 26. Activity preceding bursts could be either zero (figure 26b) or non-zero (Figure 26a). During uncorrelated firing, fluctuations in the activity have been observed (Figure 26c).

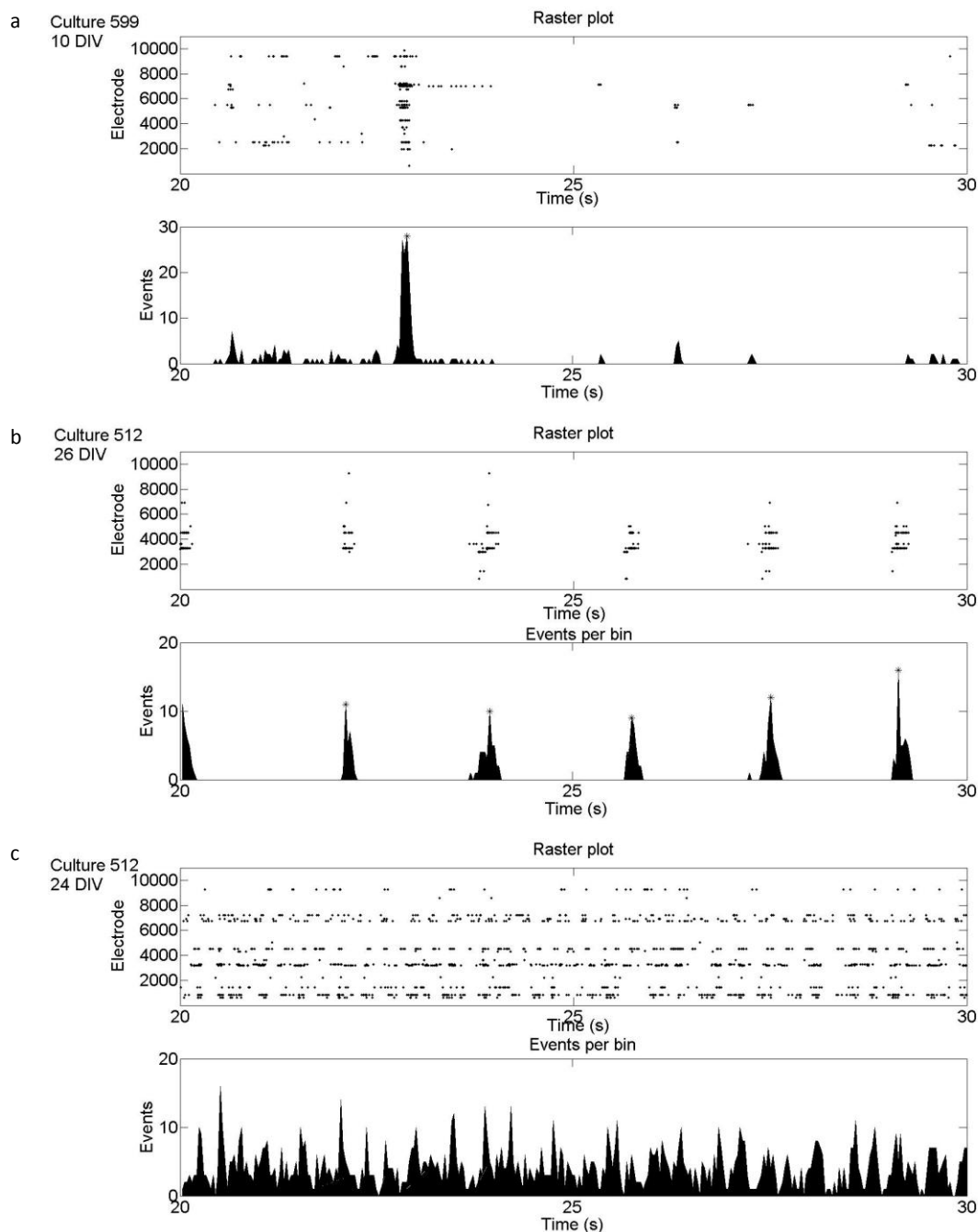


Figure 26. Raster plots of different cultures illustrating the uncorrelated firing (c) and the appearance of synchronized firing (a,b). In culture 599 (a) the synchronized firing (burst) is preceded by some activity. On the other hand, bursts of culture 512 (b) are preceded and followed by absence of activity. On the top, a raster plot is shown. The bottom plot indicates the number of events in each bin (bin size is 30ms). Spike trains were divided in segments of 2.5 minutes. For each segment, the bursting threshold was set to 9.5 times the mean firing rate for the specific segment.

### 3.2.2 Firing rates and active electrodes

Analysis of firing and burst rates (Figure 27) agrees with the raster plots. During the first stages of development all cultures exhibit low mean firing rates (MFR, figure 27 first row) and low, but not zero mean bursting rates (Figure 27, second row), with the exception of culture 599 which initially (10 DIV) showed increased burst frequency. MFR reached a plateau at 21-26 DIV depending on the culture and declined afterwards. The number of spikes per minute for cultures 512 and 599 at 11 DIV was higher than 1000. MBR increased substantially in the later stages of development, when the MFR showed a decrease. Accordingly, the percentage of events in bursts occupied a large fraction of the total events reaching values of more than 70% (culture 512, 26 DIV).

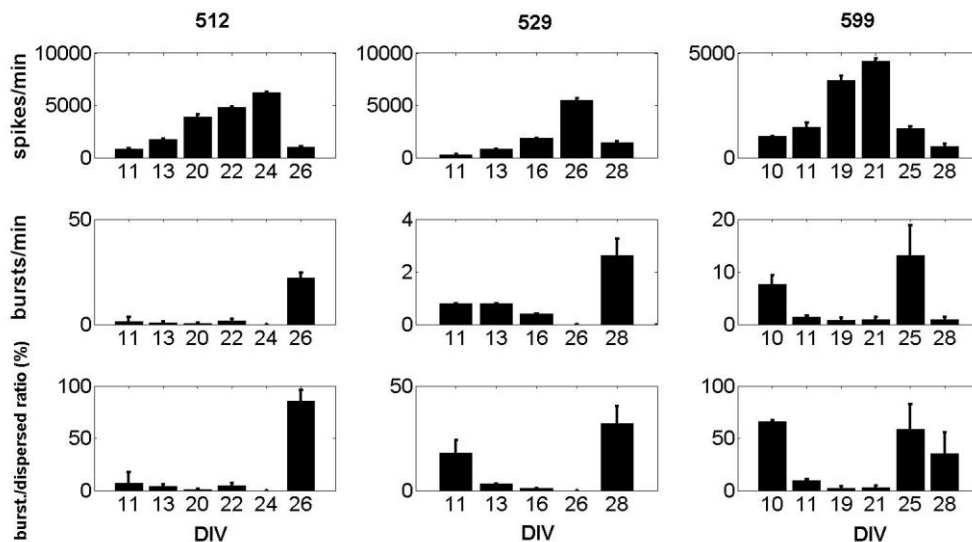


Figure 27. Firing rates for all three cultures analyzed. First row shows the mean firing rates (spikes/minute), the second row shows the mean burst rate (bursts/minute) while the third row shows the burst/dispersed ratio. This ratio is the ratio of the number of events in bursts divided by the total number of events. Spike trains were divided in segments of 2.5 minutes and averaged to produce the final value. Errorbars represent the std of these averages. For each segment, the bursting threshold was set to 9.5 times the mean firing rate for the specific segment.

The MFR of individual electrodes fluctuates much more than that of the whole network. Electrodes with the highest activity showed MFR patterns similar to that of the culture's MFR (e.g. Figure 28a). Less active electrodes showed more stochastic transitions between active (with low MFR) and inactive phases. Plots for all individual electrodes can be found in the appendix.

Figure 28b shows the normalized, averaged MFR of individual electrodes and it is evident that they follow that of the whole network, although with a very large standard deviation. The number of active electrodes (Figure 28c) also corresponds to the culture's MFR. Depending on the culture, after 20 – 25 DIV the number of active electrodes decreases. Out of the 126 electrodes used in the random configuration, a maximum of about 25 electrodes showed activity at the same day for culture 529. Furthermore, in different stages of development, different electrodes show activity as is illustrated from the high number of electrodes becoming active or inactive from one experiment to the next (Figure 28d). Only a few electrodes become active after 20 DIV.

### 3.2.3 Burst profiles

Burst profiles as identified by the burst-detection algorithm reveal a change in the burst profiles. Figure 29 shows the burst profiles for all cultures at various, selected, DIV. Culture 529 showed fewer bursts than the other two cultures and only at 28 DIV, so one burst profile is shown for this culture. At a young age, bursts are symmetric, while at a later age, 26 DIV and older, burst profiles, together with burst frequency, change dramatically. Bursts have a very fast rising phase (e.g. around 100 ms for culture 529), with the falling phase being much slower (e.g. around 300 ms for culture 529). Profiles of cultures 512 and 599 at 26 and 28 DIV are similar to that of culture's 529 at 28 DIV. All shapes, especially the ones in the later stages of development are reproducible. However, in the earlier stages of development (10 – 11 DIV) the burst's amplitude fluctuates more than that in the later stages of development (26 – 28 DIV).

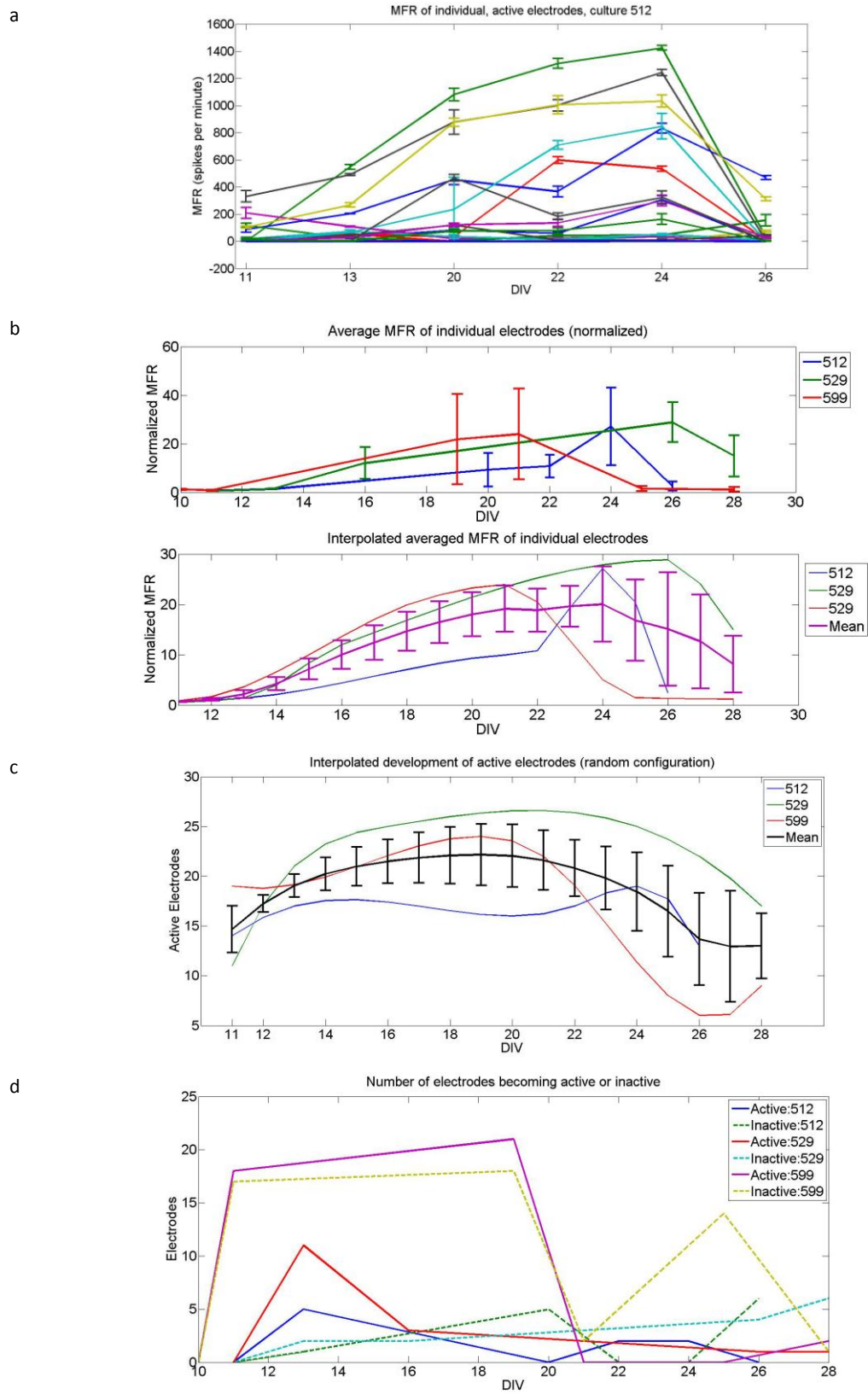


Figure 28. Electrode analysis. A) MFR for individual electrodes. B) The top plot shows the normalized, averaged MFR of individual electrodes and the bottom plot shows the same results, interpolated. Data from each electrode were normalized to the average of the first two points to produce the normalized data which were then averaged to give one data-series for each culture. C) Development of the number of active electrodes in each experiment (interpolated). D) number of electrodes becoming active or inactive from one experiment to the next.

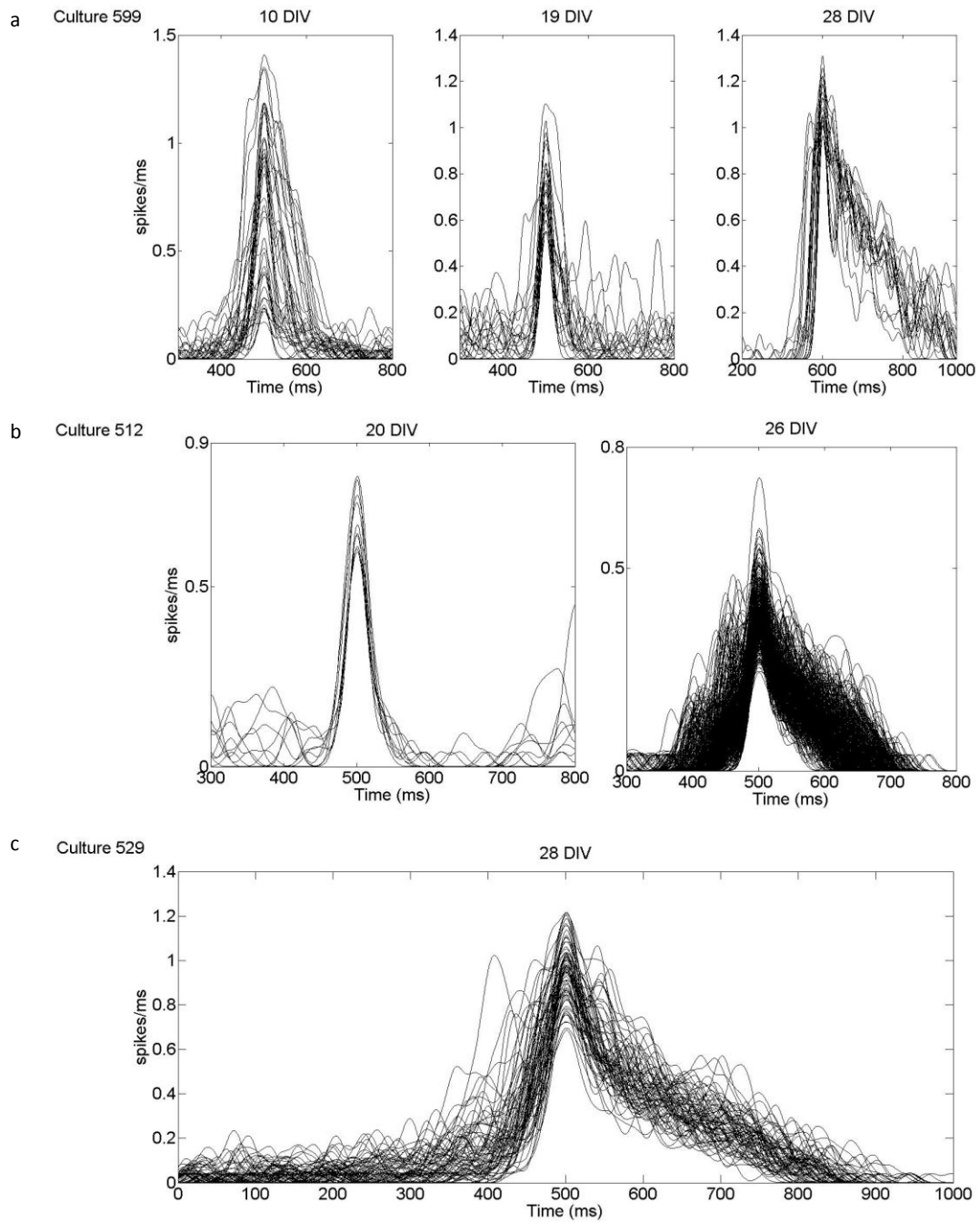


Figure 29. Smoothed burst profiles as identified by our burst-detection algorithm for all cultures. Burst profiles, especially in the later stage of development are reproducible. Bursts were identified using a threshold based algorithm, 9.5 times the MFR of each time-segment (spikes/bin).

### 3.2.4 Spike shape clustering

The properties of spike shapes for culture 512 (Figure 30a) show a very clear transition. The peak to peak amplitude increases, whereas the peak balance decreases. This means that the second phase becomes more pronounced compared to the first one. The other two cultures have more dispersed properties but culture 529 at 11 DIV (Figure 30b) mostly exhibits spikes of negative balance which also indicates that the second positive phase is much higher than the first one. Four spike shape categories were generally observed and up to 20000 spikes from each experiment were then classified to one of these categories. Class 1 is monophasic, class 2 biphasic with a large first positive phase, class 3 biphasic with a large second positive phase and class 4 triphasic. Figure 31 shows representative examples from each culture (a-c) as well as the percentage of each spike shape. Monophasic spikes occupy less than 50% with the lowest percentage (23%) in culture 512. On the contrary, triphasic spikes reached values of up to 33% in culture 599.

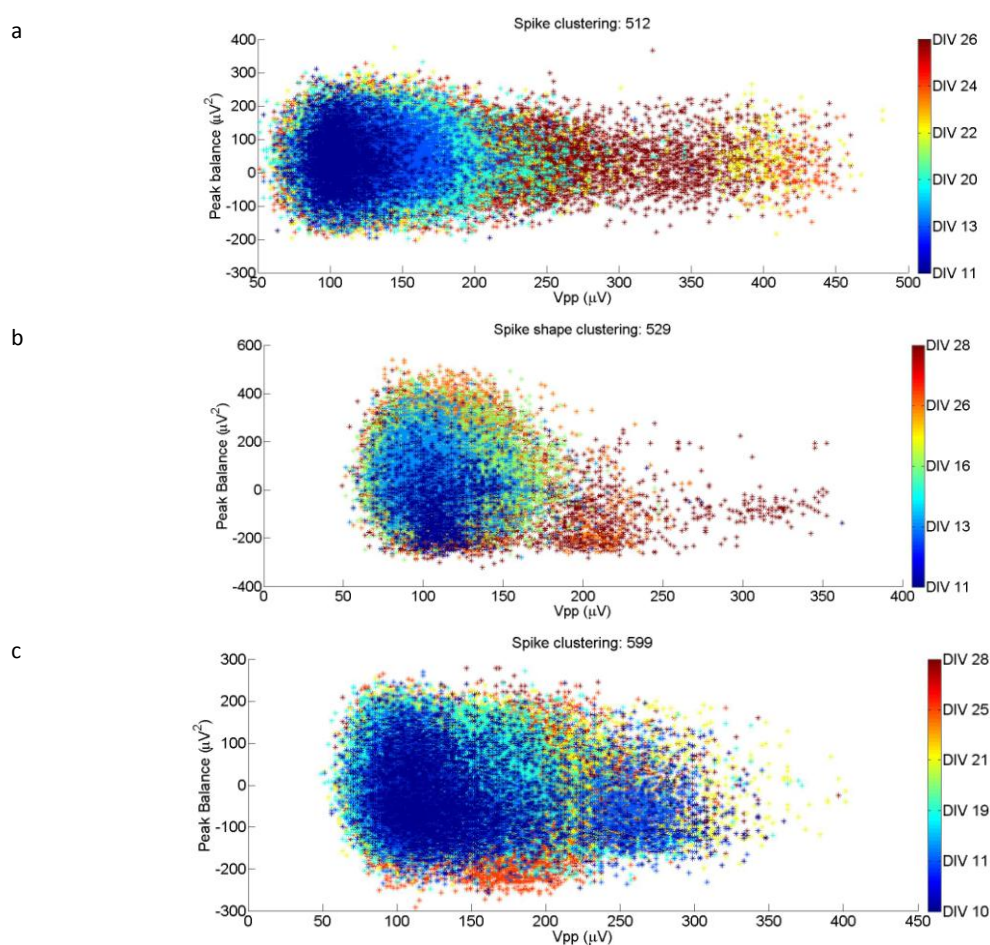


Figure 30. Spike shape clustering for culture 512 (a), 529 (b) and 599 (c). The peak to peak value of the spike and the peak balance were used. The peak balance is the difference of the areas of the two identified positive peaks (before and after the negative phase), if any.

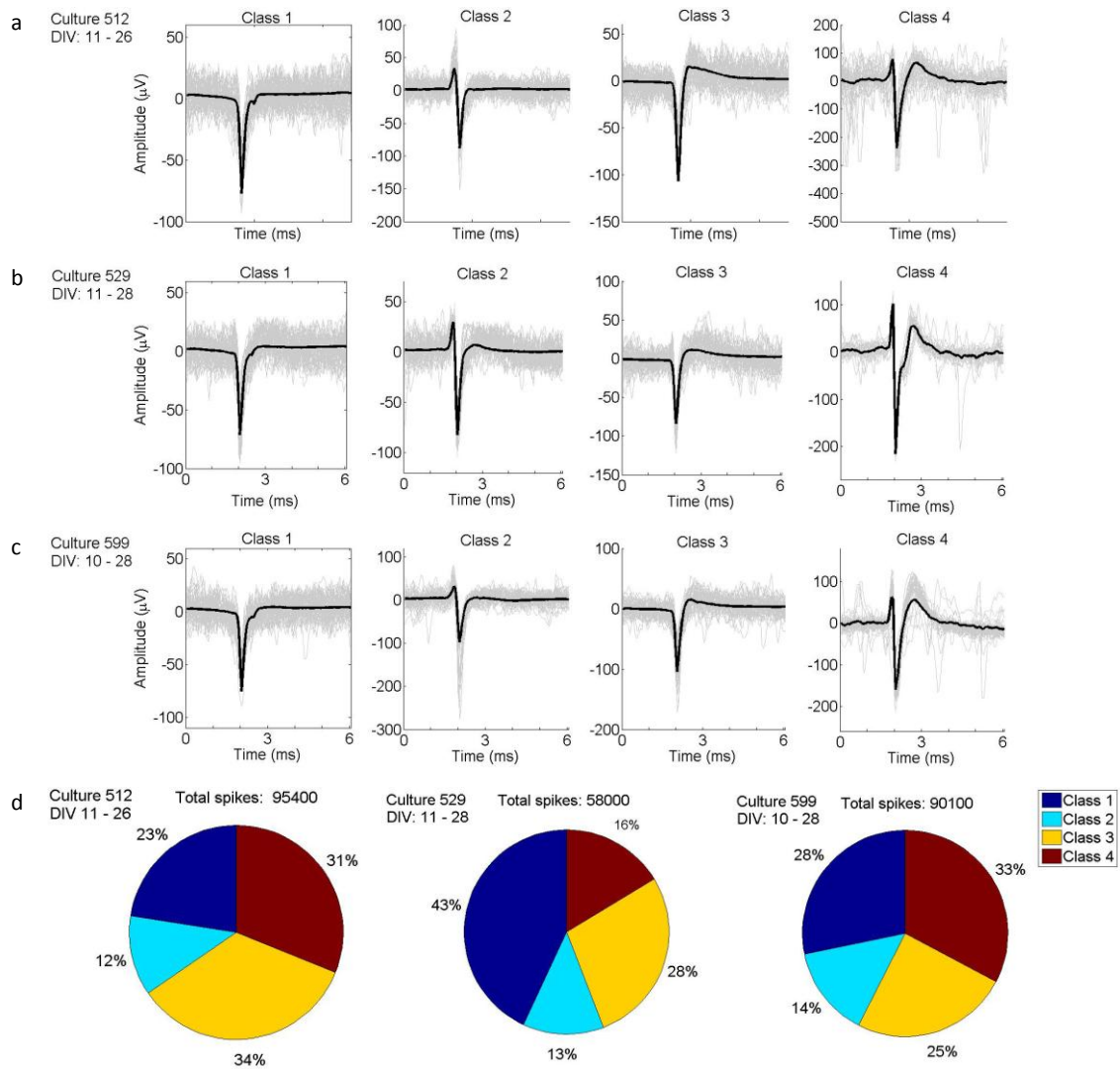


Figure 31. Spike shape clustering for culture 512 (a), 529 (b) and 599 (c). Four different classes were identified in all experiments and representative examples are shown. The percentage of each class for each culture is depicted in (d) together with the total number of spikes in the dataset. From each experiment, a maximum of 20000 spikes were taken (where available).

### 3.3 Electrode configurations

Different random and block configurations were tested (Figure 32 and Figure 33 respectively). In both cases the MFR changes but the MBR either remains stable and in almost zero levels (for the random configurations) or changes (block configurations) The array scanning algorithm was then used to scan the whole array for activity (on-line event detection) and colormaps of the MFR, average amplitude and noise levels are illustrated in Figure 34 for culture 529 and 512. In both cases, the patterns of active electrodes are diagonal and for culture 512 small clusters can be identified. Noise levels as shown are quite stable for both cultures. Based on this, the effect of MFR threshold and average amplitude on the number of suitable electrodes (electrodes that passed the thresholds) was investigated, with the results indicated in Figure 34b. Finally, one of the optimum configurations was compared to a random, a block and a configuration representing the conventional MEAs. Analysis of the results is indicated in Figure 35. The block, random and conventional configurations have similar MFR and MBR but the optimum configuration exhibits a much higher MFR but lower MBR and burst/dispersed ratio. We then obtained the burst profiles for each configuration. The random and conventional configurations exhibit burst profiles of similar amplitude and shape. With the block configuration fewer bursts were identified but their amplitude surpassed that from the random or conventional configuration. Finally, with the optimum configuration almost zero levels of bursts were identified.

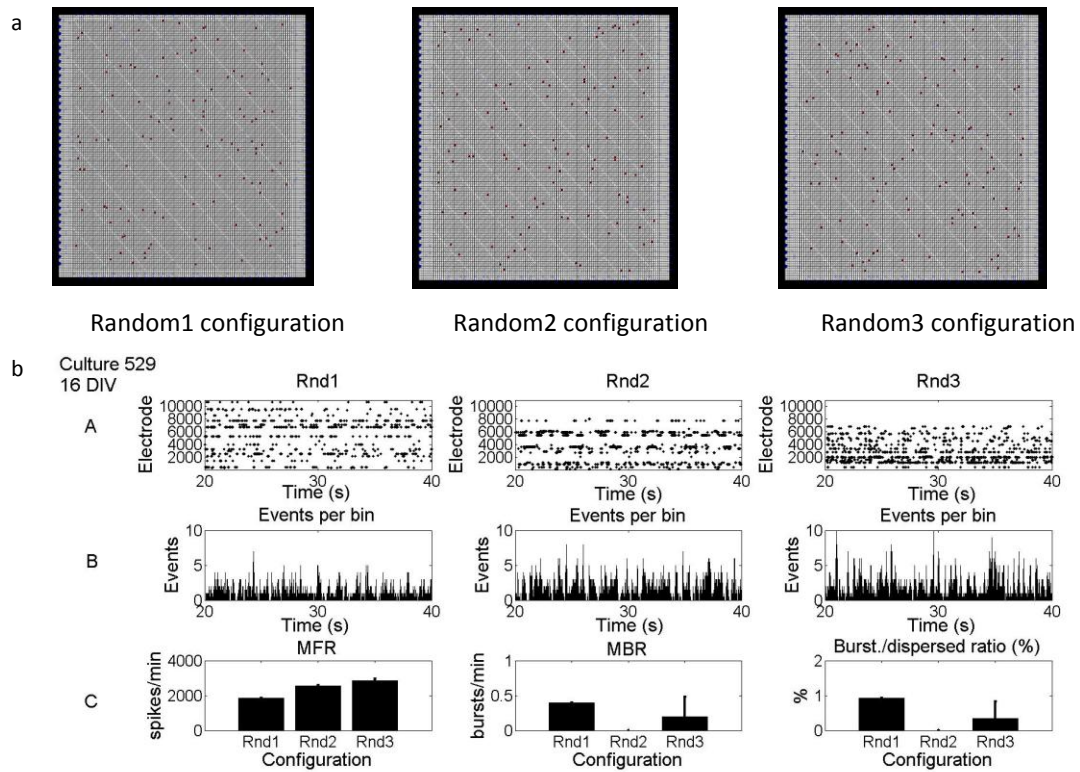


Figure 32. Comparison of activity for three different random configurations performed in culture 529, 16 DIV. The electrode configurations used are shown (a) and in b) a summarized activity analysis. Top row (A) shows raster plots for configurations random1 (first column), random2 (second column) and random3 (third column). The second row shows the number of events per bin (bin size 30 ms) and asterisks indicate identified bursts. The third row shows the MFR (spikes per minute), MBR (bursts per minute) and the burst/dispersed ratio for all configurations. Spike trains were divided in data segments of 2.5 minutes. For each segment, the burst threshold was set to 9.5 times the MFR of the specific segment.

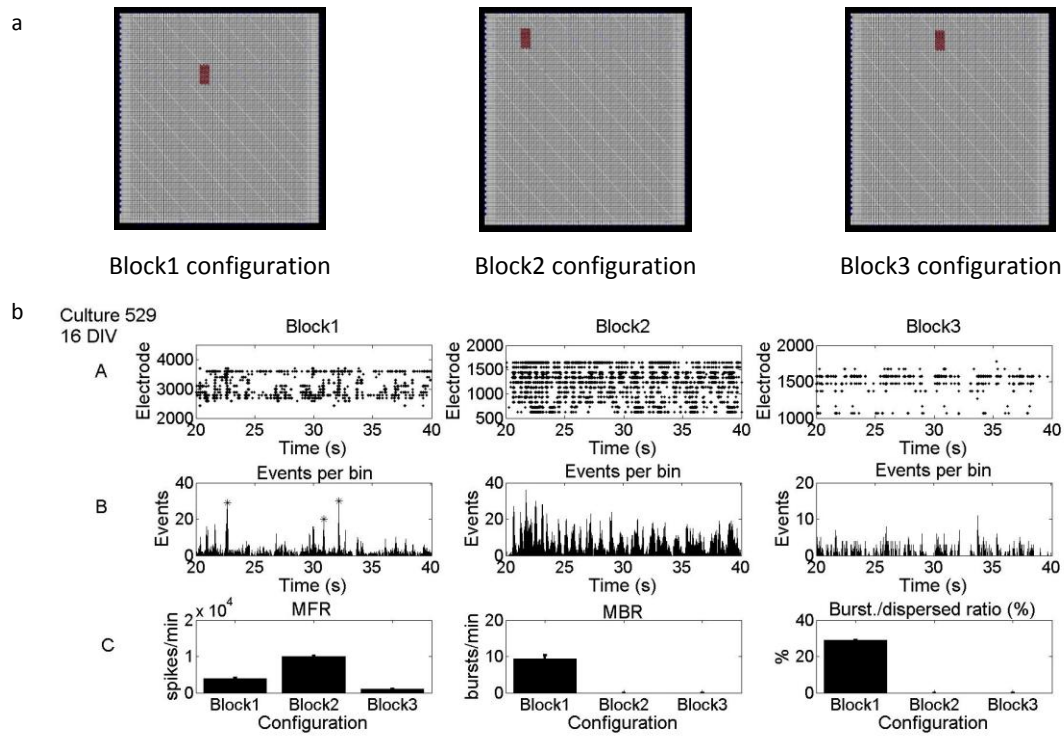


Figure 33. Comparison of activity for three different block configurations performed in culture 529, 16 DIV. The electrode configurations used are shown (a) and in (b) a summarized activity analysis. Top row shows raster plots for configurations block1 (first column), block2 (second column) and block3 (third column). The second row shows the number of events per bin (bin width 30 ms) and asterisks indicate identified bursts. The third row shows the MFR (spikes per minute), MBR (bursts per minute) and the burst/dispersed ratio for all configurations. Spike trains were divided in data segments of 2.5 minutes. For each segment, the burst threshold was set to 9.5 times the MFR of the specific segment.

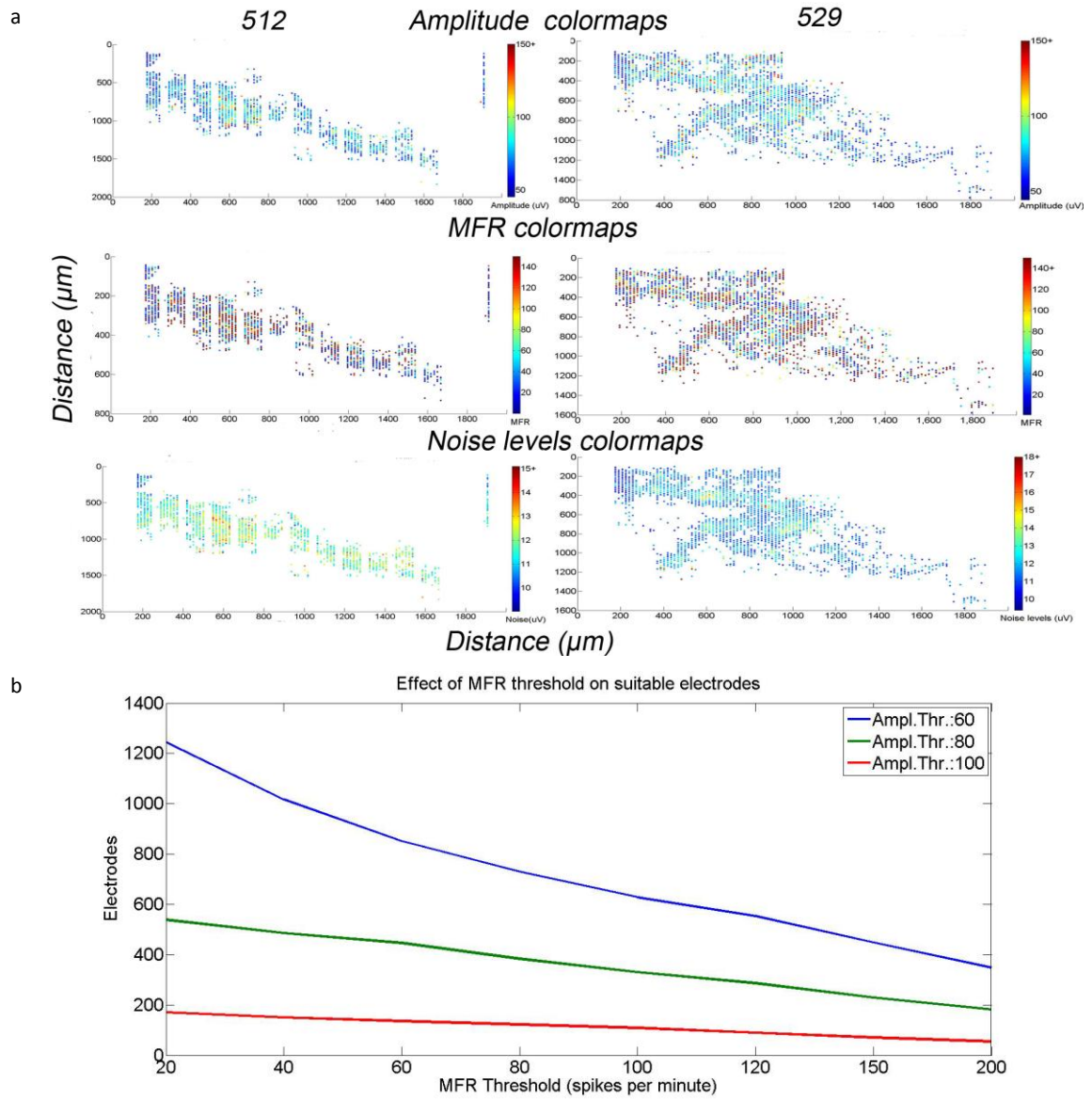


Figure 34. Colormaps of selected parameters, during the scanning algorithm for cultures 512 (left column) and 529 (right column). Indicated in the colormaps are the MFR, the average amplitude of the spikes recorded from each electrode and the averaged noise levels during the events. Only active electrodes could be analyzed since it is the result of an online event-detection algorithm. Blank electrodes are electrodes with no activity. Noise levels in all electrodes were previously found to be relatively stable (13 -14  $\mu\text{V}$ ). (b) shows the number of identified suitable electrodes with increasing MFR (spikes per minute) threshold and for different amplitude thresholds.

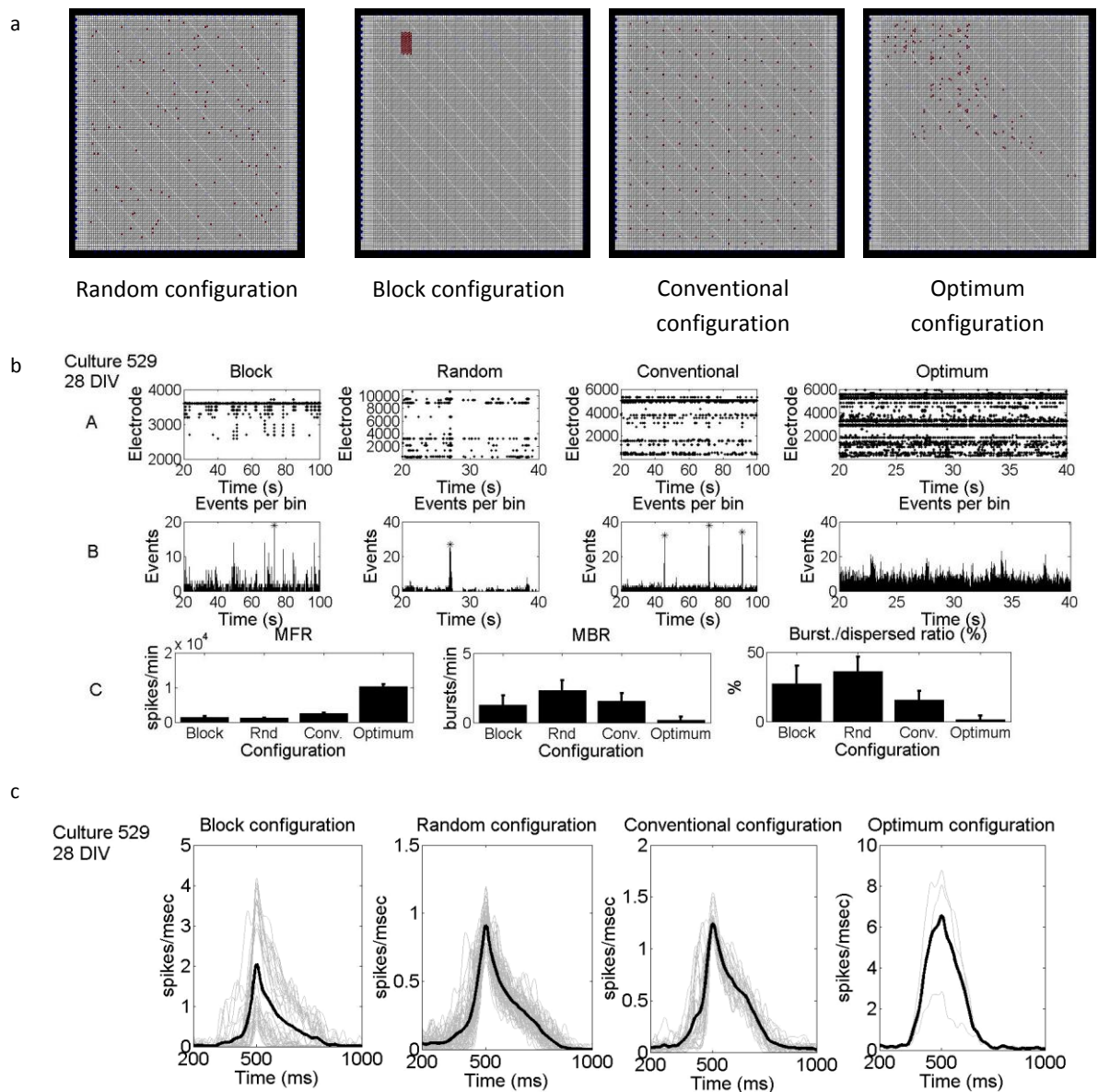


Figure 35. Comparison of four different electrode configurations for culture 529, 28 DIV in order to analyze the performance of the electrode selection algorithm. A block, random, conventional and an “optimum” configuration were used as illustrated in (a). (b) Top row (A) shows raster plots for the different configurations (different columns) while the second row (B) shows the number of events per bin (bin size 30 ms) and identified bursts (asterisk). Row (C) indicates MFR, MBR and burst/dispersed ratio in all configurations. All spike trains were divided in segments of 2.5 minutes and averaged. Errorbars represent the std of these averages. For each segment, the burst threshold was set to 9.5 times the MFR of the specific segment. (c) Burst profiles were identified and shown for each respective configuration. Grey lines represent individual burst profiles and the thick black line is their average.

### 3.4 Neurochemical treatment (Magnesium)

As a last step, we added magnesium in two cultures (529 and 599) for verification purposes. Figure 36 shows the results for culture 529. The optimum configuration as found in the previous section was used. In the baseline and control phase the MFR and MBR are similar, in the magnesium phase there are no spikes or bursts and in the washout phase the MFR returns to previous levels but the MBR is significantly lower. It is evident from the raster plot of the washout phase that the activity pattern changes, with fewer large fluctuations. The burst/dispersed ratio is also much lower. However, despite the lower number of bursts identified their profiles seem similar to the profiles of the baseline and control phase. Culture 599 showed similar properties but did not survive the experiment and after washout we recorded no activity.

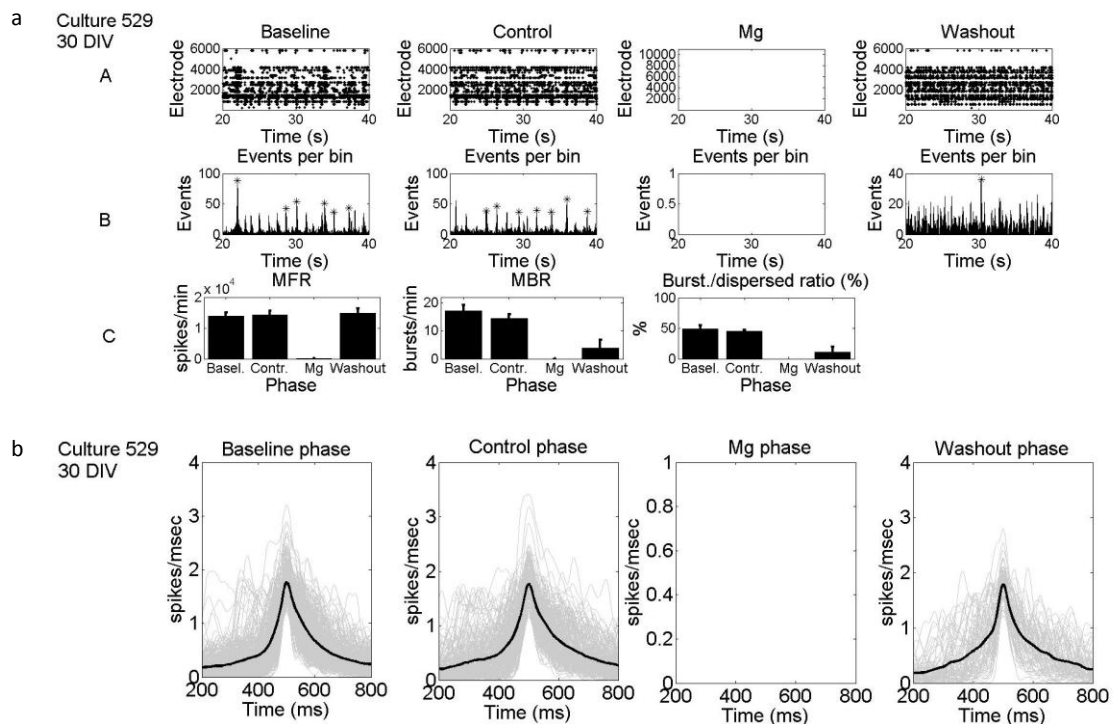


Figure 36. Magnesium effects on culture 529, 30 DIV. (a) Top row (A) shows raster plots for the different phases (different columns) while the second row (B) shows the number of events per bin (bin size 30 ms) and identified bursts (asterisk). Row (C) indicates MFR, MBR and the burst/dispersed ratio in all phases. All spike trains were divided in segments of 2.5 minutes and averaged. Errorbars represent the std of these averages. For each segment, the burst threshold was set to 9.5 times the MFR of the specific segment. (b) shows the burst profiles for each phase of the experiment. Grey lines represent individual burst profiles and the thick black line is their average.

## 4. Discussion and conclusions

### 4.1 Overview

This project presented the development of a 11000 electrode system for neural network recording. Previously, this system has been successfully used from various groups [56, 59, 62]. Noise levels found in the literature for electrodes of comparable size vary from 7 – 11  $\mu\text{V}$  rms [13, 52, 54, 63]. In our experiments we measured stable noise levels of 11 – 14  $\mu\text{V}$  rms. As the electrode size decreases, the electrode impedance and the thermal noise increase. Furthermore, the chips include amplifiers which are realized with transistors. Active components also introduce noise. Thermal noise from the electrodes are seen as input from the amplifiers, which also add their own noise sources. Furthermore, since transistors are made of semi-conductors and contain PN junctions they are inherently sensitive to light, which is another noise source. Active components dissipate heat which can increase the thermal noise of a resistor. When a culture is active, activity from distant cells is measured as biological noise and cell growth can also influence the electrode impedance [64]. The ADC finally, contributes  $0.5 \cdot \text{LSB}$  quantization noise. In our experiments, we placed the cultures into an incubator which made it susceptible to vibrations. However, recordings from the university of Kaiserslauten exhibit same noise levels [60], making it unlikely that we had any substantial vibrations.

Signals observed are more noisy than with conventional MEAs. On the other hand, the electrode size is smaller. Simulation and experimental results illustrate that the SNR of the recording is higher when a neuron completely covers an electrode [65-66]. The diameter for somata of neuronal cells is usually from 10 to 50  $\mu\text{m}$  for vertebrates [67-68]. In our system the electrodes' diameter was 7  $\mu\text{m}$  and the electrode pitch 18  $\mu\text{m}$ . Thus, as the electrode diameter and pitch decrease the probability of a neuron completely covering an electrode increases, at least when the culture is confluent. Furthermore, by using pt-black the effective surface of an electrode increases which in turn, decreases its impedance.

From the 11011 electrodes a subset must be selected for long – term recordings. When using a random electrode configuration only 20 – 25 % of the electrodes were found to be active. To the author's knowledge such an analysis has not been before, so the reasons behind this are not completely clear yet. One possible explanation is that due to the high noise levels we could not observe spikes of low amplitude. Another possibility is that the cells were not alive in some regions, or they did not successfully attach to the substrate. Colormaps of activity indeed revealed some clustering of identified activity (MFR). Noise levels on the other hand are not clustered in such a way. Therefore, the most possible explanation is that the cells were either dead or detached/not-adhered at some regions. The reason behind cell

death might be increased temperature [69]. During our saline recordings, the temperature was measured for 50 minutes and the curves are not completely stable at the end of the measurement. Since recordings with active cultures took much longer than 50 minutes it is possible that the cells died because of increased temperature. Increased temperature also results in water evaporation which can change the osmolarity of the medium, killing the cells. Indeed, medium evaporation was observed when a culture was left in the incubator for more than 24 hours. Notice, however, that the lid was not perfectly sealed and may explain the observed evaporation.

In retrospect, when the temperature recordings took place, the duration of the experiments was not clear yet and the focus was on short recording times (meaning less than 50 minutes). The temperature problem is also mentioned on the wiki [60]. They found (authors unknown, probably the ETH group) that the temperature is 1.6 degrees Celcius above the ambient temperature, although the temperature sensor was inside the black hood and not contacting the chip directly. In the author's opinion our measurement is more accurate since the sensor was placed exactly under the chip. However, the most accurate measurement would be with the sensor placed inside the medium.

Besides the slow death of parts of the culture, they survived for almost 30 DIV and afterwards they were cleaned in order to try other platings. The original HIDENS software with its labview interface and matlab toolkit does not allow long recordings. For recordings of less than a minute more than 20mbs are required. With our online event-detection algorithm we could efficiently record for more than 2 hours non-stop, after solving some disconnection problems (these were attributed to lost connection between the neurolizer and the chip pcb).

Overnight recordings can take place, provided the culture's health can be preserved. With long-term recordings plasticity and learning can be investigated [16, 18-19, 22-24, 70]. For example, Stegenga et al. [23] have investigated the effect of learning on bursting and le Feber et al. [19] have shown that slow electrical stimuli induces changes in functional connectivity, although uncontrolled. Such experiments lasted around 10 hours and are now possible if there are no disconnection problems, if the lid is properly sealed, preventing water evaporation and if the temperature stays below 37 degrees Celsius. However, in this project we did not investigate the stimulation capabilities of the device.

The large number of electrodes certainly allows more detailed experiments. For example, after visualization of the network, one could record from monosynaptically connected neurons and investigate plasticity. Gritsun et al. [71] have shown by means of modeling, that on small timescales short-term plasticity may affect firing rates during bursts. With this system it can be also tested experimentally. However, the non-transparent nature of silicon makes observation of the culture's

development under the light microscope impossible. Other ways have to be found to visualize the network. One possible way is to use cell staining. Furthermore, the complexity of the system makes it vulnerable to disturbances. Different electronic hardware systems need to communicate between them exchanging data packets every 20 – 50 msec. This imposes restriction on the communication pathway which should have a large SNR. Data are digitized but a low SNR results in slow transmission speeds between the FPGA and the computer.

Unfortunately, not all of the questions could be answered during this project. A lot of reasons contributed to this. First batches of chips were not working at all, some were accidentally damaged, the internal reference electrode was not working and there were many disconnection problems besides the low success rate of platings and the death of puppets

## 4.2 Data analysis

Analysis of MFR and MBR is a de facto analysis of a culture's development . It has been established that both the MFR and MBR first show an initial increase in their frequency and later on, a decrease is observed [10-11, 13, 15]. The MFR in our experiments agrees with that concept, although a very fast and profound decrease was observed in the later stages of development. Wagenaar [50] found that although the MFR decreases after the third WIV, the Burstiness Index (BI) continues to increase. This means that the activity of the culture decreases but the percentage of spikes in bursts increases. On the other hand, Chiappalone et al. [10] report a decrease in this ratio after 14 DIV. In our case, both the MBR and the burst/dispersed ratio (which is equivalent to Wagenar's BI) were almost zero until the third WIV and later on they increased. It is therefore speculated that each culture has its own characteristic development between uncorrelated firing and bursting.

Chiappalone et al. [10] report a maximum averaged firing rate of 2 spikes per second. It is also shown in raster plots that (almost) all sites are active, which translates to a maximum of 9000 spikes/minutes summed activity of the network at 21 DIV. In our experiments we observed slightly more than 5000 spikes per minute at 21 – 26 DIV, but from a much lower number of electrodes. Van pelt [11-13] found that individual sites (electrodes) display highly irregular firing rate profiles on a time scale of days. We analyzed the activity of individual sites and found that their averaged activity is similar to the culture's MFR but the individual electrodes show irregular transitions of high and low activity from one experiment to the next. This irregularity in the firing rates has been also observed in other studies on cortical cell cultures by Ramakers et al. [72].

The presence of bursts was verified in our recordings in accordance with previous studies of burst occurrences [13, 61, 73-74]. Stegenga et al. [61] report on bursts appearing as early as 7 DIV and present up to 61 DIV. Several characteristics were identified such as a long tail, a distinct second mode and differences in the rising and falling phase. Kamioka et al. [73] reports burst duration of 100 ms to 450 ms. No systematic approach took place to calculate the width of the burst but judging from the figures our results agree with theirs with a rough estimation of 200 ms to 600 ms.

Developmental changes of burst profiles are reported by van Pelt et al. [13] who found a drastic shortening of the rising phase by about one month in vitro. Furthermore, a detailed look in the burst profiles produced shows a large variety among them. Two characteristic profiles are one symmetric, and one with a long tail on the falling phase. In our experiments, we observed a sudden onset of the network burst and a long falling phase at about 1 month in vitro. Stegenga et al. [61] report on similar burst profiles, with a long falling phase, from 12 to 19 DIV. In our case, at 10 – 11 DIV the bursts appear symmetric and with a large variability in the peak amplitude but at 26 – 28 DIV bursts are reproducible and with a long falling phase. Bursts appear to be reproducible at a given day even with a different electrode configuration, although the burst's amplitude might be altered. Due to the smoothing algorithm, some variation is lost but the main features of the bursts are preserved.

Bursts observed at 10 DIV for culture 599 (Figure 30) have similar shapes but the variability in their peak amplitude is quite high. Taking a look at the MBR for this culture (Figure 27) we observe that only at 25 DIV the MBR is high. It could be the case that due to large variability of the burst profiles at 10 DIV and due to the low MBR up to 25 DIV these burst profiles are false positives. However, a look into Figures 24 and 25 which indicate the raster plots clearly shows a bursting behavior at 10 DIV. For this reason, in the authors opinion the majority of these burst profiles although variable in their peak amplitude represent bursts.

Besides bursts, waveshapes of action potential shapes were classified with a procedure similar to that of van Staveren et al. [75]. In MEA recordings the most commonly observed waveform is monophasic (class 1). In our experiments we distinguished 4 different classes of spike shapes and class 1 was not often observed. Classes 2 and 3 were biphasic while class 4 was triphasic. Furthermore, variations within the classes were large, also found by van Staveren et al. [75]. However, they identified less than 42000 spikes, whereas in our case this number was larger than 240000 spikes.

The extracellular action potential recorded by an electrode depends on a variety of parameters [35, 37] including electrode position and the conductance density profiles. Since the procedure in our group for the preparation of the culture on the

chip is the same as with the conventional MEAs the difference in the recorded waveshapes should be attributed to the chip's properties.

Van pelt et al. [13] have also investigated the wave shapes of spontaneous neuronal activity in cortical cultures. They showed that the amplitude of the negative peak can fluctuate as the culture matures and a lack of systematic development was observed. In this project, one culture (512) showed a clear transition from low to high peak to peak amplitudes whereas the other two were fluctuating.

Last but not least, the electrode evaluation algorithm proved, in principle, to be working but there is an obvious drawback. The MFR of the optimum configuration is much higher than in other configurations. However, the MBR and the burst/dispersed ratio (%) showed a significant decrease. This can be explained by the fact that no burst criterion was used in the electrode evaluation algorithm, so it is biased towards tonically firing neurons. Beggs et al. [76] report that bursts might be an optimum way of information transfer. In that respect, ignoring bursts would have a profound negative effect on data analysis.

On the other hand, the activity pattern of the culture, for a specific electrode configuration, might change from uncorrelated firing to bursting (or the other way around) in a matter of days. Compare for example the activity pattern of the optimum configuration of culture 529 at 28 DIV (Figure 35) and at 30 DIV (figure 36, baseline phase). In 2 days the activity changed pattern. Furthermore, the scanning algorithm takes about 2,5 hours. From our current results it was obvious that both the MFR and the pattern of activity might drastically change in a matter of days. It may be necessary therefore, to re-evaluate the electrodes every 2-3 days.

All results as presented in this report are based on specific definitions as described in the methods and materials sections. In some cases, different definitions might give rise to different results so, one should be aware of that fact. For example, for the bursting criterion it is very common to use a specific threshold of e.g. 9 for the minimum product of the spikes and the number of electrodes. Several burst criterion protocols were tried but these protocols did not work and the one presented here was selected after careful evaluation of the algorithm's performance for our data (as presented in the appendix). The main problem was that the MFR was decreasing but bursts were observed. Setting a low value would result in many false positive detections during high uncorrelated firing. Setting a high value would exclude the bursts from cultures of low MFR. Furthermore, since when the MFR is low also the number of active electrodes is low we set the minimum number of electrodes to 4, a rather low value so as to include bursts from a low number of active electrodes, since taking a look at the raster plots shows a burst-like behavior (sudden onset of collective behavior). This procedure is thought to be the best procedure for the specific data and it should by no means taken to mean that it is a universally effective criterion.

As a last step, we added magnesium to verify that the recorded data were indeed spikes from living cells and to check for an effect on the firing rates or the burst profiles. After washout, the MFR remained the same but the MBR decreased, reaching almost zero levels. This can be explained by the fact that the cultures went through some treatment, neurochemical and physical. The culture had to be taken out of the incubator and the medium was changed a couple of times. However, the control phase is similar to the baseline phase which means that the change in the activity pattern was not from the physical/mechanical treatment. Rather, it should be attributed to the magnesium itself or the medium washout. In the author's opinion it is mainly due to the medium washout since, during a previous project this was found to have a large effect on the network's activity. Furthermore, we observed a decrease in the number of bursts, whereas Wagenaar observed an increase after moving the cultures [50].

## 5. Future work and Recommendations

In this project we used high density cultures. Due to unexpected problems (damaged chips, infections etc...) only 3 cultures could be used for long-term experiments. It is now proven that the hardware and the software work. The procedures generated, like the scanning algorithm and the electrode selection procedure, also work but the later is biased. A bursting evaluation criterion should be added, which should not occupy more than a couple of Matlab code. The next step is to use low-density cultures together with cell-staining for a more in-depth analysis of neural networks.

When using Cell Tracker Green make sure the work is done as much as possible in the dark. For the recordings, the incubator used is dry, so one should not leave the culture for many hours/days in it. In one case, it was found that after two days inside the incubator, all of the medium evaporated and the culture died.

If there are any disconnection problems, all connections should be checked. The connection from the PC to the FPGA, FPGA to the LVDS etc... The most important one is the connection between the Neuroizer and the chips and between the Neuroizer and the FPGA. Writing data to external hard drives should be avoided. The speed is slow and a disconnection problem will arise. Only write to the internal hard-disk.

If signals are saturated, lower gain amplification should be used. The DC-offset compensation algorithm should be applied each time a configuration is changed or the amplification settings are altered.

To get a good signal for the chip many settings need to be correctly selected, most of them in the AVR-shell. The Mosr voltage, the reference cable and the V2 stage reference are three of them. The WIKI [60] contains a lot of details.

Furthermore, the server's buffer should be observed during the experiment. If data reading is slow errors will arise. Especially when using the scanning algorithm it is imperative to set the reading style to "live". Otherwise, data from a previous configuration may be registered with the new configuration. If data reading is too slow plots in the Labview software should be disabled. Also note that Labview itself does not actually do anything. Rather, it sends commands to the server. In case of any problems the server's capabilities should be checked together with the Labview code.

## Appendix

### A.1 Experimental set-up for temperature recordings

Five experiments were conducted for measuring the chips' temperature. The first two had external temperature levels of 34.7°C, the internal reference electrode was used and the hood was applied to cover the chips. Later, I noticed that in some chips the internal reference electrode was not working, so the next 3 experiments (external temperature 33°C) were done with the external PCB attached and without the hood.



Figure A1. Measurement of the chip's temperature. A hood was used to cover the chips.



Figure A2. Measurement of the chip's temperature. No hood was used to cover the chips and the PCB extension cable was used to provide an external reference electrode.

## A.2 Trial hippocampal recordings – verifying integrity of our software

We obtained trial hippocampal recordings from the university of Kaiserslautern and used these data to verify our on line software. They are composed of two ntk files (approximate size 130mbs) of duration 1 minute each. The first task was to verify that our online software correctly reads data from the server. A recorded file was sent to the server with the help of the “stream\_server” program. Then we used our software to read and write the data from the server to a file. We then loaded the original ntk file to the Hidens toolkit and compared the data to the data produced from our software. Results showed that our software correctly reads the data from the server as the recorded data are exactly the same with the data from the Hidens toolkit. A raster plot and some sample events are also shown. The threshold used for spike detection was set to 5.5 times the noise level and negative only threshold-crossings were accepted.

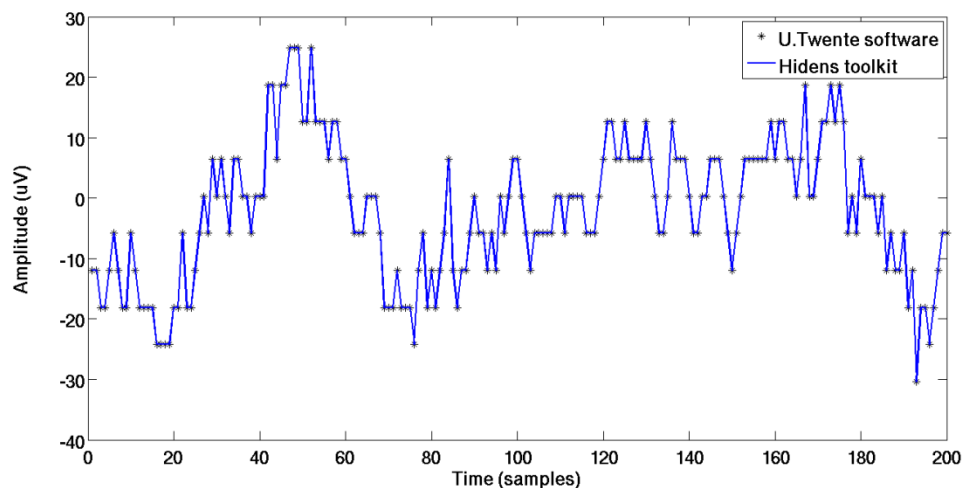


Figure A3. Verification of our software’s integrity in reading data from the server. The data read from the server is the same, regardless of the software used.

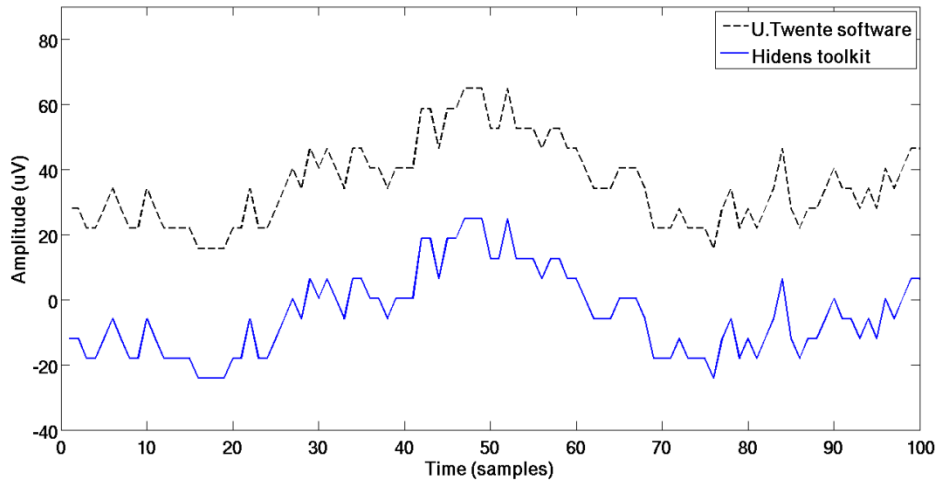


Figure A4. Verification of our software's integrity in reading data from the server. The data read from the server is the same, regardless of the software used.

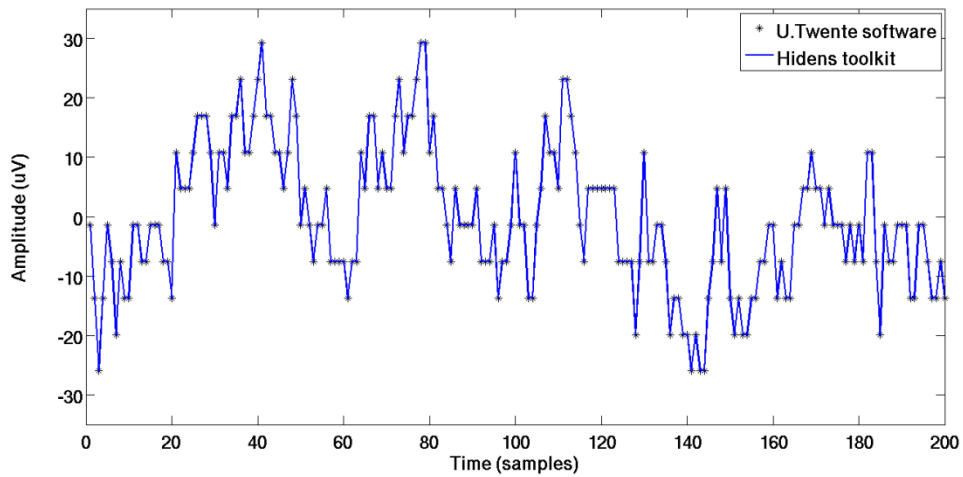


Figure A5. Verification of our software's integrity in reading data from the server. The data read from the server is the same, regardless of the software used.

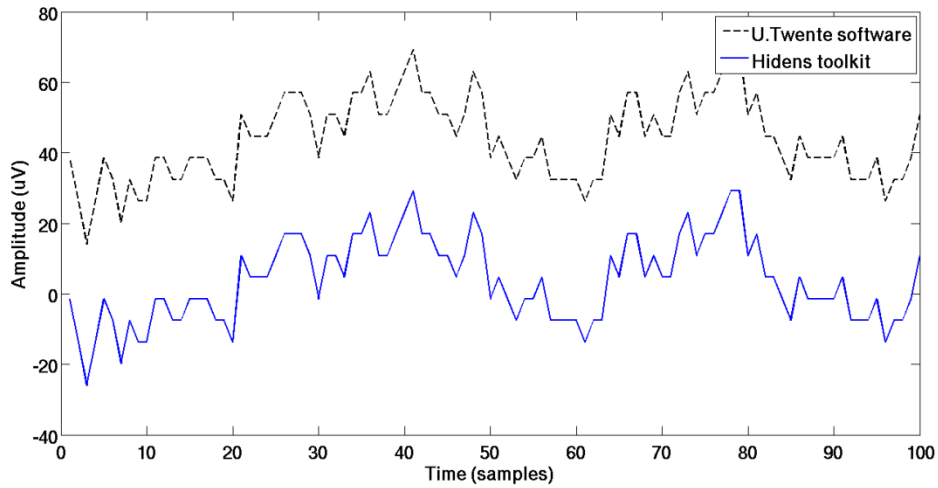


Figure A6. Verification of our software’s integrity in reading data from the server. The data read from the server is the same, regardless of the software used.

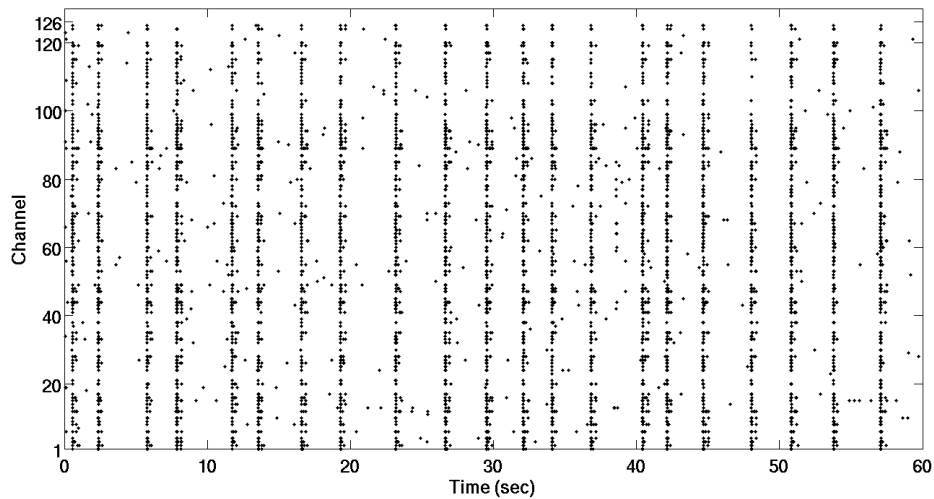


Figure A7. Raster plot from a 1-minute recording from the University of Kaiserslautern. Bursts and tonic firing can be seen.

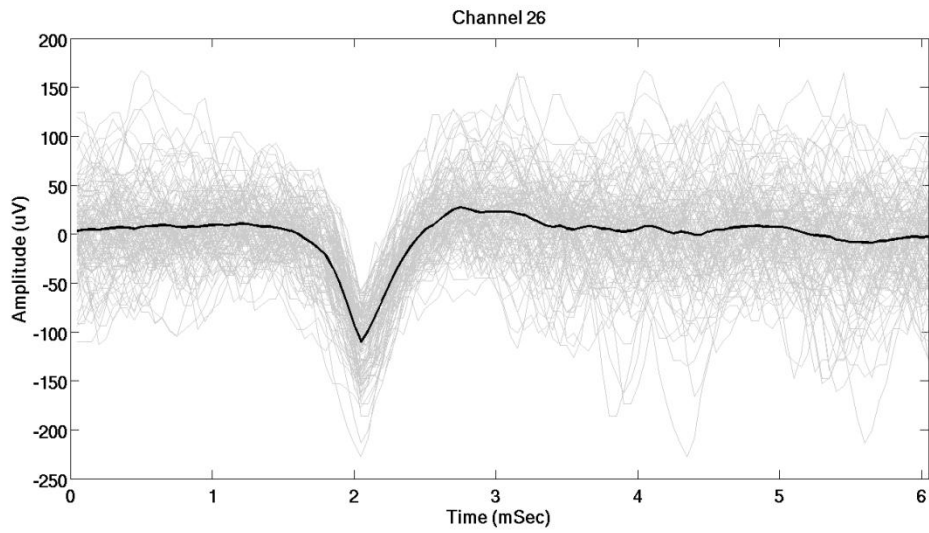


Figure A8. Illustration of events as identified from our online spike-detection algorithm. Grey lines are individual events while the thick, black line is their average.

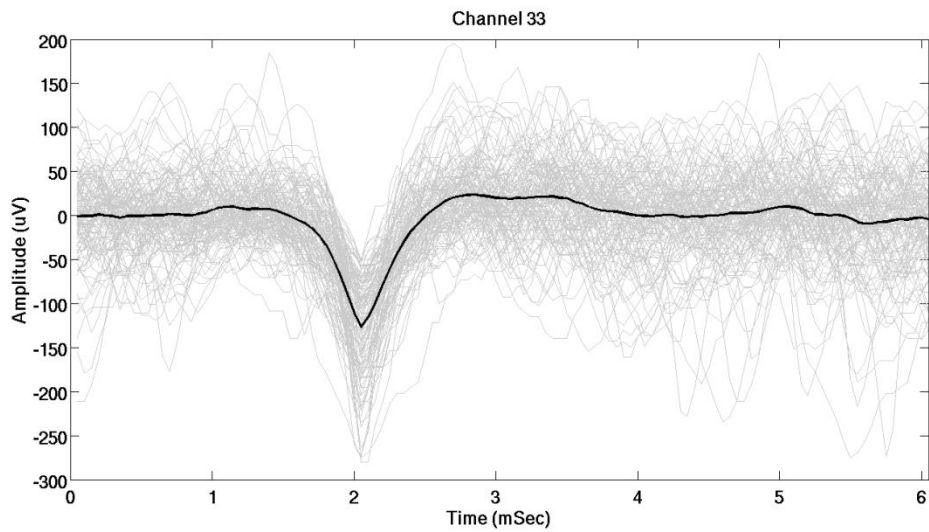


Figure A9. Illustration of events as identified from our online spike-detection algorithm. Grey lines are individual events while the thick, black line is their average.

### A.3 Selecting burst criterion

Here we present our rationale for selecting the used burst criterion. Firstly, one of the commonly used criterion was tested. The threshold was set to a fixed value of spikes per minute. Figure A10a illustrates a raster plot with the identified bursts for a value of 10 spikes/bin. It is evident that the number of identified bursts is quite high and even small fluctuation in the activity are identified as bursts. A value of 20 spikes/bin successfully eliminated the small fluctuations (Figure A10b) but it also eliminated bursts of the same culture at 26 DIV (Figure A10c). Other values showed similar results and we could not find an appropriate value that would give an acceptable performance. Next, we tried several other protocols such as setting the product of the number of spiked times the number of active electrodes to fixed values as presented in [13] which showed similar drawbacks. Another approach is presented in [61] where the threshold is set to two spikes for each active electrode. This approach takes into account the number of active electrodes and is a more dynamic threshold which can accommodate changes in the MFR. However, this protocol also failed in capturing the bursts of culture 512 at 26 DIV since the number of electrodes is quite low, but the patterns showed in the raster plot (figure A11a) clearly show a bursting behavior.

Therefore we deemed necessary to use a more dynamic threshold which can take into account the fact that the MFR might decrease but bursts might still appear. The main problem was the large difference in the MFR of each culture's development. Therefore, we calculated the average number of spikes per bin in each segment of 2.5 minutes. The threshold for each segment was then dependent on the MFR with the formula  $Th = A * BinMFR$ , where A is a constant and BinMFR the averaged MFR of the bins. We then tried several values for A from 4 to 10.5 with a step of 0.25. To analyze its performance we used 3 raster plots which clearly showed tonic firing (e.g. Figure A11b) and 3 raster plots in which bursts dominate (e.g. Figure A11c). The purpose was to have as few as possible identified bursts in the first dataset and as many bursts as possible in the second dataset. The MBR was calculated for each raster plot of each dataset and the three values (for the three raster plots) were then summed up. Figure A11d shows the summed MBR for different values of A. Based on this, we decided to choose the value of 9.5 for A.

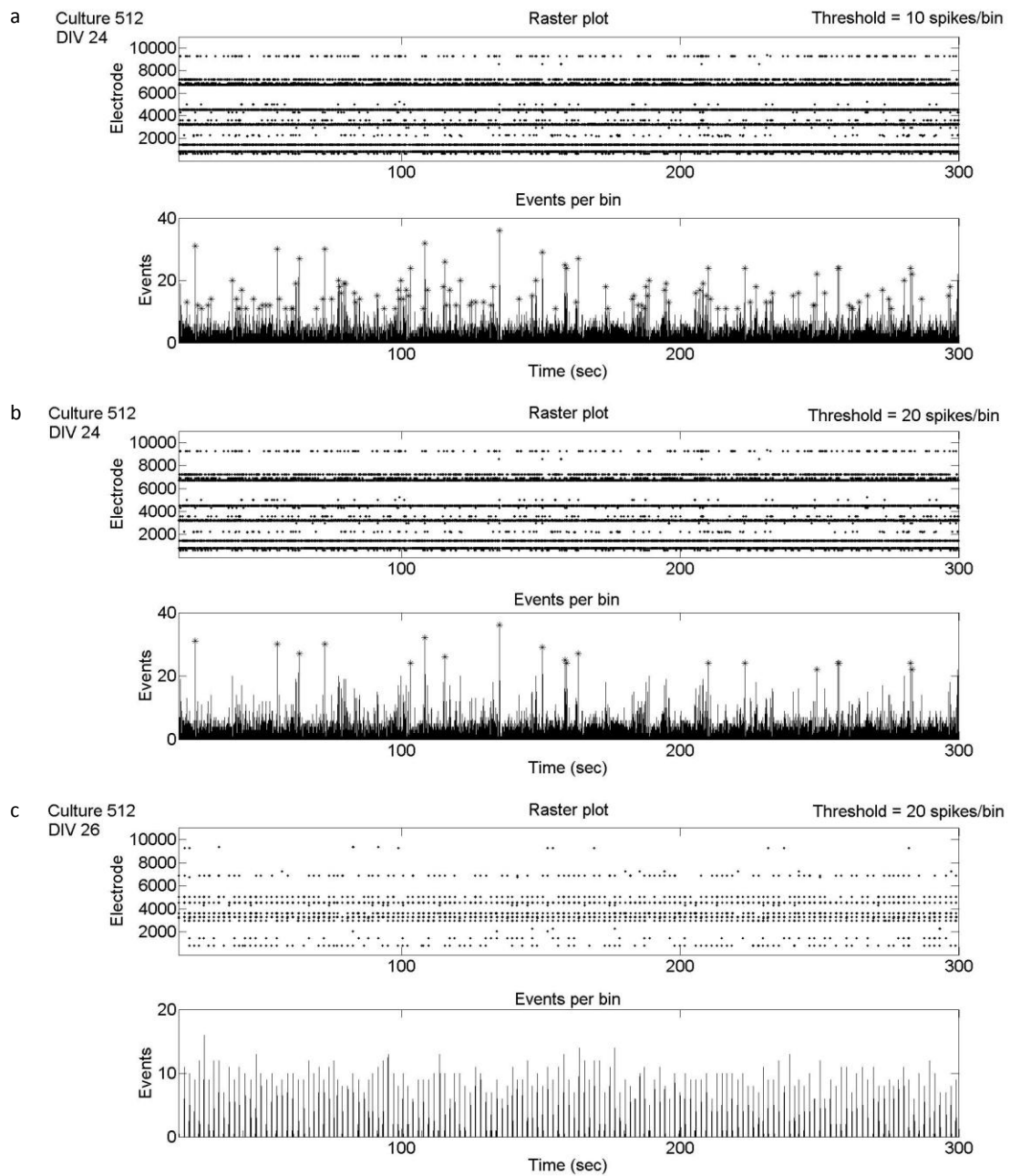


Figure A10. Raster plots indicating the effect of different threshold values for static threshold.

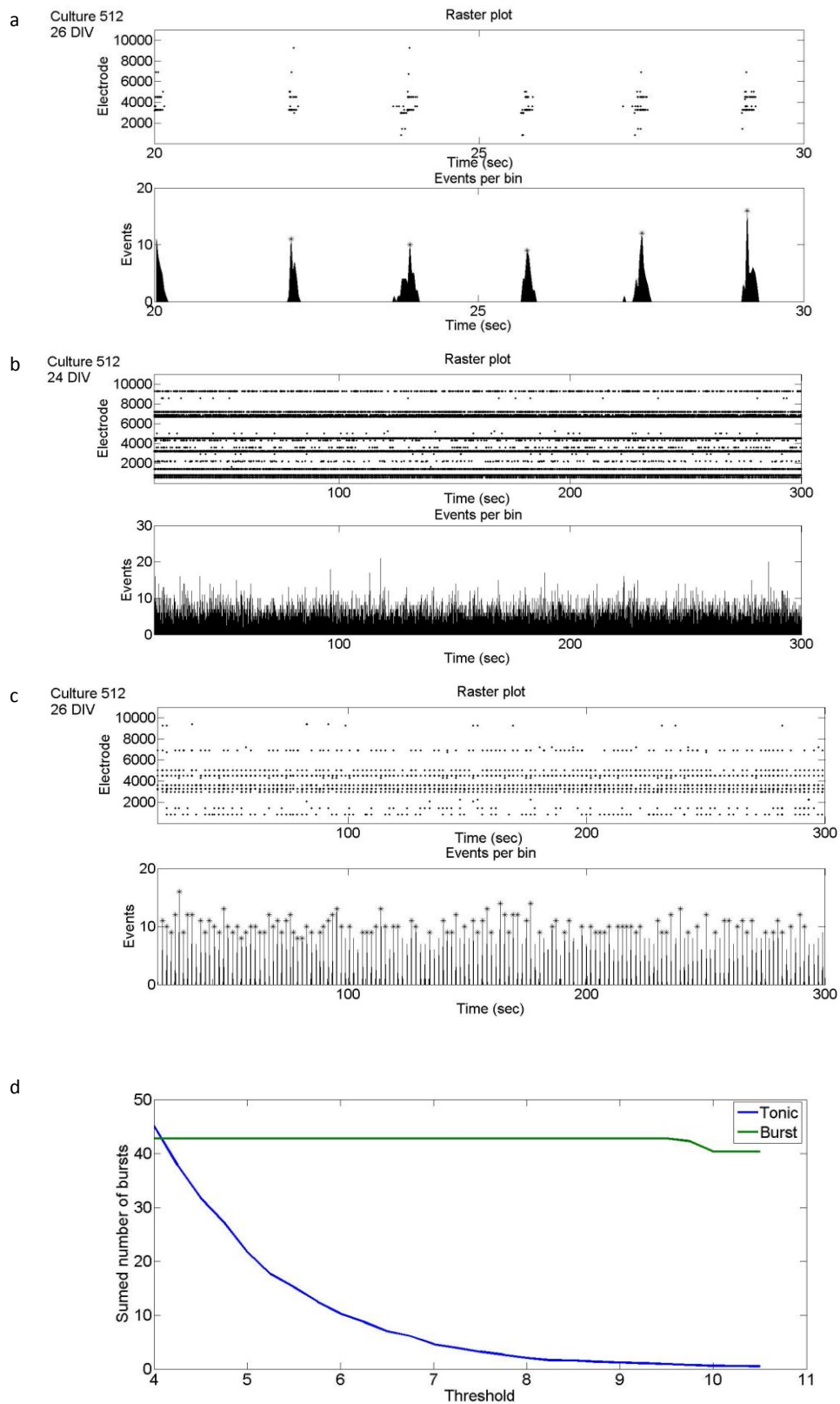
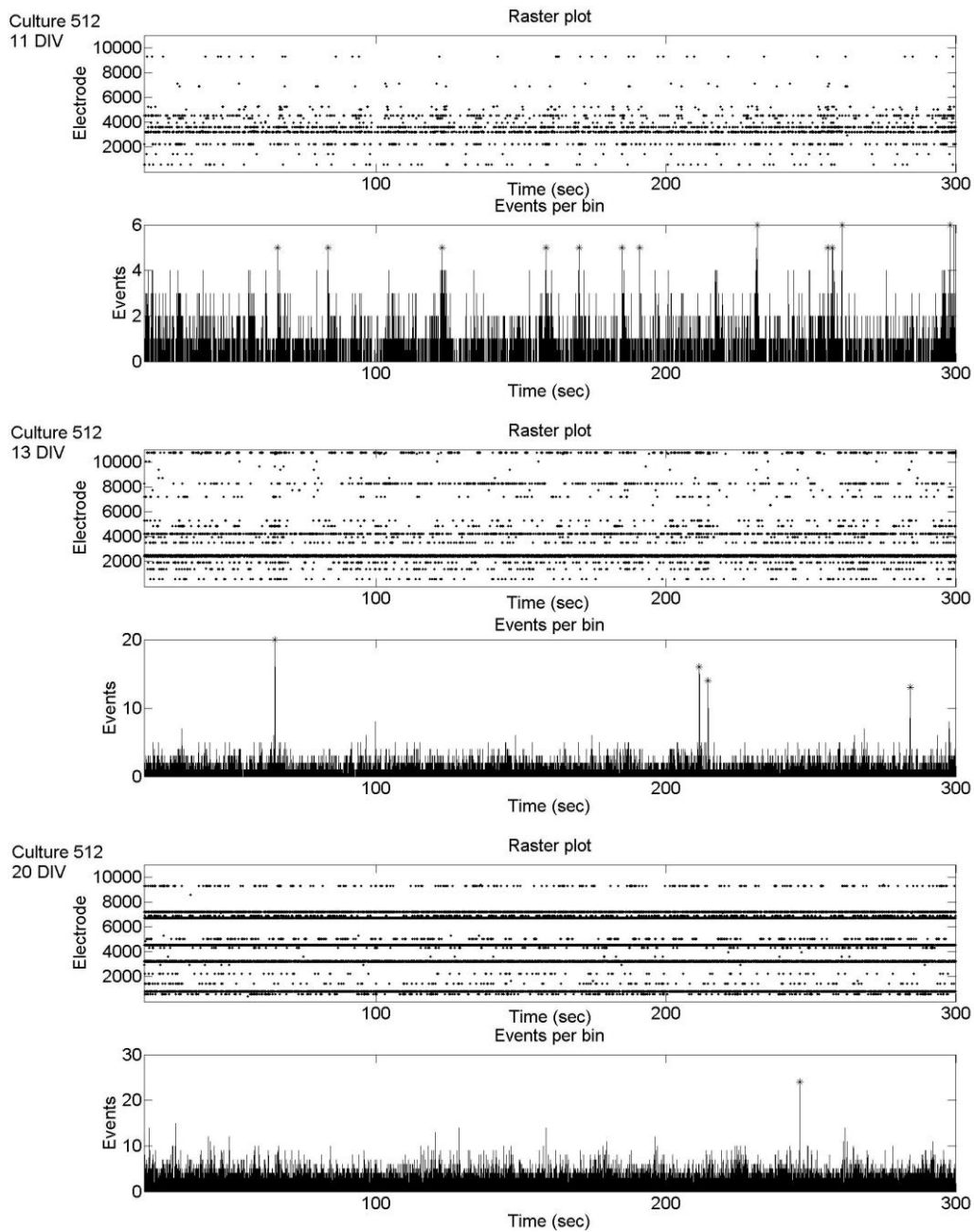


Figure A11. (a) Bursts were composed even from few electrodes. (b) illustration of a raster plot where tonic firing dominates. (c) illustration of a raster plot where bursting dominates. (d) effect of the value of  $A$  (threshold constant) to the MBR on raster plots where either tonic activity or bursting dominates.

## A.4 Complementary raster plots

### A.4.1 Culture 512



(continued on next page)

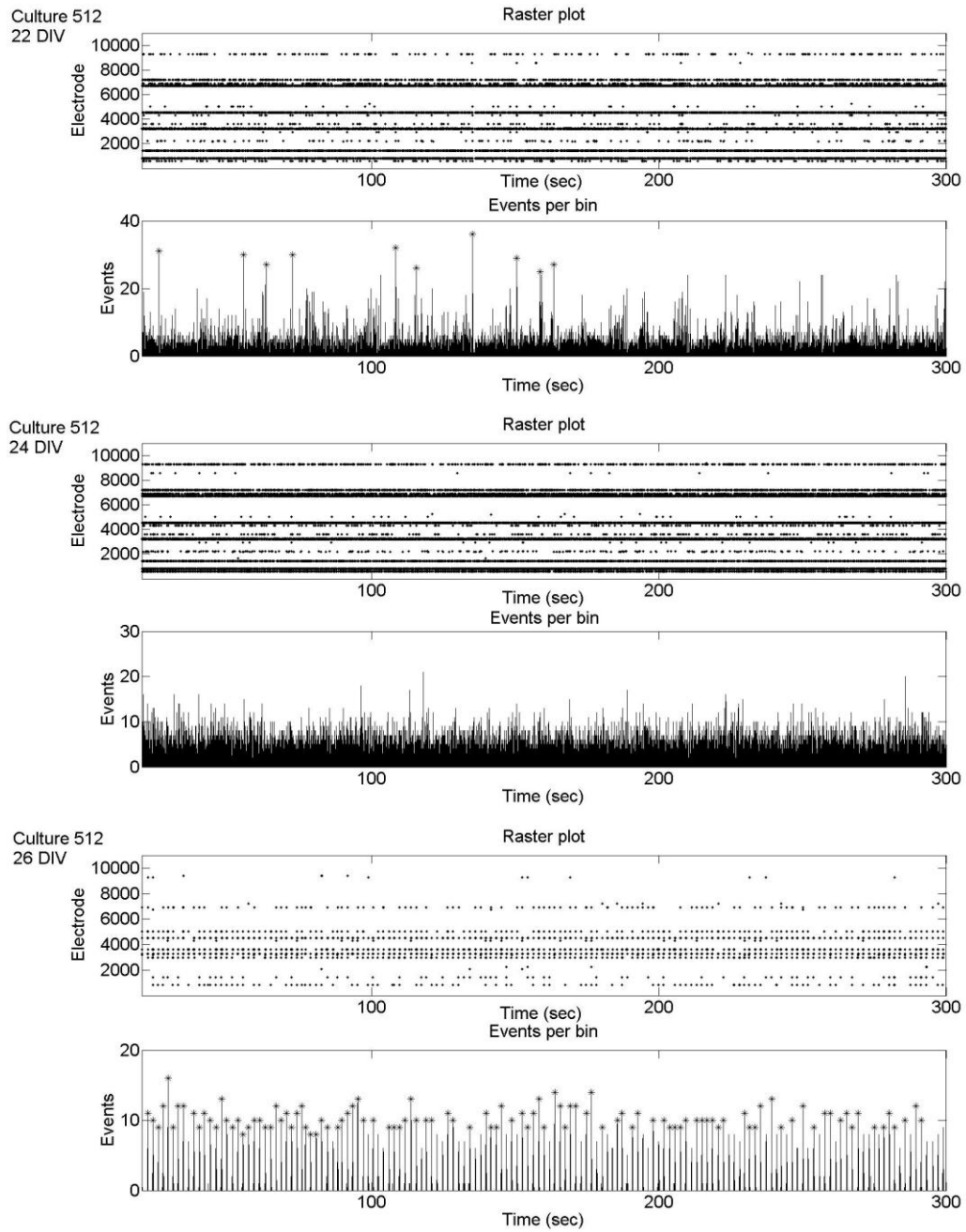
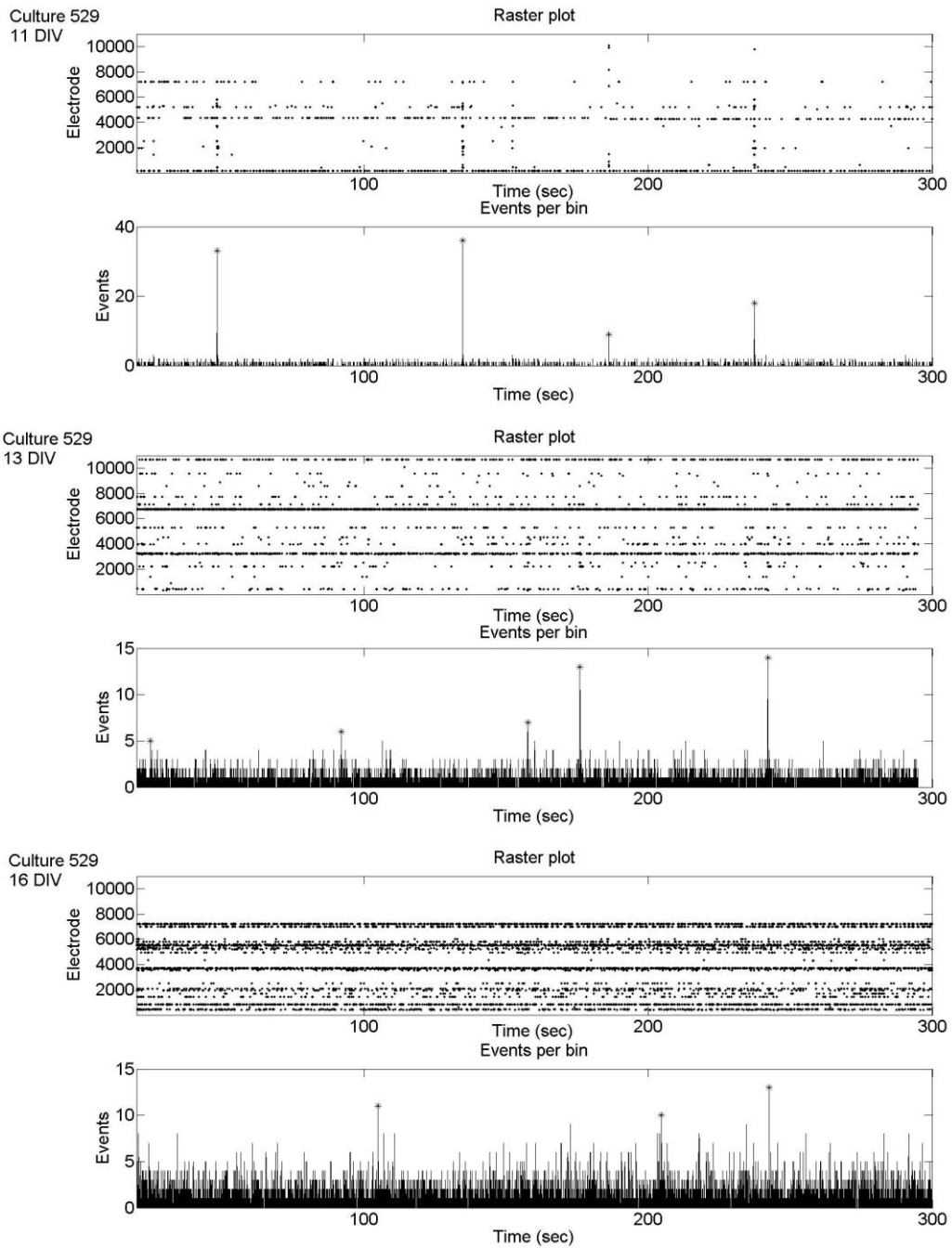


Figure A12. Raster plots for culture 512.

## A.4.2 Culture 529



Continued on next page

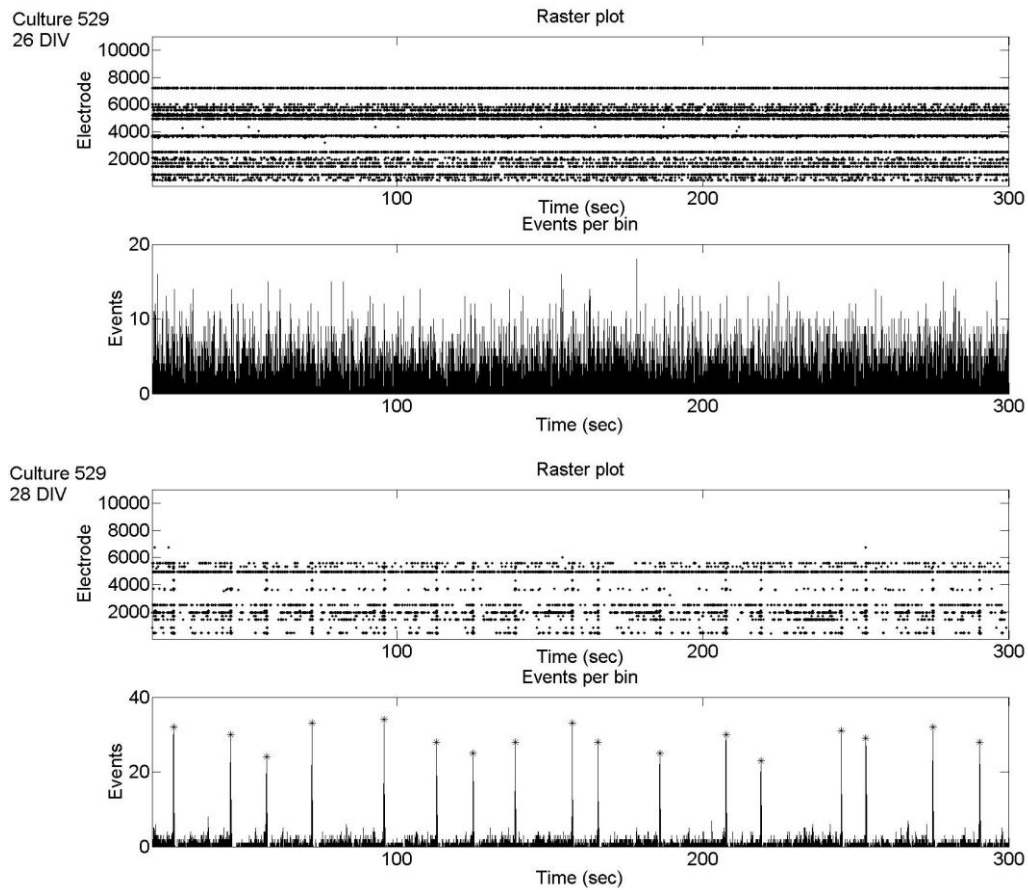
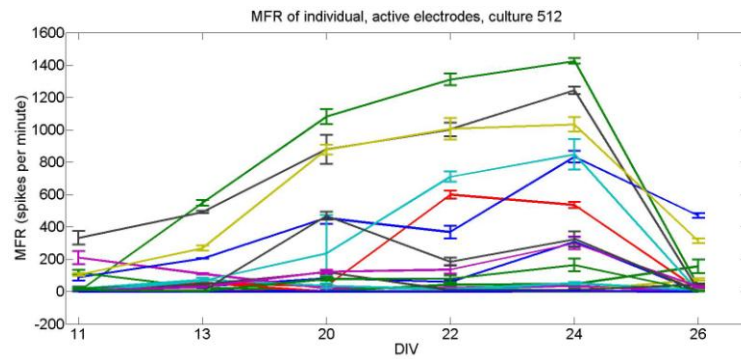


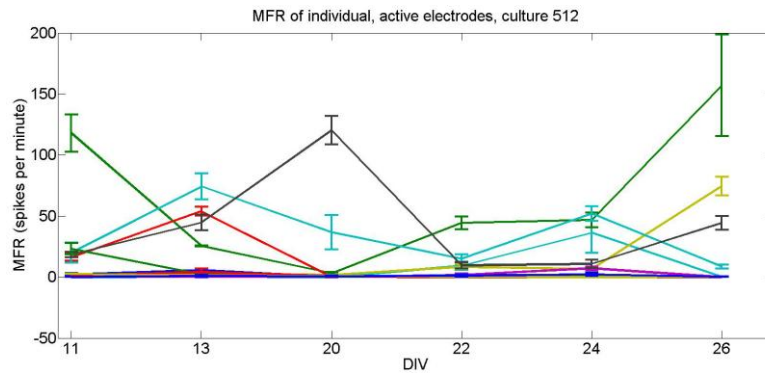
Figure A13. Raster plots for culture 529.

## A.5 MFR of individual electrodes

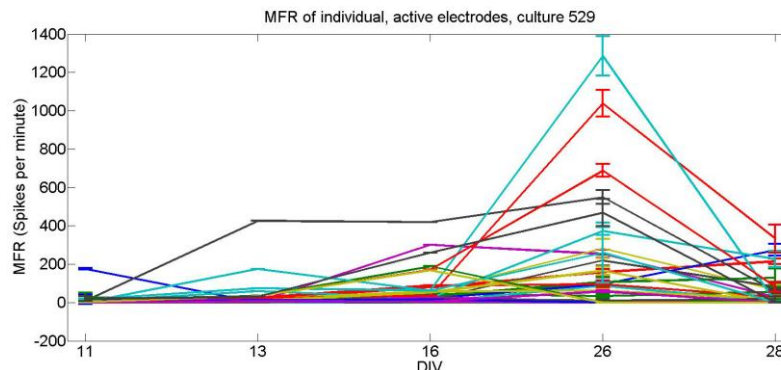
a



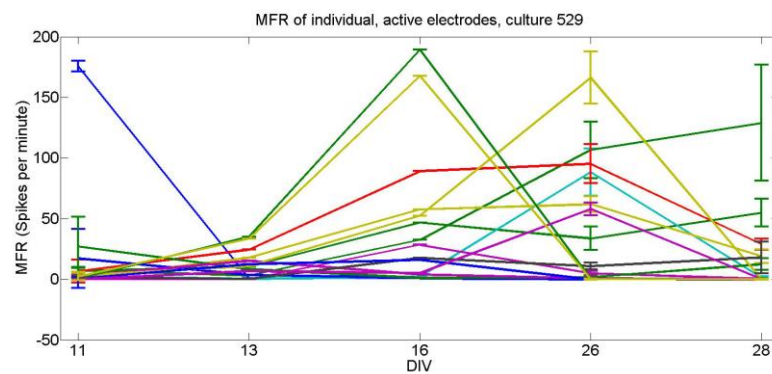
b



c

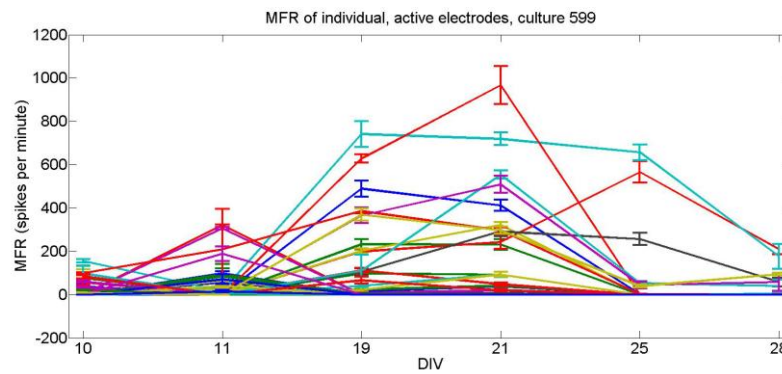


d



Continued on next page

e



f

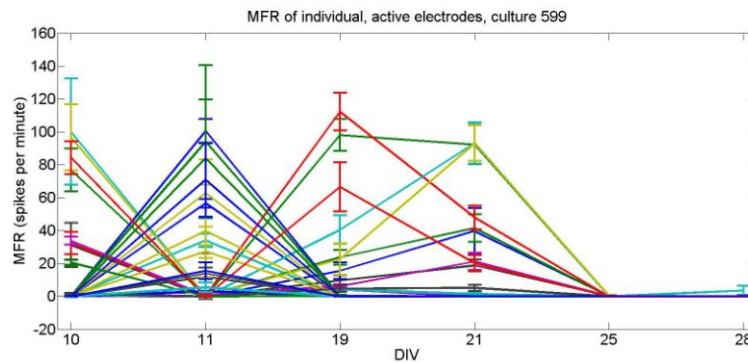


Figure A14. (a) MFR of individual electrodes for culture 512 and a zoom in (b). (c) MFR of individual electrodes for culture 529 and a zoom in (d). (e) MFR of individual electrodes for culture 599 and a zoom in (f).

## A.6 Software description

### A.6.1 Hidens neurodish router

The NeuroDishRouter handles the array routing. It controls the electrode to channel mapping and is also used to visualize configurations. Type “NeuroDishRouter” in the shell to run the program and then, the first thing you have to do (even before you try loading a previously-generated file) is to construct the chip. You will then see something similar to Figure A15.

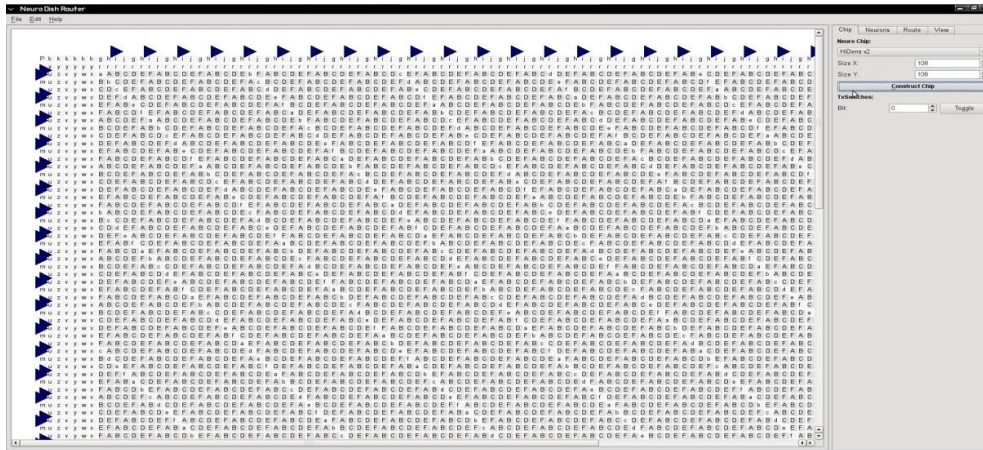


Figure A15. Initialization of NeuroDishRouter.

There are four tabs in the program's main window. “Chip”, “Neurons”, “Route” and “View”. After the chip construction we will mainly use the “Neurons” and “Route” tabs. The most important tab for creating the configuration is the “Neurons” tab, Figure A16.

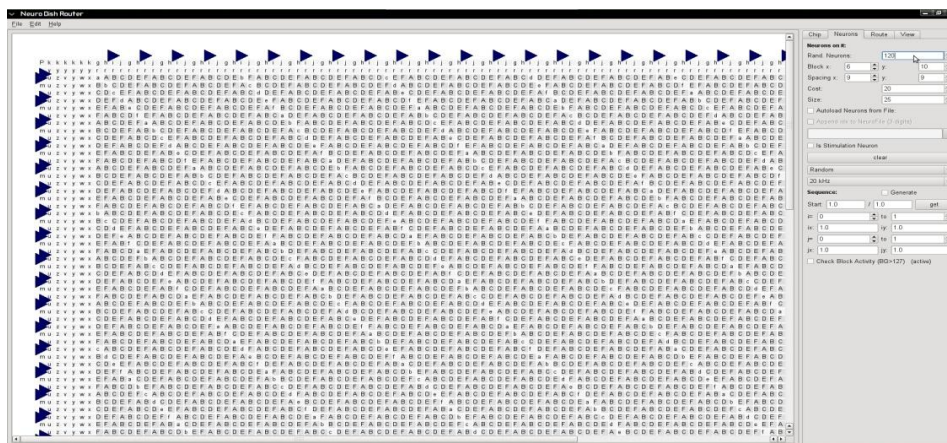


Figure A16. The “Neurons” tab.

We will first briefly describe the controls of this tab and then proceed with some examples for a random configuration, a block configuration and a block(s) sequence that scans the whole array. The first five controls in the “Neurons” tab are labeled: Random neurons, block(x,y), spacing(x,y), cost and size. “Random neurons” controls the number of neurons that you want to add when using a random configuration. Remember, a neuron is an interesting spot. It is neither an electrode nor a channel. Furthermore, because it is interesting for you it does not mean it will be routed. By creating an interesting spot you declare that you would like this position to be analyzed. So, the algorithm tries to map a channel to an electrode nearby this area. It could be the closest electrode or the second closest etc...

The “block(x,y)” tabs control the number of neurons in the x and y axis. For example if you set x = 1 and y = 10 you will get a nice column of ten neurons. If you set x = 10 and y = 1 you will get a nice row of ten neurons, Figure A17.

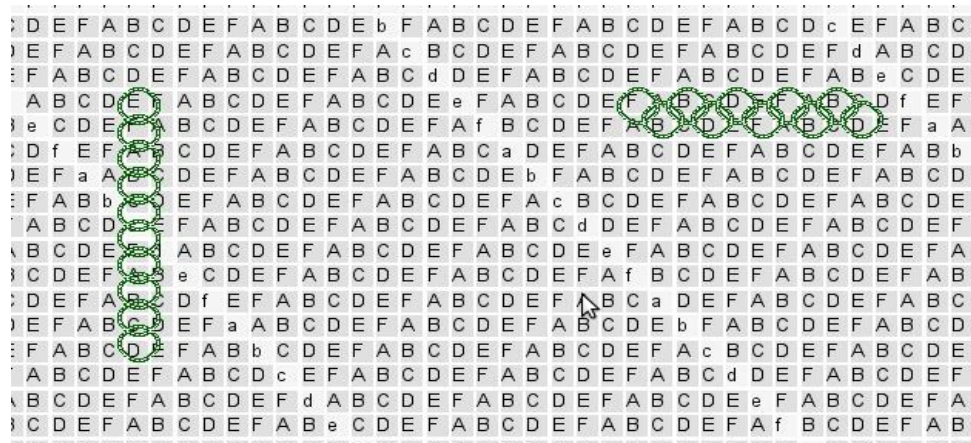


Figure A17. A column of ten neurons (left) can be created by setting block(x) = 1, block(y) = 10. A row of ten neurons (right) can be created by setting block(x) = 10 and block(y) = 1.

The “spacing(x,y)” controls the spacing of neurons. For example, when you want to generate block spaced neurons, the spacing(x,y) controls this spacing (block). In Figure A18 imagine some “blocks” between individual neurons of size(x,y) = (5,9).

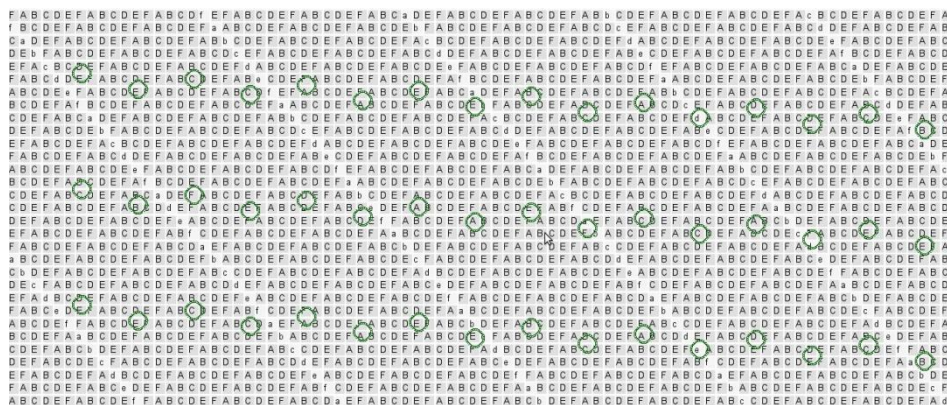


Figure A18. Block spaced neurons

The “cost” and “size” controls, are about the cost of each neuron in the optimization algorithm and the size (diameter) of each neuron respectively. It is advised to leave these settings to their default values.

After these controls there are the controls labeled “clear”, “random”, “20kHz”. The second one controls the type of configuration you want to create: random, block or block spaced. The first one clears the existing configuration, allowing you to create a new one and the last one controls the sampling rate. However, the higher the

sampling rate the less channels can be used. 8 channels for 20kHz can be “exchanged” by one channel of 160kHz.

Generation of random, single, block or block spaced configuration

- Press “clear” to clear any previously defined configuration
- For random neurons select the number of random neurons from the control “Rand.Neurons”
- For single neurons only the cost and size are important, but is advised to leave the default values.
- For blocks of neurons, select the block(x,y) size.
- For block spaced select the spacing(x,y)
- Select from the appropriate list Random,Single,Block or Block spaced
- Click once in the device figure on the left to place the neuron(s)

Generation of blocks-sequence configurations for a complete scan:

Under the “Sequence” label in the “Neurons” tab are the necessary controls for sequence generation. The Start control defines the starting point (coordinates) of the first neuron/block. There are six other controls: i, ix, iy, j, jx, jy. Roughly, the I and j act like For loops while the x's and y's define the spacing between consecutive loop iterations. A simple pseypo-algorithm for that is given below:

```
For i = a to b-1
  for j = c to d-1
    CreateBlock(x,y)
  end
end
```

where a,b,c,d are the values you enter in the controls. Then, the function Createblock(x,y) is something like:

CreateBlock(x,y) = Start(x,y) + i\*i(x,y) + j\*j(x,y)

By setting ix =0, iy =5, jy = 0, jx = 5 you can create a block sequence in which in the first iterations (j loops) it moves on the x axis (because the j loop is inside the i loop it executes “first”). When this loop is finished, due to ix=0,iy=5 the block will move in

the y-direction from the original place. Then it will start a new j loop in the x direction. To sum up:

A starting point is chosen and the j loop executes. The i-loop then shifts the block to a new position and the j loop executes again.

The  $i(x,y)$  and  $j(x,y)$  should depend on the values of the block  $(x,y)$ . For example, if your block has  $\text{block}(x,y) = (6,10)$  then you could set  $j_x \geq 6$  and  $i_y \geq 10$ . Otherwise, your generated blocks might overlap.

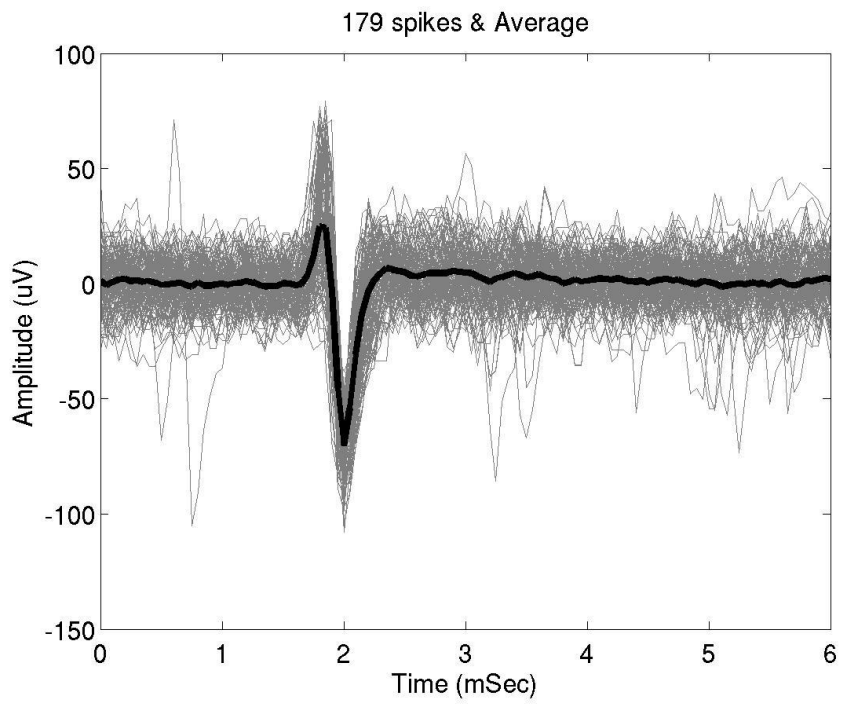
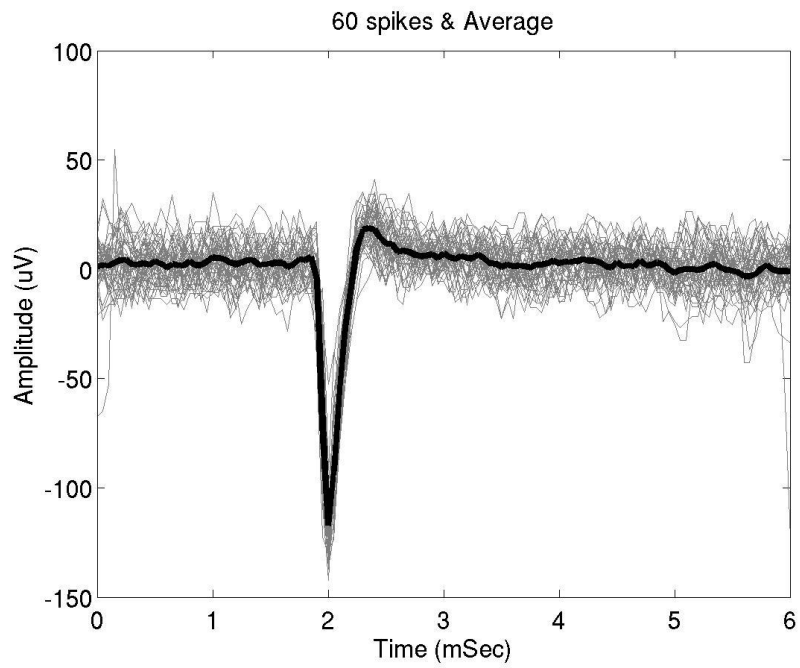
### A.6.2 Labview software overview

The software developed in its final form contains two main parts. One is the original HIDENS labview client and the second is an on-line spike detection software. Both of them can be used at any time, although when used together the CPU seems to be quite under heavy load.

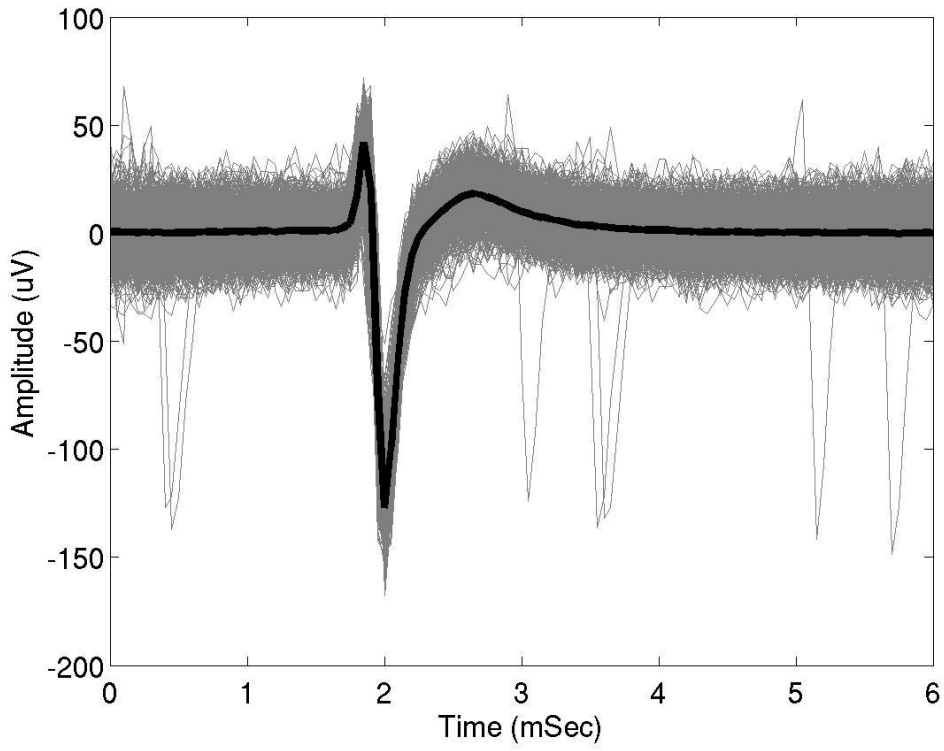
The original Hidens client allows for real-time observation of the signals. It provides with information about the DC-values of each electrode's signals, allows sending new configuration to the chip and make recordings. There are two options for recording, one is a single recording in which case one ntk file is produced with data from a single configuration. The recording file also contains information about the channel to electrode configuration, gain etc... The second option is to make a sequence recording. In this case you need first to generate sequence configurations with the Neurodish router which are then used one by one to record individual ntk files. Then you get as many number of ntk files as the number of recordings, each one with its own configuration. A disadvantage of this client is that it only allows for continuous data recording which is very demanding in terms of hard disk space and processing time later on.

The online spike detection algorithm was created to solve this problem. It takes exactly the same data as the Hidens client from the server and allows for full recording or for storing only spike-events. Events are detected with a threshold-crossing algorithm which can be set during the operation of the software. Typical values are 4-5 times the estimated noise. An image of the array is also visible, and when an event is detected the corresponding electrode position in the array lights up.

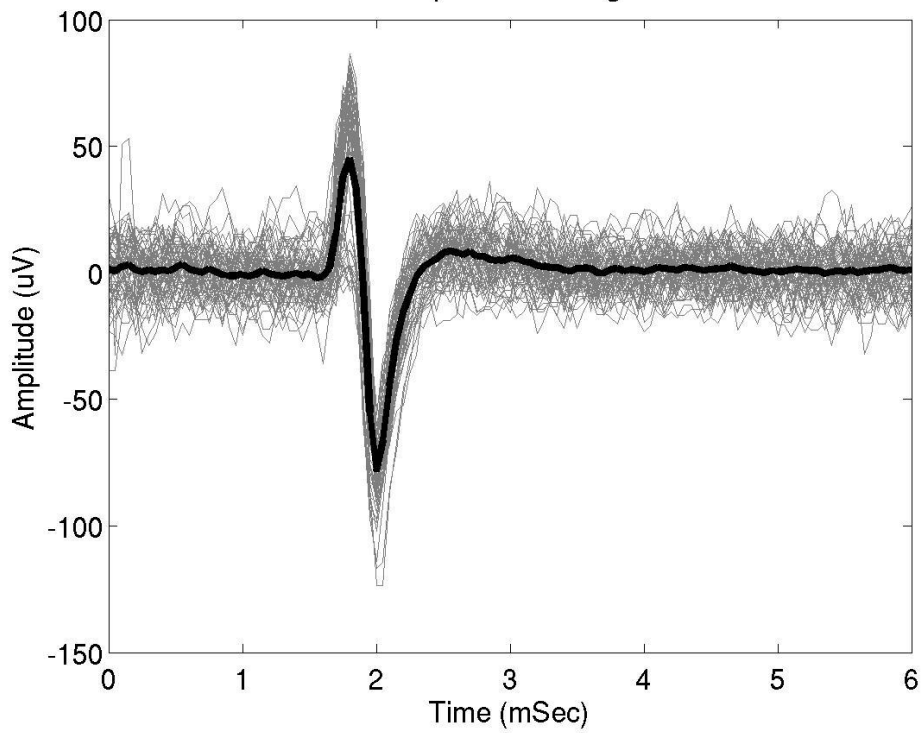
## A.7 Spike shapes

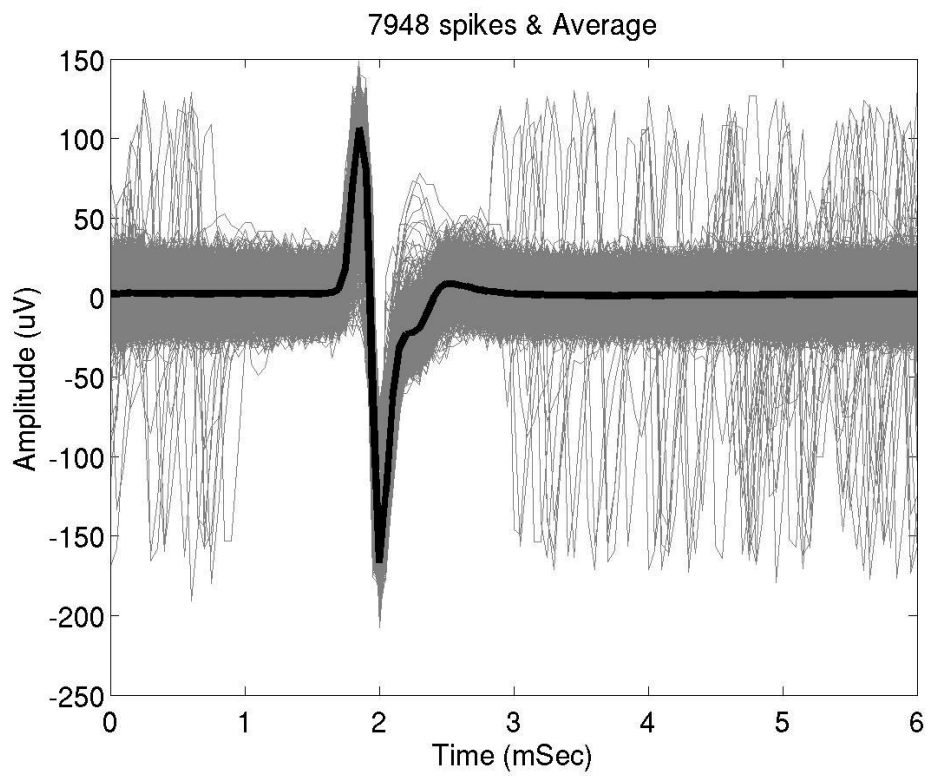
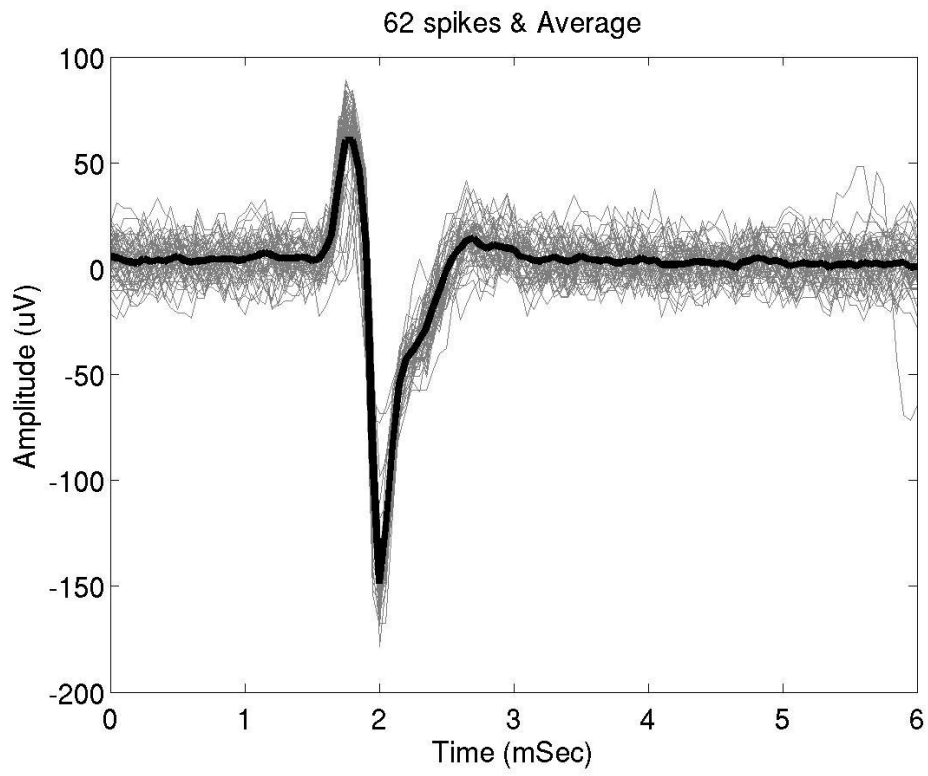


1412 spikes & Average

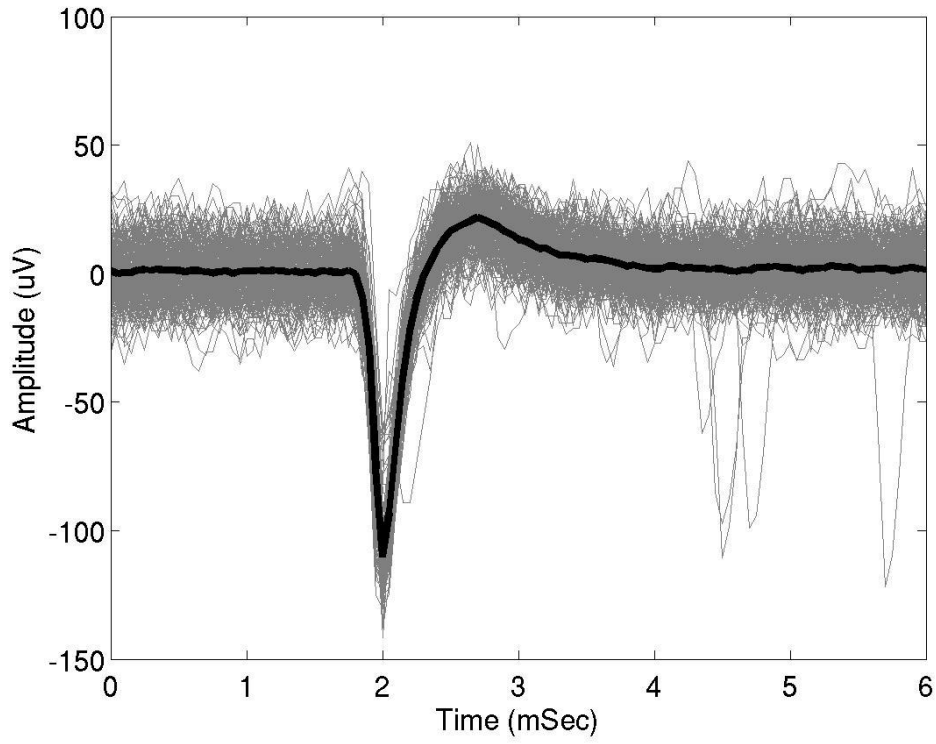


69 spikes & Average

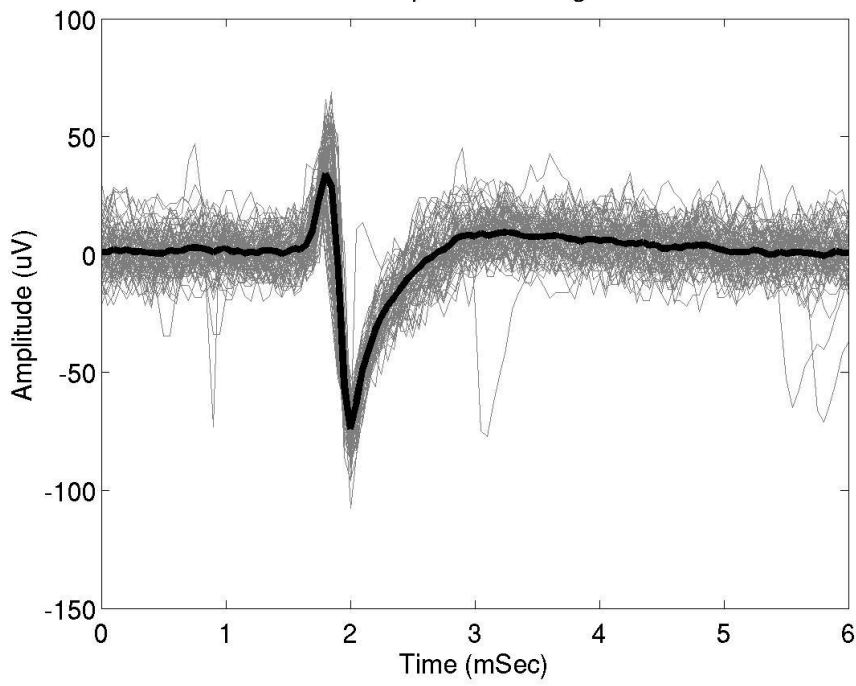


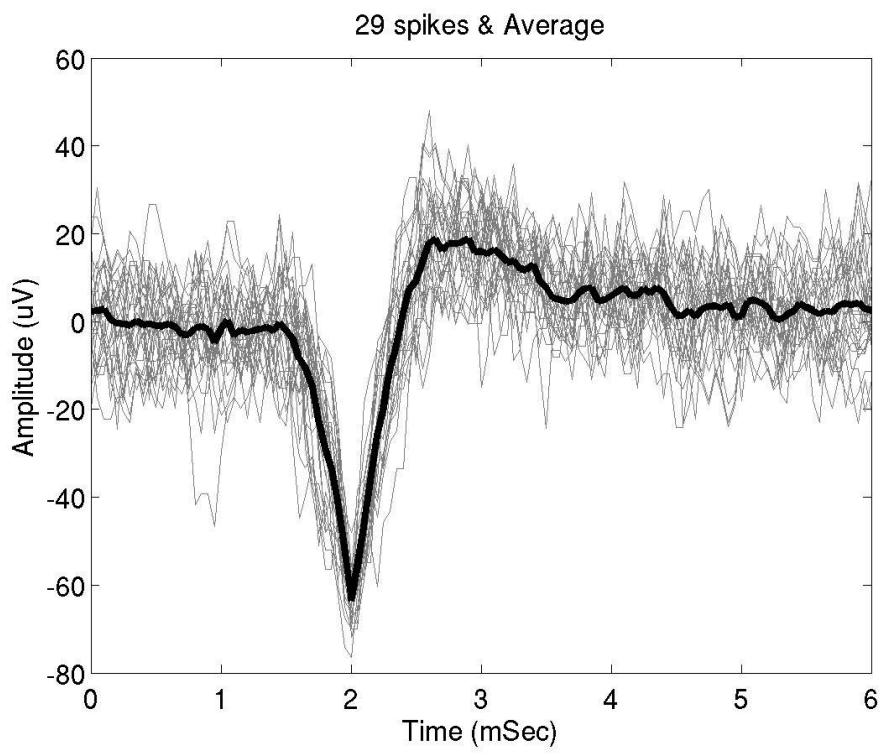
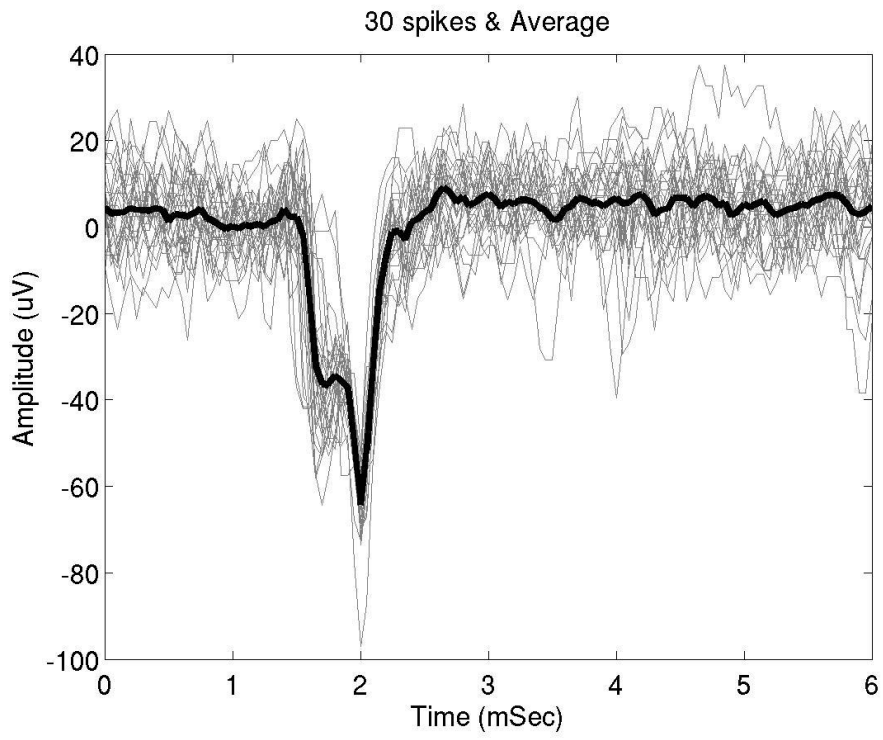


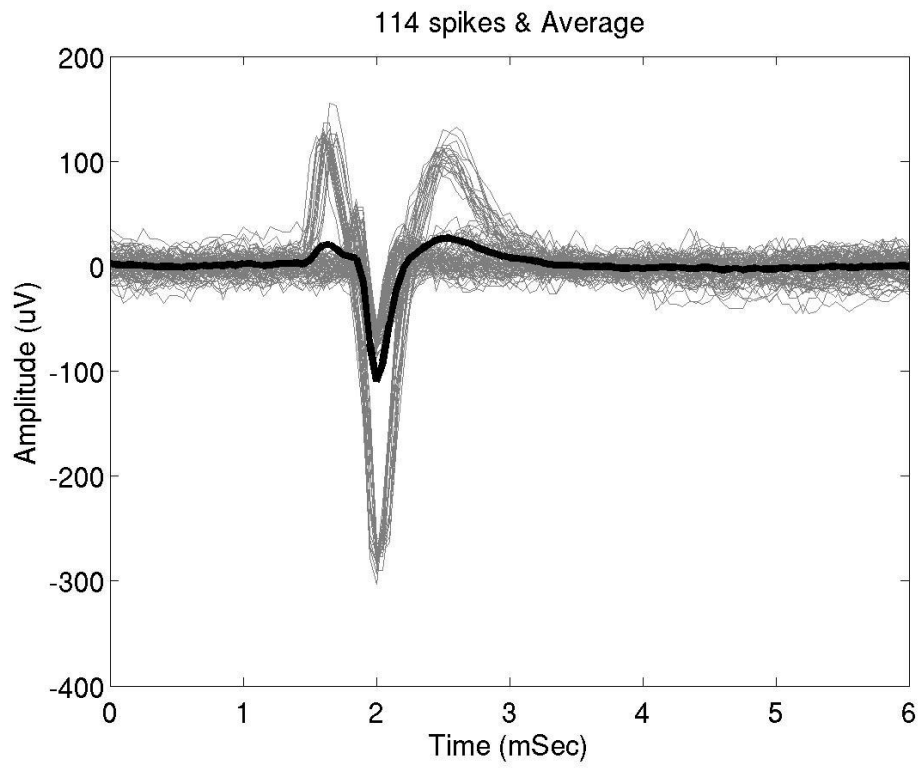
293 spikes & Average



100 spikes & Average









## References

1. GREVE, F., *MICROMACHINED PLATFORMS FOR MANIPULATING AND RECORDING FROM CELLS*. 2006, SWISS FEDERAL INSTITUTE OF TECHNOLOGY ZURICH.
2. Purves, D., et al., *Neuroscience*. Sunderland, MA. Sinauer Associates., 2001: p. 2008.
3. Marom, S. and G. Shahaf, *Development, learning and memory in large random networks of cortical neurons: lessons beyond anatomy*. Quarterly Reviews of Biophysics, 2002. **35**(01): p. 63-87.
4. Heer, F. and A. Hierlemann, *Integrated Microelectrode Arrays*. 2007. p. 207-258.
5. Bonifazi, P., M. Ruaro, and V. Torre, *Statistical properties of information processing in neuronal networks*. European Journal of Neuroscience, 2005. **22**(11): p. 2953-2964.
6. Johnstone, A., et al., *Microelectrode Arrays: A Physiologically-based Neurotoxicity Testing Platform for the 21st Century*. NeuroToxicology, 2010.
7. Morin, F., Y. Takamura, and E. Tamiya, *Investigating neuronal activity with planar microelectrode arrays: achievements and new perspectives*. Journal of bioscience and bioengineering, 2005. **100**(2): p. 131-143.
8. Rutten, W., *SELECTIVE ELECTRICAL INTERFACES WITH THE NERVOUS SYSTEM*. Annual Review of Biomedical Engineering, 2002. **4**(1): p. 407-452.
9. Rutten, W., et al., *Neuro-electronic interfacing with multielectrode arrays*. IEEE Engineering in Medicine and Biology Magazine, 1999. **18**(3): p. 47-55.
10. Chiappalone, M., et al., *Dissociated cortical networks show spontaneously correlated activity patterns during in vitro development*. Brain research, 2006. **1093**(1): p. 41-53.
11. Van Pelt, J., et al., *Longterm stability and developmental changes in spontaneous network burst firing patterns in dissociated rat cerebral cortex cell cultures on multielectrode arrays\* 1*. Neuroscience letters, 2004. **361**(1-3): p. 86-89.
12. van Pelt, J., et al., *Dynamics and plasticity in developing neuronal networks in vitro*. Development, dynamics and pathology of neuronal networks: from molecules to functional circuits: proceedings of the 23rd International Summer School of Brain Research, held at the Royal Netherlands Academy of Arts and Sciences, Amsterdam, the Netherlands, from 25-29 August 2003, 2005: p. 173.
13. Van Pelt, J., et al., *Long-term characterization of firing dynamics of spontaneous bursts in cultured neural networks*. IEEE Transactions on Biomedical Engineering, 2004. **51**(11): p. 2051-2062.
14. Wagenaar, D., J. Pine, and S. Potter, *An extremely rich repertoire of bursting patterns during the development of cortical cultures*. BMC neuroscience, 2006. **7**(1): p. 11.
15. Ben-Ari, Y., *Developing networks play a similar melody*. TRENDS in Neurosciences, 2001. **24**(6): p. 353-360.
16. Feber, J., et al., *Conditional firing probabilities in cultured neuronal networks: a stable underlying structure in widely varying spontaneous activity patterns*. Journal of neural engineering, 2007. **4**: p. 54.
17. Le Feber, J., J. Van Pelt, and W. Rutten, *Latency-related development of functional connections in cultured cortical networks*. Biophysical Journal, 2009. **96**(8): p. 3443-3450.
18. le Feber, J., J. Stegenga, and W. Rutten. *Do external stimuli, applied to train cultured cortical networks, disturb the balance between activity and connectivity?* 2008.
19. Le Feber, J., J. Stegenga, and W. Rutten, *The Effect of Slow Electrical Stimuli to Achieve Learning in Cultured Networks of Rat Cortical Neurons*. 2010.
20. Marom, S. and D. Eytan, *Learning in ex-vivo developing networks of cortical neurons*. Development, dynamics and pathology of neuronal networks: from molecules to

- functional circuits: proceedings of the 23rd International Summer School of Brain Research, held at the Royal Netherlands Academy of Arts and Sciences, Amsterdam, the Netherlands, from 25-29 August 2003, 2005: p. 189.
21. Shahaf, G. and S. Marom, *Learning in networks of cortical neurons*. Journal of Neuroscience, 2001. **21**(22): p. 8782.
  22. Stegenga, J., *Live learning neuronal networks: plasticity of bursts*. 2009.
  23. Stegenga, J., et al., *The effect of learning on bursting*. Biomedical Engineering, IEEE Transactions on, 2009. **56**(4): p. 1220-1227.
  24. Van Staveren, G., et al. *The effect of training of cultured neuronal networks, can they learn?* 2005.
  25. Bonzano, L., M. Bove, and S. Martinoia, *Effects of NMDA and non-NMDA receptors antagonists on the dynamic behavior of cultured cortical networks*. Neurocomputing, 2006. **69**(16-18): p. 1897-1903.
  26. Eytan, D., et al., *Dopamine-induced dispersion of correlations between action potentials in networks of cortical neurons*. Journal of neurophysiology, 2004. **92**(3): p. 1817.
  27. Gross, G., M. Rhoades Hassan, and K. Barry, *The use of neuronal networks on multielectrode arrays as biosensors*. Biosensors and Bioelectronics, 1995. **10**(6-7): p. 553-567.
  28. Li, Y., et al., *Dynamics of learning in cultured neuronal networks with antagonists of glutamate receptors*. Biophysical Journal, 2007. **93**(12): p. 4151-4158.
  29. Martinoia, S., et al., *Electrophysiological activity modulation by chemical stimulation in networks of cortical neurons coupled to microelectrode arrays: A biosensor for neuropharmacological applications*. Sensors & Actuators: B. Chemical, 2005. **108**(1-2): p. 589-596.
  30. Nagy, J. and L. Laszlo, *Increased sensitivity to NMDA is involved in alcohol-withdrawal induced cytotoxicity observed in primary cultures of cortical neurones chronically pre-treated with ethanol*. Neurochemistry international, 2002. **40**(7): p. 585-591.
  31. Ruardij, T., M. Goedbloed, and W. Rutten, *Adhesion and patterning of cortical neurons on polyethylenimine-and fluorocarbon-coated surfaces*. Biomedical Engineering, IEEE Transactions on, 2002. **47**(12): p. 1593-1599.
  32. Ruardij, T., M. Goedbloed, and W. Rutten, *Long-term adhesion and survival of dissociated cortical neurons on miniaturised chemical patterns*. Medical and Biological Engineering and Computing, 2003. **41**(2): p. 227-232.
  33. Ruardij, T., M. van den Boogaart, and W. Rutten, *Adhesion and growth of electrically active cortical neurons on polyethylenimine patterns microprinted onto PEO-PPO-PEO triblockcopolymer-coated hydrophobic surfaces*. NanoBioscience, IEEE Transactions on, 2003. **1**(1): p. 4-11.
  34. Rutten, W., et al., *Cultured neural networks: Optimization of patterned network adhesiveness and characterization of their neural activity*. Applied Bionics and Biomechanics, 2006. **3**(1): p. 1-7.
  35. Gold, C., et al., *On the origin of the extracellular action potential waveform: a modeling study*. Journal of neurophysiology, 2006. **95**(5): p. 3113.
  36. Quiroga, Q., *What is the real shape of extracellular spikes?* Journal of neuroscience methods, 2009. **177**(1): p. 194-198.
  37. Gold, C., D. Henze, and C. Koch, *Using extracellular action potential recordings to constrain compartmental models*. Journal of Computational Neuroscience, 2007. **23**(1): p. 39-58.
  38. Huettner, J. and R. Baughman, *Primary culture of identified neurons from the visual cortex of postnatal rats*. Journal of Neuroscience, 1986. **6**(10): p. 3044.

39. Neale, E., et al., *Glutamate decarboxylase immunoreactivity and gamma-[3H] aminobutyric acid accumulation within the same neurons in dissociated cell cultures of cerebral cortex*. Journal of Neuroscience, 1983. **3**(2): p. 376.
40. Romijn, H., F. Van Huizen, and P. Wolters, *Towards an improved serum-free, chemically defined medium for long-term culturing of cerebral cortex tissue*. Neuroscience & Biobehavioral Reviews, 1984. **8**(3): p. 301-334.
41. Ito, D., et al., *How many neurons do we need to record synchronized bursts in dissociated culture using multi-electrode arrays?* Neuroscience Research, 2009. **65**(Supplement 1): p. S198-S198.
42. Gopal, K. and G. Gross, *Auditory cortical neurons in vitro: cell culture and multichannel extracellular recording*. Acta oto-laryngologica, 1996. **116**(2): p. 690-696.
43. Claverol-Tinture, E. and J. Pine, *Extracellular potentials in low-density dissociated neuronal cultures*. Journal of neuroscience methods, 2002. **117**(1): p. 13-21.
44. Jun, S., et al., *Low-density neuronal networks cultured using patterned poly-l-lysine on microelectrode arrays*. Journal of neuroscience methods, 2007. **160**(2): p. 317-326.
45. Jungblut, M., et al., *Triangular neuronal networks on microelectrode arrays: an approach to improve the properties of low-density networks for extracellular recording*. Biomedical Microdevices, 2009. **11**(6): p. 1269-1278.
46. Mok, S.Y., Y.M. Lim, and S.Y. Goh, *A device to facilitate preparation of high-density neural cell cultures in MEAs*. Journal of neuroscience methods, 2009. **179**(2): p. 284-291.
47. Ito, D., et al., *Minimum neuron density for synchronized bursts in a rat cortical culture on multi-electrode arrays*. Neuroscience, 2010. **171**(1): p. 50-61.
48. Van Huizen, F., *Significance of bioelectric activity for synaptic network formation*. 1986, PhD Thesis, University of Amsterdam.
49. Van Huizen, F., H. Romijn, and A. Habets, *Synaptogenesis in rat cerebral cortex cultures is affected during chronic blockade of spontaneous bioelectric activity by tetrodotoxin*. Developmental Brain Research, 1985. **19**(1): p. 67-80.
50. Wagenaar, D., *Development and control of epileptiform bursting in dissociated cortical cultures*. 2006.
51. Scholl, M., et al., *Ordered networks of rat hippocampal neurons attached to silicon oxide surfaces*. Journal of neuroscience methods, 2000. **104**(1): p. 65-75.
52. Berdondini, L., et al., *Active pixel sensor array for high spatio-temporal resolution electrophysiological recordings from single cell to large scale neuronal networks*. Lab on a Chip, 2009. **9**(18): p. 2644-2651.
53. Imfeld, K., et al., *Large-scale, high-resolution data acquisition system for extracellular recording of electrophysiological activity*. IEEE Transactions on Biomedical Engineering, 2008. **55**(8): p. 2064-2073.
54. Berdondini, L., et al., *Extracellular recordings from locally dense microelectrode arrays coupled to dissociated cortical cultures*. Journal of neuroscience methods, 2009. **177**(2): p. 386-396.
55. DeBusschere, B. and G. Kovacs, *Portable cell-based biosensor system using integrated CMOS cell-cartridges*. Biosensors and Bioelectronics, 2001. **16**(7-8): p. 543-556.
56. Heer, F., et al., *CMOS microelectrode array for bidirectional interaction with neuronal networks*. IEEE Journal of Solid-State Circuits, 2006. **41**(7): p. 1620-1629.
57. Jimbo, Y. and H. Robinson, *Propagation of spontaneous synchronized activity in cortical slice cultures recorded by planar electrode arrays*. Bioelectrochemistry, 2000. **51**(2): p. 107-115.

58. Lambacher, A., et al., *Electrical imaging of neuronal activity by multi-transistor-array (MTA) recording at 7.8  $\mu\text{m}$  resolution*. Applied Physics A: Materials Science & Processing, 2004. **79**(7): p. 1607-1611.
59. FREY, U., et al., *Switch-Matrix-Based High-Density Microelectrode Array in CMOS Technology*. IEEE Journal of Solid-State Circuits, 2010. **45**(2): p. 467-482.
60. *CMOS D-BSSE CMOS-MEAs*. March - December 2010]; Available from: <http://wiki-bsse.ethz.ch>.
61. Stegenga, J., et al., *Analysis of cultured neuronal networks using intraburst firing characteristics*. Biomedical Engineering, IEEE Transactions on, 2008. **55**(4): p. 1382-1390.
62. Frey, U., et al., *Microelectronic system for high-resolution mapping of extracellular electric fields applied to brain slices*. Biosensors and Bioelectronics, 2009. **24**(7): p. 2191-2198.
63. Berdondini, L., et al., *High-density electrode array for imaging in vitro electrophysiological activity*. Biosensors and Bioelectronics, 2005. **21**(1): p. 167-174.
64. Huang, X., et al., *Simulation of microelectrode impedance changes due to cell growth*. Sensors Journal, IEEE, 2004. **4**(5): p. 576-583.
65. Buitengeweg, J., et al., *Measurement of sealing resistance of cell-electrode interfaces in neuronal cultures using impedance spectroscopy*. Medical and Biological Engineering and Computing, 1998. **36**(5): p. 630-637.
66. Regehr, W., et al., *Sealing cultured invertebrate neurons to embedded dish electrodes facilitates long-term stimulation and recording*. Journal of neuroscience methods, 1989. **30**(2): p. 91-106.
67. *BSSE wiki* Available from: <http://wiki-bsse.ethz.ch>.
68. Bear, M., B. Connors, and M. Paradiso, *Neuroscience: Exploring the brain*. 2007: Lippincott Williams & Wilkins.
69. Potter, S. and T. DeMarse, *A new approach to neural cell culture for long-term studies*. Journal of neuroscience methods, 2001. **110**(1-2): p. 17-24.
70. Wagenaar, D., J. Pine, and S. Potter, *Searching for plasticity in dissociated cortical cultures on multi-electrode arrays*. Journal of negative results in biomedicine, 2006. **5**(1): p. 16.
71. Gritsun, T., et al., *Explaining burst profiles using models with realistic parameters and plastic synapses*. 2008.
72. Ramakers, G., M. Corner, and A. Habets, *Development in the absence of spontaneous bioelectric activity results in increased stereotyped burst firing in cultures of dissociated cerebral cortex*. Experimental Brain Research, 1990. **79**(1): p. 157-166.
73. Kamioka, H., et al., *Spontaneous periodic synchronized bursting during formation of mature patterns of connections in cortical cultures\* 1*. Neuroscience letters, 1996. **206**(2-3): p. 109-112.
74. Maeda, E., H. Robinson, and A. Kawana, *The mechanisms of generation and propagation of synchronized bursting in developing networks of cortical neurons*. Journal of Neuroscience, 1995. **15**(10): p. 6834.
75. Van Staveren, G., et al. *Wave shape classification of spontaneous neuronal activity in cortical cultures on micro-electrode arrays*. 2002: IEEE.
76. Beggs, J. and D. Plenz, *Neuronal avalanches are diverse and precise activity patterns that are stable for many hours in cortical slice cultures*. Journal of Neuroscience, 2004. **24**(22): p. 5216.